

國立交通大學

環境工程研究所

博士論文

一個控制細微粒及奈米微粒排放的
電極線-平板型濕式靜電集塵器

A Wire-in-Plate Wet Electrostatic Precipitator for Controlling
Fine and Nanosized Particle Emission

研究生：林冠宇

指導教授：蔡春進 教授

中華民國九十九年八月

一個控制細微粒及奈米微粒排放的
電極線-平板型濕式靜電集塵器

A Wire-in-Plate Wet Electrostatic Precipitator for Controlling
Fine and Nanosized Particle Emission

研究生：林冠宇

Student : Guan-Yu Lin

指導教授：蔡春進

Advisor : Chuen-Jinn Tsai



博士論文

A thesis
Submitted to Institute of Environmental Engineering
National Chiao Tung University
in Partial Fulfillment of the Requirements
for the Degree of
Doctor of Philosophy
in
Environmental Engineering
August 2010
Hsinchu, Taiwan, Republic of China

中華民國九十九年八月

一個控制細微粒及奈米微粒排放的 電極線-平板型濕式靜電集塵器

學生：林冠宇

指導教授：蔡春進

國立交通大學環境工程研究所

摘要

本研究設計並開發一個高效率電極線-平板型濕式靜電集塵器用以控制細微粒及奈米微粒污染物。本集塵器之寬為 75 mm，有效微粒沉降長度及氣膠通道間隙分別為 48 mm 及 9.0 mm。本濕式靜電集塵器之收集板表面經噴砂處理後塗敷 TiO₂ 奈米微粒，以提高表面親水性，用以取代親水性薄膜的設計；電暈放電電極由三條黃金電極線(直徑為 100μm)所構成；一個氣體脈衝閥用以連續且規律的清潔附著在電極線表面之粉塵，使集塵器維持最佳的集塵效率。本濕式靜電集塵器之設計目的在於解決以下傳統乾式靜電集塵器在使用上之問題：粉塵沉降於收集板表面及放電電極上使集塵效率下降、背電暈及粉塵再揚起。最後，我們在起始乾淨條件下及經過高濃度粉塵負荷後進行濕式靜電集塵器集塵效率測試，並與乾式靜電集塵器之測試結果做比較。

實驗結果顯示當施加電壓為 4.3 kV、氣膠流量為 5 L/min (微粒停留時間為 0.39 s) 時，本濕式靜電集塵器在起始乾淨狀況下對 16.8-615 nm 電移動度粒徑之奈米微粒去除效率為 96.9-99.7%。在相同操作條件下經過 1.2±0.06 g/plate 之 TiO₂ 高粉塵濃度負荷後，濕式集塵器對於 16.8-615 nm 之玉米油微粒之去除效率仍可維持在 94.7-99.0%。

本研究首先建立了一個拉式數值模式來推估靜電集塵器對粒徑分佈為 $0.1 \leq d_p \leq 10$ μm 之微粒的集塵效率。微粒的充電及運動方程式係利用四階 Runge-Kutta 法來求解，以

求得微粒的帶電量及微粒移動軌跡。比對結果發現，模擬出的收集效率與 Huang and Chen (2002)及 Chang and Bai (1999)的實驗值相符，誤差範圍分別為 0.68-14.57 %及 1.49-12.46 %。但此模式僅適用於推估靜電集塵器對 $d_p \geq 100 \text{ nm}$ 之微粒的集塵效率，無法有效計算出部分充電效應對奈米微粒收集效率的影響。

為了準確預估單極電極線-平板靜電集塵器對奈米微粒($d_p \leq 100 \text{ nm}$)的收集效率，本研究建立了一個 2 維數值歐拉模式來模擬電場、離子濃度分佈，及微粒充電量。集塵器內部的流場係利用 SIMPLER 方法來計算之，而電場強度及離子濃度分佈則利用 Poisson 方程式及對流擴散方程式來求解。帶電微粒的濃度分佈及微粒去除效率分別利用對流擴散方程式及 Fuch 充電理論進行計算。

針對 6-100 nm 之奈米微粒，本研究模擬之微粒收集效率與 Huang and Chen (2002) 的實驗數據比對結果發現，模擬值與實驗值吻合(氣膠流量: 100 L/min, 施加電壓: -15.5~-21.5 kV)。進一步比對模擬的收集效率值與濕式靜電集塵器(Lin et al. 2010)的收集效率實驗值結果發現，模擬值與集塵器對單徑分佈、粒徑為 10 及 50 nm 的食鹽微粒及多徑分佈、粒徑分佈範圍為 5.23-107.5 nm 之銀微粒的去除效率實驗值相符(氣膠流量: 5 L/min, 施加電壓: +3.6~+4.3 kV)。

本單極電極線-平板型濕式靜電集塵器在高濃度粉塵負荷下可有效的去除細微粒及奈米微粒。預期本濕式靜電集塵器可作為高效率微粒去除設備及奈米微粒採樣器。本研究建立的數值模式可用於設計大型的單極平板濕式靜電集塵器，以解決傳統乾式靜電集塵器在實際操作上所面臨的問題。

A Wire-in-Plate Wet Electrostatic Precipitator for Controlling Fine and Nanosized Particle Emission

Student: Guan-Yu Lin

Adviser: Dr. Chuen-Jinn Tsai

Institute of Environmental Engineering

National Chiao Tung University

ABSTRACT

In this study, an efficient parallel-plate single-stage wet electrostatic precipitator (wet ESP) with a width of 75 mm, effective precipitation length of 48 mm and gap of 9.0 mm was designed and tested to control fine and nanosized particles without the need of rapping. The collection plates are made of sand-blasted copper plates coated with TiO₂ nanopowder instead of hydrophilic membranes. Three gold wires (diameter: 100 μm) were used as the discharge electrodes and a pulse jet valve was used to regularly purge the wires. The design of the present wet ESP is aimed at solving the problems of traditional dry ESPs: reduction of the collection efficiency due to particle deposition on the discharge electrodes and collection electrodes, back corona, and particle re-entrainment. The collection efficiency at initially clean and heavy particle loading conditions was tested and compared to a similar dry ESP.

Experimental results showed that when the wet ESP was initially clean, the particle collection efficiency ranged from 96.9-99.7% for particles ranging from 16.8 to 615 nm in electrical mobility diameter at an aerosol flow rate of 5 L/min (residence time of 0.39 sec) and an applied voltage of 4.3 kV. After heavy loading with TiO₂ nanopowder about 1.2±0.06 g/plate, the collection efficiency of the present wet ESP for corn oil particles was shown to

reduce only slightly to 94.7-99.0 % for particles from 16.8 to 615 nm in diameter.

In order to predict collection efficiency for particles with $0.1 \leq d_p \leq 10 \mu\text{m}$, a numerical model based on Lagrangian method was developed. The equation of particle charging and particle motion were solved by using the fourth order Runge-Kutta integration to obtain particle charges and trajectory. The simulated particle collection efficiencies based on Lagrangian method were shown to agree reasonably with the experimental data in Huang and Chen (2002) and Chang and Bai (1999) with deviation of 0.68-14.57 % and 1.49-12.46 %, respectively. This model, which can't be used to predict partial charging effect on nanoparticle collection efficiency, is appropriate to be used to predict collection efficiency of ESPs for particles with $d_p \geq 100 \text{ nm}$

In order to predict nanoparticle ($d_p \leq 100 \text{ nm}$) collection efficiency in single-stage wire-in-plate ESPs accurately, the electric field, the ion concentration distribution, and the particle charge were obtained by a 2-D numerical model based on the Eulerian method. Laminar flow field was solved by using the Semi-Implicit Method for Pressure-Linked Equation (SIMPLER Method), while electric field strength and ion concentration distribution were solved based on Poisson and convection-diffusion equations, respectively. The charged particle concentration distribution and the particle collection efficiency were calculated based on the convection-diffusion equation with particle charging calculated by Fuchs diffusion charging theory.

The simulated collection efficiencies of 6-100 nm nanoparticles were compared with the experimental data of Huang and Chen (2002) for a wire-in-plate dry ESP (aerosol flow rate: 100 L/min, applied voltage: -15.5~-21.5 kV). Good agreement was obtained. The simulated particle collection efficiencies were further shown to agree with the experimental data obtained in the study for a wire-in-plate wet ESP (Lin et al. 2010) (aerosol flow rate: 5 L/min, applied voltage: +3.6~+4.3 kV) using monodisperse NaCl particles of 10 and 50 nm in diameter, and polydisperse Ag particles of 5.23-107.5 nm in diameter.

The present single-stage wire-in-plate wet ESP was found to remove fine and nanosized particle effectively under heavy loading conditions. It is expected that the present wet ESP could be used as efficient particle removal equipment or a nanoparticle sampler. The present model could facilitate the design and scale-up of the single-stage wire-in-plate wet ESP to control fine and nanosized particles without the typical problems associated with dry ESPs.

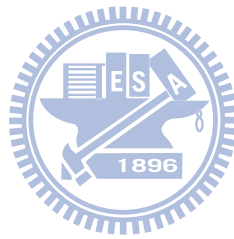
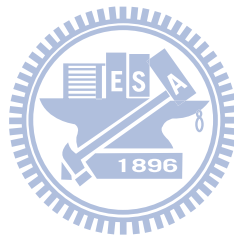


TABLE OF CONTENTS

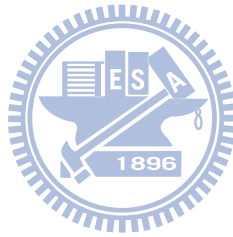
摘要.....	I
ABSTRACT	III
TABLE OF CONTENTS	VI
LIST OF TABLES	VIII
LIST OF FIGURES	IX
LIST OF SYMBOLS	XII
CHAPTER 1 INTRODUCTION.....	1
1.1 Motivation	1
1.2 Objective.....	2
1.3 Content of this thesis	3
CHAPTER 2 LITERATURE REVIEW.....	5
2.1 Experimental studies on wet ESPs for particle control	5
2.2 Numerical model for predicting collection efficiency of ESPs	7
CHAPTER 3 METHODS	16
3.1 Experimental method	16
3.1.1 The present parallel-plate wet ESP	16
3.1.2 Particle collection efficiency experiment and loading test.....	22
3.2 Numerical method	28
3.2.1 Flow field.....	28
3.2.2 Electric field and ion concentration distribution	29
3.2.3 Particle collection efficiency based on Eulerian method.....	33
3.2.4 Particle collection efficiency based on Lagrangian method	36
3.2.4 Turbulent flow field in a pilot scale wet ESP	38
CHAPTER 4 RESULTS AND DISCUSSION	40
4.1 Experimental results for the particle collection efficiency of the wet ESP.....	40
4.1.1 Flow rate, uniformity and thickness of the water film.....	40
4.1.2 Particle collection efficiency of the wet ESP at different aerosol flow rates and applied voltages	41
4.1.3 Particle loading test	49
4.2 Numerical results based on Lagrangian method for the nanoparticle collection efficiency of ESPs	54
4.2.1 Particle charging and particle trajectory in the ESP.....	54
4.2.2 Comparing the particle collection efficiency in the dry ESP of Huang and Chen (2002) and Chang and Bai (1999)	58
4.3 Numerical results based on Eulerian method for the nanoparticle collection efficiency of ESPs.....	62
4.3.1 Characteristics of the V-I curve, electric field and ion concentration	

<i>distribution</i>	62
4.3.2 <i>Comparing the particle collection efficiency in the dry ESP of Huang and Chen (2002)</i>	69
4.3.3 <i>Comparing the particle collection efficiency in the present wet ESP</i>	74
4.4 Numerical modeling of a pilot scale wet ESP	81
CHAPTER 5 CONCLUSIONS AND RECOMMENDATIONS	87
5.1 Conclusions	87
5.2 Recommendations	89
REFERENCES	91
VITA	97
PUBLICATION LIST	98



LIST OF TABLES

Table 2.1 Arrangement of literature reviews in experimental studies of wet ESPs.	14
Table 2.2 Arrangement of literature reviews in numerical studies of particle collection efficiencies in wire-in-plate ESPs.	15
Table 3.1 Characteristics of the test particles	25
Table 4.1 Comparison of different models for particle charging by field, diffusion, and combined charging.	55
Table 4.2 Ion molecular weight, ion mobility, and the corresponding ion diffusion coefficient used in previous researches.	64
Table 4.3. Combination coefficient of positive ion with 50 and 10 nm NaCl particles calculated by using different ion molecular weights shown in Table 1 based on Fuchs theory.	76
Table 4.4 Typical design parameter for ESPs (http://yosemite.epa.gov/oaqps/EOGtrain.nsf/DisplayView/SI_412A_0-5?OpenDocument).	83

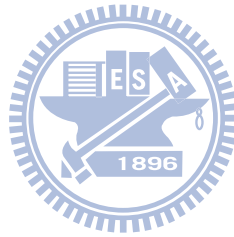


LIST OF FIGURES

Figure 3.1 Schematic diagram of the parallel-plate wet ESP. Plexiglass plates (M), enter piece (C), frosted glass plate (FG), sand-blasted copper plate (G), overflowing reservoir (OR), collecting reservoir (CR), golden wire (GW), liquid inlet (LI), liquid outlet (LO), aerosol inlet (AI), aerosol outlet (AO), pulse jet valve (PJ), air hole (AH).....	17
Figure 3.2 SEM image of micromorphological characteristic of the frosted copper plate coated with TiO ₂ nanopowder. (a) X 70,000, (b) X 100,000.	20
Figure 3.3 Water contact angle on three copper plate surfaces. (a) smooth surface, (b) sand-blasted surface, and (c) sand-blasted surface coated with TiO ₂ nanopowder.	21
Figure 3.4 Experimental setup for particle collection efficiency and particle loading tests.	26
Figure 3.5 Experimental setup for monodisperse NaCl particle collection efficiency.....	27
Figure 3.6 Calculation domain (a) the single-stage wire-in-plate dry ESP (Huang and Cheng 2002), (b) the single-stage wire-in-plate wet ESP (Lin et al. 2010). (unit: m).....	32
Figure 4.1 Corona current as a function of applied voltage in the dry and wet ESPs.	42
Figure 4.2 Collection efficiency of the present wet ESP for corn oil particles at the aerosol flow rate 5 and 10 L/min and the applied voltage of 4.3 kV. Each test was repeated 6 times.	43
Figure 4.3 Collection efficiency of the present wet ESP for corn oil particles under different applied voltages. The aerosol flow rate is fixed at 5 L/min. Each test was repeated 6 times.	46
Figure 4.4 Collection efficiency of the present wet ESP for corn oil particles under different applied voltages. The aerosol flow rate is fixed at 10 L/min. Each test was repeated 6 times.	47
Figure 4.5 Electrostatic precipitation and diffusive deposition efficiencies of the polydisperse corn oil particles in the present wet ESP when the aerosol flow rate and the applied voltage are 5 L/min and 4.3 kV, respectively. Each test was repeated 6 times.	48
Figure 4.6 Collection efficiency for corn oil particles in the dry ESP at different TiO ₂ nanopowder loadings. The applied voltage and aerosol flow rate are 4.3 kV and 5 L/min, respectively.	51
Figure 4.7 Particle reentrainment test in dry ESPs. The aerosol flow rate and applied voltage were 5 L/min and 4.3 kV.	52
Figure 4.8 Collection efficiency for corn oil particles in the wet ESP at different TiO ₂ nanopowder loadings. The applied voltage and aerosol flow rate are 4.3 kV and 5 L/min, respectively.	53
Figure 4.9 Comparison of the simulated particle trajectory between the present numerical results and those in Goo and Lee (1997) (Line: the present numerical results;	

open symbol: the numerical results in Goo and Lee (1997)).	56
Figure 4.10 Comparison of the simulated particle charging between the present numerical results and those in Goo and Lee (1997) (Line: the present numerical results; open symbol: the numerical results in Goo and Lee (1997)).	57
Figure 4.11 Comparison of particle collection efficiency in the single-stage wire-in-plate dry ESP between numerical results and experimental data in Huang and Chen (2002) at the aerosol flow rate of 100 L/min.	60
Figure 4.12 Comparison of particle collection efficiency in the single-stage wire-in-plate dry ESP between numerical results and experimental data in Chang and Bai (1999) at an aerosol flow rate of 109 L/min and an applied voltage of 27.0 kV.	61
Figure 4.13 Comparison of Corona current as a function of applied voltage between theoretical results and experimental data in the ESP.	65
Figure 4.14 Comparison of electric field strength and ion concentration distribution between numerical results and analytical solutions in a wire-in-tube ESP for (a) positive ions, and (b) negative ions.	66
Figure 4.15 Electric potential distribution at the applied voltage of +3.7 kV in the wet ESP. (Note: The scale in y direction is magnified 4.5 times relative to that in x direction.)	67
Figure 4.16 Ion concentration distribution at the applied voltage of +3.7 kV in the wet ESP. (Note: The scale in y direction is magnified 4.5 times relative to that in x direction.)	68
Figure 4.17 Comparison of particle collection efficiency in the single-stage wire-in-plate dry ESP between numerical results and experimental data in Huang and Chen (2002) at the aerosol flow rate of 100 L/min.	72
Figure 4.18 Number concentration distribution of 6 nm particles carrying 0 and 1 charges in the single-stage wire-in-plate dry ESP (Huang and Chen 2002) when the applied voltage and air flow rate was -15.5 kV and 100 L/min, respectively. (a) 0 charge, (b) 1 charge.	73
Figure 4.19 Comparison of particle collection efficiency in the single-stage wire-in-plate wet ESP between numerical results and experimental data at the air flow rate of 5 L/min.	77
Figure 4.20 Number concentration distribution of 50 nm particles carrying 0-4 charges in the single-stage wire-in-plate wet ESP when the applied voltage and air flow rate was +3.7 kV and 5 L/min, respectively. (a) 0 charge, (b) 1 charge, (c) 4 charges. (Note: The scale in y direction is magnified 4.5 times relative to that in x direction.)	78
Figure 4.21 Collection efficiencies of the polydisperse silver particles in the present wet ESP when the aerosol flow rate and the applied voltage are 5 L/min and	

	+3.7-+3.9kV, respectively. Each test was repeated 6 times.	80
Figure 4.22	Turbulent flow field in the simulated pilot scale wet ESP, (a) simulated result calculated by using SIMPLER algorithm (Patankar 1980), and using (b) the CFD commercial code, Star CCM.....	84
Figure 4.23	Collection efficiencies of particles in the pilot scale wet ESP under different design parameters. The applied voltage was 70 kV.	85
Figure 4.24	Comparison of the collection efficiency for particles with $5 \leq d_p \leq 100$ nm in ESPs which have 3, 6, or 9 discharge wires (diameter=2.5 mm). (a) The ESPs have 3 and 6 wires, (b) The ESP have 6 and 9 wires.	86



LIST OF SYMBOLS

A	total collection area (m^2)	
a	radius of particles (m)	
C_c	Cunningham slip correction factor	
C_D	empirical drag coefficient	
$C_{in}(d_p)$	particle inlet concentration (cm^{-3})	
$C_{out}(d_p)$	outlet concentration (cm^{-3}) for particle of diameter d_p	
\bar{c}_i	mean thermal speed of the ions (m/s)	
d_p	particle diameter (nm)	
D_0	turbulent dispersion coefficient within the turbulent core of the flow (m^2/s)	
D_H	hydraulic diameter (m)	
D_i	diffusion coefficient of ions (m^2/s)	
D_B	Brownian diffusion coefficient of particles (m^2/s)	
D_{eddy}	Eddy diffusivity of a particle (m^2/s)	
E	electric field strength (V/m)	
E_c	corona initiating electric field (V/m)	
E_{ave}	average electric field strength (V/m)	
E_x	electric field strength in x direction (V/m)	
E_y	electric field strength in y direction (V/m)	
e	elementary electrical charge	1.6×10^{-19}
f	wire roughness factor	
f_r	friction factor	
G_{IN}	first iterate correction to the flux	0.26.
h	distance from the wall to the interface between the region of a linearly increasing dispersion coefficient and that of a constant dispersion coefficient (m)	
I	total current per discharge wire (A)	
J_p	average current density at the collection plate (A/m^2)	
K_E	constant of proportionality	
Kn	Knudsen number	
k	turbulent kinetic energy (J/s-kg)	
k^c	constant	0.4~0.6
k_b	Boltzmann constant J/K	1.38×10^{-23}
l	wire length (m)	
l_c	length of collection electrode (m)	

M_i	molecular weights of ions (kg/mol)	
M_{air}	molecular weights of air (kg/mol)	
N_a	Avogadro number 1/mol	6.023×10^{23}
N_i	ion number concentration (m^{-3})	
$N_{p,q}$	concentration of particles carrying q elementary charges (m^{-3})	
$N_{p,0,total}(y)$	inlet uncharged particle number concentration (m^{-3})	
$N_{p,q,outlet}(y)$	outlet number concentration of particles carrying q elementary charges (m^{-3})	
P_0	pressure (atm)	1 (atm)
Q	air flow rate (m/s)	
q	number of charges carried by particles	
q_{sat}	saturation charge (C)	
r	distance between particles and ions center (m)	
r_a	apsidal distance (m)	
Re	Reynolds number based on the hydraulic diameter	
Re_p	particle Reynolds number	
r_{eff}	equivalent cylinder radius (m)	
r_c	wire radius (m)	
S_c	generation of particles with $q-1$ charges.	
s_x	half wire to wire spacing (m)	
s_y	wire to plate spacing (m)	
T	temperature (K)	
T_0	temperature (K)	293 (K)
u	air velocity in x direction (m/s)	
u^*	velocity distribution of a fully developed turbulent flow (m/s)	
u_{ave}	average air velocity (m/s)	
u_p	particle velocity in x direction (m/s)	
v	air velocity in y direction (m/s)	
v_p	particle velocity in y direction (m/s)	
V	potential (Volt)	
V_0	applied voltage (kV)	3.6-4.3
V_c	corona onset voltage (V)	
V_{TE}	particle migration velocity (m/s)	
$V_{TE,k}$	average migration velocity of particles (m)	
W_{loaded}	quantity of particles in the ESP per plate (g)	
W_{out}	particles that penetrated through the ESP (g)	

W_{total}	total particle dispersed by the Jet-O-Mizer (g)	
W_{ex}	particles in the excess flow (g)	
Z_i	ion mobility ($m^2/s-V$)	
Z_p	particle electrical mobility ($m^2/s-V$)	
α_q	combination coefficient of ions for particles carrying q elementary charges (m^3/s)	
$\eta_{total}(d_p)$	particle collection efficiency of the wet ESP	
λ_{ion}	mean free path of ions (nm)	
δ	relative density of air	
δ_r	radius of the limiting sphere (m)	
ρ_{air}	air density (kg/m^3)	
ρ_c	ion density at the boundary of the ionized sheath ($A \cdot sec/m^3$)	
ρ_i	space charge density (C/m^3)	
κ_d	dielectric constant of particle (salt)	6.2
ε	turbulent dissipation rate ($J/s\text{-kg}$)	
ε_0	permittivity of free air (F/m)	8.85×10^{-12}
ξ	striking probability	
ξ_p	turbulent dispersion coefficient within the turbulent core of the flow (m^2/s)	
ϕ	electrostatic potential between the particle and the ion	
μ_{air}	viscosity ($kg/m\text{-s}$)	
μ_t	turbulent viscosity ($kg/m\text{-s}$)	

CHAPTER 1

INTRODUCTION

1.1 Motivation

In recent year, the applications of nanomaterials are increasing rapidly in many industries including textile, optics, electronics, medical devices, biosensors, and environmental remediation (Smith et al. 2007). During manufacturing and shipping of nanomaterials, nanoparticles could be released into environment posing adverse effects on aquatic species and human health (Griffitt et al. 2007; Oberdörster et al. 2005). Thus, efficient control of nanoparticle emissions effectively has become an important research topic.

Electrostatic precipitators (ESPs), including dry and wet types, have been widely used to remove particles emitted from various industrial processes. ESPs are capable of handling large flow rates of exhaust gas with low electrical power consumption because of its low pressure drop through the collection chamber (USEPA 1999). When particles are introduced into a single-stage ESP, they are charged by diffusion and field charging mechanisms and are collected by electrostatic forces on the collection electrodes (Hinds 1999). In a well-designed dry ESP, the collection efficiency for micron and submicron particles can reach up to 95% as shown in several experimental (Huang and Chen 2002; Marek et al. 2005) and numerical studies (Oglesby and Nichols 1978; Yoo et al. 1997; Goo and Lee 1997). However, aerosol penetration was found to increase with increasing operation time due to the deposition of particles on both the discharge wires and collection electrodes. Huang and Chen (2003) constructed a laboratory-scale, single-stage, wire-plate dry ESP to investigate the loading effect of particles on the collection efficiency. Their results showed that the aerosol penetration for fine cement particles of 0-600 nm in diameter increased after 120 min of particle loading due to the reduction of the ion current. The maximum penetration increase of

4 % (from 3.5 to 7.5 %) occurred at 300 nm. In addition to the decrease in collection efficiency from the accumulated dust cake, back corona also reduced the efficiency by decreasing the particle charging ratio and migration velocity (Chang and Bai 1999). Furthermore, dry ESPs can not be used to control sticky or oily particles, which are difficult to remove from the collection electrodes by rapping (Altman et al. 2001).

The objective of this study was to develop a wire-in-plate single-stage wet ESP to enhance the collection efficiency of fine and nanosized particles. The design of the present wet ESP was aimed at solving the problems of the traditional dry ESPs: reduction of the collection efficiency due to particle deposition on the discharge electrodes and collection electrodes, back corona, and particle re-entrainment.

1.2 Objective

Wet ESPs have been developed to solve the problems associated with the traditional dry ESPs. Previous works on particle collection efficiency of wet ESPs include the experimental studies of Lungren et al. (1995), Kim et al. (2000), Pasic et al. (2001), Bayless et al. (2004) and Saiyasitpanich et al. (2006; 2007). However, most of the researchers focused on investigation of collection efficiency for particles with diameter (d_p) of 0.1-10 μm . The nanoparticle collection efficiency after heavy particle loading is still rarely discussed. Moreover, in order to enhance the uniformity of the water film on the collection electrode surfaces, high scrubbing water flow rate was used in previous researches (Lungren et al. 1995; Saiyasitpanich et al. 2006, 2007), which resulted in thick water film and would reduce the strength of the electric field because of the resistivity of water. Thus, hydrophilicity of the collection plate surfaces should be increased to diminish the scrubbing water flow rate used in wet ESPs.

To predict particle collection efficiency in ESPs, many researchers developed numerical model including Goo and Lee (1997), Yoo et al. (1997), Park and Kim (2000; 2003), Park and

Chun (2002), Talaie (2001; 2005) and Li and Christofides (2006). However, previous numerical model was found to over-predict the collection efficiency for particles with $d_p \leq 100$ nm. This is because charging models were not adopted appropriately to calculate particle charges. Besides, no researchers have ever developed a numerical model to predict nanoparticle collection efficiency accurately in the wet ESP. That is, an accurate numerical model which can be used to facilitate design of an efficient wet ESP for nanoparticle control needs to be developed.

The objectives of this study are summarized below:

1. To use both numerical and experimental methods to investigate the collection efficiencies of fine and nanosized particles in the single-stage wire-in-plate wet ESP and determine the optimum operation conditions.
2. To conduct collection efficiency by using high concentration of TiO₂ nanopowder to examine heavy particle loading effect on collection efficiency of both dry and wet ESP.
3. To compare numerical particle collection efficiencies calculated by using the Lagrangian and Eulerian methods with experimental data and determine the applicability of each method for predicting the particle collection efficiency.

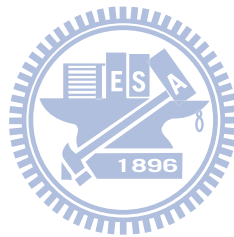
1.3 Content of this thesis

In chapter 2, previous experimental studies on wet ESPs for particle control are reviewed. The numerical models for predicting particle collection efficiency based on the Lagrangian and the Eulerian methods in ESPs are also discussed.

In chapter 3, the method to increase the hydrophilicity of the collection plates is introduced. Then the experimental methods for particle collection efficiency in the present wet ESP under initial clean and heavy loading conditions are presented. Next is the description of numerical methods for predicting the flow field, the electric field strength, and the ion concentration distribution. Charging models for predicting particle charges in the

transition and continuum regimes are described. Finally, the methods to solve charged particle concentration distribution and particle trajectory are presented.

In chapter 4, particle collection efficiency in the present wet ESP under initial clean and different operation conditions are discussed. Then the heavy particle loading effect on particle collection efficiency in the present wet ESP is compared with that of the dry ESP experimentally. Subsequently, the numerical results based on Lagrangian and Eulerian methods are compared with the experimental data published in the previous researches (Chang and Bai 1999; Huang and Chen 2002) and obtained for the present wet ESP. Finally, the numerical results for the parametric study of a pilot scale wet ESP are presented. In chapter 5, conclusions of this thesis are drawn and future work is recommended.



CHAPTER 2

LITERATURE REVIEW

2.1 Experimental studies on wet ESPs for particle control

Wet ESPs have been developed to control a wider variety of particulate pollutants and exhaust gas conditions compared to dry ESPs, especially for particles that are sticky, corrosive, or have high resistivity (Altman et al. 2001a; Altman et al. 2001b). The periodic or continuous scrubbing water flow, used to wash the collection electrode surfaces, was found to prevent particle re-entrainment caused by rapping, which occurs in dry ESPs (USEPA 2003). The traditional methods to distribute water uniformly on the collection plate surfaces include vapor condensation or spraying (Altman et al., 2001b; Bayless et al., 2004). In the vapor condensation method, moisture in the gas condenses to form water film on the collection plate surfaces due to the temperature differential between the cold surface and the hot gas. In the spraying method, water droplet is emitted by nozzles at the top or bottom of ESPs to wash the collection plates. However, aqueous mist used in these two methods will result in sparkover to reduce electric field strength and particle collection efficiency (Bayless et al. 2004).

Lungren et al. (1995) invented a wire-in-tube wet ESP in which the charging electrode consisted of a tapered section, a rod and four discs to enhance particles charging efficiency. Scrubbing water was first introduced onto a diamond-shaped plate, which was used to equalize the water flow, and then flowed into the inner surface of the collection electrode to remove the collected particles. They found that the opacity of the flue gas was reduced from 35 to 0 % in the pilot unit when the applied voltage was increased from 30 to 75 kV. However, the collection efficiency for different particle diameters and particle loadings was not discussed. Similar types of wire-in-tube wet ESPs were used to control the emissions of incinerator flue gas (Kim et al. 2000) and diesel particulate matter (Saiyasitpanich et al. 2006; Saiyasitpanich et al. 2007). The collection efficiency of particle mass of the wet ESP for

10-1000 nm diesel particles was measured to be from 92 to 69 % when the gas velocity was from 1.38 to and 5.61 m/s (or the corresponding residence time from 0.4 to 0.1 sec) (Saiyasitpanich et al. 2007), respectively.

However, the collection efficiency under heavy particle loading conditions for long time periods was not studied. Moreover, the previous study used a high flow rate of scrubbing water (4.44-6.22 L/min/m² of collection area), which resulted in a thick water film, thus decreasing the electric field strength due to water's resistivity.

To improve the uniformity of the liquid film over the collection electrodes without having to supply the scrubbing water at high flow rate, Pasic et al. (2001) invented a membrane electrostatic precipitator which used hydrophilic membranes made of corrosion resistant woven fibers as the collection electrodes. The tensile apparatuses were needed to stretch the membranes during operation of the wet ESP to prevent channeling effect due to uneven surfaces. In the bench scale test, Bayless et al. (2004) compared the membrane-based and steel plate wet ESPs for the collection efficiency of fly ash, iron oxide and calcium carbonate having particle sizes of 20-25, 1-5 and 2-3 μm in diameter, respectively. The collection efficiency of the membrane-based wet ESP was found to be higher than the steel plate wet ESP. In the pilot scale test, the membrane wet ESP was used to remove iron-oxide particles with the peak gas velocity of 4 m/s or the corresponding residence time of 1.9 sec. The collection efficiency of particle mass was approximately 96 % for particles from 1 to 5 μm in diameter. However, the collection efficiency of submicron particles under heavy particle loading conditions was not discussed. In addition, membranes may be expensive and not all have uniform wetting and corrosion-resistant properties, which must be carefully determined for optimal use in specific field applications (Bayless et al. 2004).

2.2 Numerical model for predicting collection efficiency of ESPs

In ESPs, particles are collected by electrostatic forces, and thus the electric field strength and particle charge are very important factors influencing the collection efficiency of ESPs. The conventional theory used to predict particle collection efficiency is based on the Deutsch-Anderson equation, which is shown as follows:

$$\eta = 1 - \exp\left(\frac{-V_{TE} A}{Q}\right) \quad (2.1)$$

$$V_{TE} = \frac{qeE_{ave} C_c}{3\pi\mu_{air} d_p} \quad (2.2)$$

where V_{TE} is particle migration velocity (m/s), A is the total collection area (m²), Q is the air flow rate (m³/s), q is the number of elementary units of charge, e is the elementary electrical charge (1.6×10^{-19} C), E_{ave} is the average electric field strength (V/m), C_c is the Cunningham slip correction factor, μ_{air} is the viscosity (kg/m-s), and d_p is the particle diameter (m). In order to predict collection efficiency more accurately, Matt and Ohnfeldt (1964) and White (1982) presented a modified Deutsch-Anderson equation as follows:

$$\eta = 1 - \exp\left(\frac{-V_{TE,k} A}{Q}\right)^{k^c} \quad (2.3)$$

where $V_{TE,k}$ is the average migration velocity of particles (m), k^c is a constant (0.4~0.6). The above semi-empirical equations can not predict collection efficiency precisely because the following assumptions were made: (1) Particles are assumed to reach their saturation charge during the collection process. (2) Particles migration velocity is not affected by air velocity and nonuniform distribution of the electric field. (3) The effects of particle reentrainment,

uneven gas flow distribution, and back corona on collection efficiency are not taken into consideration.

Many researchers developed numerical models based on charging model for continuum regime ($Kn=2\lambda_i/d_p \ll 1$, λ_i : mean free path of ions, d_p : particle diameter) to predict collection efficiency of the wire-in-plate dry ESPs for particles ranging from 0.3-10 μm in diameter. Good agreement between experimental data and numerical results was obtained (Goo and Lee 1997; Park and Kim 2000, 2003; Park and Chun 2002; Talaie 2001, 2005). For example, a numerical model based on Lagrangian method with turbulent electrohydrodynamic (EHD) flow field was developed to predict particle collection efficiency and further validated with experimental data of Kihm (1987) (Goo and Lee 1997). The particle charging rate was calculated by using combined charging model of Fuchs model (1947) for diffusion charging and Pauthenier and Moreau-Hanot's model (1932) for field charging (The combined charging model shown in section 3.2.4 was also used in the present study to predict the charge for particles with $d_p \geq 100$ nm). The calculated results were found to be lower than the experimental data at the applied voltage of 6.5~13 kV for 4 μm particles. The deviation between the calculated values and the experimental data is probably due to the difficulty in estimating exact charging properties of particles, the inlet conditions of flow and particles, and the experimental error.

The effects of the EHD flow and turbulent diffusion on the collection efficiency of particles in a wire-cavity plate dry ESP was further studied by using a numerical model based on Eulerian method (Park and Kim, 2000; 2003). Particle charges were obtained by solving White's equation (1967), which is given by

$$q_{white} e = \frac{3\kappa_d}{1 + \kappa_d} \pi \varepsilon_0 d_p^2 E_{ave} \quad (2.4)$$

where κ_d is the dielectric constant of particles, ε_0 is the permittivity of free air (F/m). Good agreement between experimental and computational data of collection efficiency was obtained for 4.5 μm Al_2O_3 particles when the applied voltage and air velocity were 7.5~15 kV and 0.5~1 m/s, respectively.

Park and Chun (2002) developed a numerical model to investigate the effect of turbulent dispersion on particle collection efficiency without considering the nonuniform distribution of electric field and ion concentration in a wire-in-plate dry ESP. The eddy diffusivity of a particle is given as follows:

$$D_{eddy} = \xi_p \frac{y}{h}, 0 \leq y \leq h \quad (2.5)$$

$$D_{eddy} = \xi_p, h \leq y \leq s_y \quad (2.6)$$

$$\xi_p = 0.4u^* h \quad (2.7)$$

$$h = 0.1s_y \quad (\text{Oron et al., 1988}) \quad (2.8)$$

where ξ_p is the turbulent dispersion coefficient within the turbulent core of the flow (m^2/s), h is the distance from the wall to the interface between the region of a linearly increasing dispersion coefficient and that of a constant dispersion coefficient (m), s_y is the wire to plate spacing (m), u^* is the velocity distribution of a fully developed turbulent flow (m/s), which is defined as

$$u^* = \sqrt{8f_r u_{ave}^2} \quad (2.9)$$



where u_{ave} is the average air velocity (m/s), f_r is the friction factor, which is given by

$$f = 0.0791Re^{-0.25} \quad (2800 < Re < 10^5) \quad (2.10)$$

where Re is the Reynolds number based on the hydraulic diameter as follows:

$$Re = \frac{\rho_{air} u_{ave} D_H}{\mu_{air}} \quad (2.11)$$

where ρ_{air} is the air density (kg/m^3), D_H is the hydraulic diameter (m). The above method for calculating turbulent dispersion coefficient of particles was adopted in the present parametric study (in turbulence flow case). To calculate particle charges, Cochet equation (1961) was used, which is given by

$$q_{Cochet} e = \left\{ \left(1 + \frac{2\lambda_i}{d_p} \right)^2 + \left(\frac{2}{1 + 2\lambda_i / d_p} \right) \left(\frac{\kappa_d - 1}{\kappa_d + 2} \right) \right\} \pi \epsilon_0 d_p^2 E_{ave} \quad (2.12)$$

The predicted collection efficiency was validated with published experimental data of Riehle and Löffler (1993) and good agreement was found for limestone particles in the size range of 0.3~10 μm at an applied voltage of 25 kV, a mean air velocity of 1 m/s, and a turbulent dispersion coefficient of 50 cm^2/s . The collection efficiency was found to increase with increasing turbulent dispersion coefficient for particles below 1 μm . For particles larger than 1 μm , the increase of turbulent dispersion coefficient led to a decrease of collection efficiency due to the effect of dispersing the particles back to the flow. The author also noted that a complete model should necessarily include a realistic particle charging model, an electrostatic

field strength distribution, and a more realistic flow field.

Except for the effect of EHD and the turbulent dispersion coefficient, the effect of polydisperse particle loading on the particle collection efficiency was also taken into consideration in Talaie et al. (2001), who developed a mathematical model based on Eulerian method to predict the collection efficiency of a double-stage wire-in-plate dry ESP. The particle charging rate was calculated by using White's equation (1967). The numerical values were in good agreement with the experimental data of Leonard (1982) for 3.5 μm oleic acid drops.

As discussed above, the numerical models for predicting collection efficiency for particles in the size range of 0.3-10 μm in wire-in-plate ESPs have been well-developed. For particles with $100 \leq d_p \leq 200$ nm, the numerical model of Yoo et al. (1997) based on Fuchs diffusion charging model (1947) and the field charging model of Pauthenier and Moreau-Hanot (1932) was able to predict the particle collection efficiency accurately. However, the combined charging model used by Yoo et al. (1997) was found to over-predict particle charge for particles with $d_p \leq 100$ nm in Lawless (1996), who concluded that 100 nm was the limit of applicability of the combined charging model.

In the transition regime ($Kn \approx 1$), Fuchs model (1963), which was used by Zhuang et al. (2000) and Li and Christofides (2006) to predict particle charge in ESPs, was shown to be accurate for particles with $d_p > 30$ nm (Adachi et al. 1985; Pui et al. 1988). However, the numerical model could not predict the experimental collection efficiency accurately for $30 < d_p < 400$ nm because the flow field and the non-uniform ion concentration distribution were not calculated in Zhuang et al. (2000). In the work of Li and Christofides (2006), non-uniform electric field and ion concentration were not considered either and simulated particle collection efficiencies were not compared with experimental data. Therefore, the applicability of the previous models (Yoo et al. 1997; Zhuang et al. 2000; Li and Christofides 2006) for $30 \leq d_p \leq 100$ nm requires further investigations.

For particles with $d_p < 30$ nm, experimental data (Huang and Chen 2002) and numerical results (Yoo et al. 1997; Zhaung et al. 2000; Li and Christofides 2006) showed that a fraction of particles was uncharged and penetrated through ESPs, resulting in decreasing collection efficiency as d_p was decreased from 30 nm to 5 nm. This is called the partial charging effect. Marlow and Brock's model (1975) was shown to provide accurate prediction of particle charge for $d_p < 30$ nm (Pui et al. 1975). However, Marlow and Brock's model has not been applied to examine the partial charging effect on the collection efficiency of the ESP. The combined charging model used in Yoo et al. (1997) over-predicted particle charge in the transition regime, as compared to the experimental data of Fjeld and MacFarland (1986), leading to an overestimation of collection efficiency for particles below 30 nm. The Fuchs model (1963) used in Zhuang et al. (2000) and Li and Christofides (2006) also over-predicted particle charge for $d_p < 30$ nm, which also led to an overestimation of the collection efficiency.

In the traditional dry ESPs, particle collection efficiency, especially for nanoparticle, decreases with increasing operation time due to particle deposition on discharge electrodes and collection electrodes (Huang and Chen 2003), back corona (Chang and Bai 1999), and particle re-entrainment (USEPA 2003). In order to solve typical problems associated with dry ESPs, wet ESPs were developed to control fine and nanoparticle effectively (Saiyasitpanich et al. 2006; Lin et al. 2010). Saiyasitpanich et al. (2006) compared measured and calculated collection efficiency by using Deutsch equation in a wire-in-tube wet ESP for particles in the size range of 20~700nm. The particle charging was calculated by solving Cochet equation (1961) and Robinson equation, which is given by

$$q_{Robinson} e = \left(\frac{3\kappa_d}{\kappa_d + 2} \right) \left(\frac{E_{ave} d_p^2}{4K_E} \right) + \frac{d_p k_b T}{2K_E e} \ln \left(1 + \frac{\pi K_E d_p \bar{c}_i e^2 N_i t}{2k_b T} \right) \quad (2.13)$$

where K_E is a constant of proportionality, \bar{c}_i is the mean thermal speed of the ions (m/s), N_i

is the ion number concentration (m^{-3}), k_b is the Boltzmann's constant ($\text{N}\cdot\text{m}/\text{K}$), and T is the temperature (K). The comparison revealed that the predicted values based on Deutsch equation underestimated the measured values.

Huang and Chen (2002) investigated aerosol penetration for particles in the size range of 7-100 nm by using a single-stage and a two-stage wire-in-plate dry ESP. A significant increase aerosol penetration was found for particles below 20 and 50 nm in the single- and two-stage dry ESP, respectively. Their experimental data could serve as a good benchmark for validating the simulation models for the nanoparticle collection efficiency in ESPs.

The above literature reviews for previous experimental and numerical studies were arranged in Table 2.1 and 2.2, respectively. In summary, according to the above discussions, an efficient wet ESP should be further designed and developed for controlling fine and nanosized particles. The optimal operation conditions for collecting nanoparticle in wet ESPs, and the collection efficiency of submicron particles under heavy particle loading conditions are needed to be investigated.

For predicting nanoparticle collection efficiency in ESPs by using numerical methods, the existing models can't predict collection efficiency very well because the electric field and ion concentration distribution were not simulated, or charging models were not adopted appropriately to calculate particle charges. Thus, a numerical model using appropriate charging model to calculate particle charges requires to be developed for predicting nanoparticle collection efficiency accurately in ESPs.

Table 2.1 Literature reviews in experimental studies of wet ESPs.

Investigator	ESP type	Particle residence time (s)	Applied voltage (kV)	Liquid flow rate (L/min/m ²)	Collection efficiency (%)
Lungren et al. (1995)	wire-in-tube wet ESP	0.9-1.9	30.0-65.0	N.A.	Opacity: 35~4
Kim et al. (2000)	wire-in-tube wet ESP	0.08-0.41	20.0	N.A.	85.7-99
Saiyasitpanich et al. (2007)	wire-in-tube wet ESP	0.1~0.4	70.0	4.44-6.22 L/min/m ²	69~92 (10-1000 nm)
Pasic et al. (2001); Bayless et al. (2004)	membrane-based wet ESP	1.9	44.0	1.68-4.57 L/min/m ²	96 (1-5 μm)

Table 2.2 Literature reviews in numerical studies of particle collection efficiencies in wire-in-plate ESPs.

Researcher	Numerical method	Particle charging model	Particle diameter	Results
Goo and Lee (1997)	Lagrangian method	combined charging model	4 μm	The calculated results were found to be lower than the experimental data.
Park and Kim (2000; 2003)	Eulerian method	White's equation	4.5 μm	Good agreement between experimental and computational data of collection efficiency was obtained.
Park and Chun	Eulerian method	Cochet equation	0.3-10 μm	The calculated collection efficiencies match with the experimental data.
Talaie et al. (2001)	Eulerian method	White's equation	3.5 μm	The numerical values were in good agreement with the experimental data.
Talaie (2005)	Lagrangian method	combined charging model	1.0-10 μm	The secondary flow and the high particle loading result in a decrease of collection efficiency.
Chang and Bai (1999)	Lagrangian method	combined charging model	0.2-10.0 μm	The simulated values match with the experimental data.
Yoo et al. (1997)	Lagrangian method	combined charging model	0.03-0.2 μm	The combined charging model is only valid for particles with $dp \geq 100 \text{ nm}$ Lawless (1996).
Zhuang et al. (2000)	Eulerian method	Fuchs model (1963)	10-100 nm	Ion concentration distribution was not simulated. Simulated collection efficiency didn't match with experimental data.
Li and Christofides (2006)	Eulerian method	Fuchs model (1963)	5-100 nm	Electric field and ion concentration distribution were not simulated. Simulated collection efficiency wasn't compared with experimental data.
Saiyasitpanich et al. (2006)	Deutsch equation	Cochet equation (1961) and Robinson equation (1971)	20-700 nm	The comparison revealed that the predicted values based on Deutsch equation underestimated the measured values.

CHAPTER 3

METHODS

3.1 Experimental method

3.1.1 *The present parallel-plate wet ESP*

The collection electrodes of the present parallel plate wet ESP were designed based the parallel-plate wet denuder in Tsai et al. (2008). As shown in Figure 3.1, the wet ESP consists of two plexiglass plates (M) on which a copper plate (G) (100 mm in length, 75 mm in width and 3.0 mm in thickness) was attached to the inner surface. A copper plate was used as collection electrode because of its high conductivity and ease with sandblasting. In order to make scrubbing water film flow uniformly on the collection electrodes (G) at low flow rates, a frosted glass plate (FG, 70 mm in length, 75 mm in width and 3.0 mm in thickness) coated with TiO₂ nanopowder (Degussa AEROXITE TiO₂ P25, Anatase, 20 nm) is attached to the inner surface (M) above the copper plate. Between the collection electrodes, a center piece (C) is sandwiched to form a 9 mm gap between the electrodes. On the center piece, three gold discharge wires (GW) (99% purity, 100 μm in diameter, Surepure Chemetals Inc.) spaced at 16 mm in the flow direction are fixed. These gold wires were used as discharge wires due to their long lifetime of more than 6 months (Asbach 2004). Two overflowing (OR) and collection reservoirs (CR) for continuous scrubbing water flow are installed at the top and bottom of the ESP, respectively. A pulse jet valve (Bag Filter Enterprise Co. Ltd., Taiwan) was used to generate pulse jet passing through 3 rows of small holes (diameter: 1.0 mm, 24 holes on each row) on the collection plates. The discharge wires were cleaned every 5 minutes with an instantaneous pressure of 2.95 atm (3.05 kg/cm²) and the instantaneous air flow rate passing through all 24 holes per wire was calculated to be 11 L/s. Pulse duration was about 0.5 sec. During pulse jet cleaning, the scrubbing water flow was stopped for two minutes to prevent sparking over due to the water mist generated by the pulse jet.

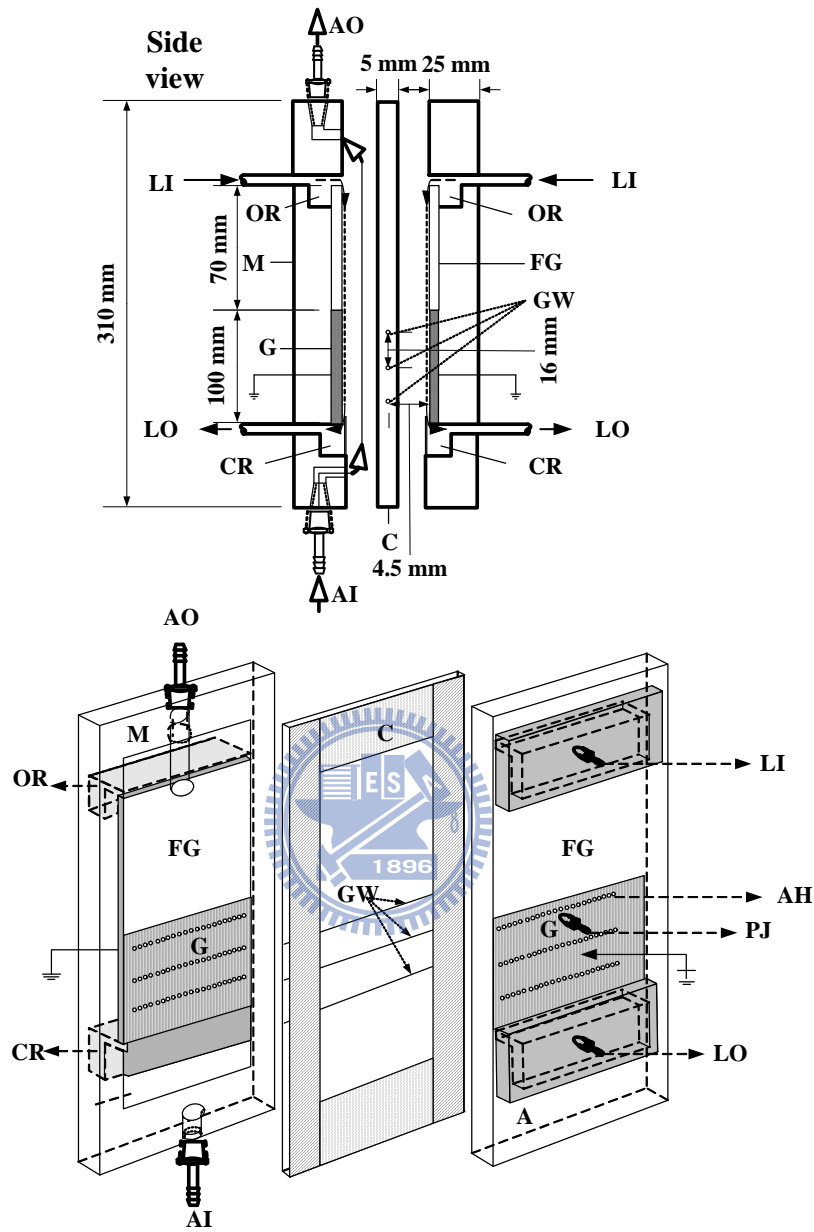


Figure 3.1 Schematic diagram of the parallel-plate wet ESP. Plexiglass plates (M), enter piece (C), frosted glass plate (FG), sand-blasted copper plate (G), overflowing reservoir (OR), collecting reservoir (CR), golden wire (GW), liquid inlet (LI), liquid outlet (LO), aerosol inlet (AI), aerosol outlet (AO), pulse jet valve (PJ), air hole (AH).

In order to increase the hydrophilicity of the collection plates, which will enhance the uniformity of the water film and reduce the scrubbing water flow rate, the copper plate surfaces were first sand blasted to an average depth of 61.0 μm and then coated with TiO_2 nanopowder (Degussa P25) based on the method described in Tsai et al. (2008). The surfaces were first sonicated with DI water (18.2 $\text{M}\Omega\text{-cm}$) and then dried by purging with compressed air. 0.5 g of TiO_2 nanopowder was well dispersed in 50 ml DI water by ultrasonication and then applied onto the sand blasted surfaces. 30 min later, the excess solution was removed, and the plates were calcinated at 300 $^\circ\text{C}$ for 90 min to facilitate thermal bonding of the TiO_2 nanopowder onto the copper plate surfaces.

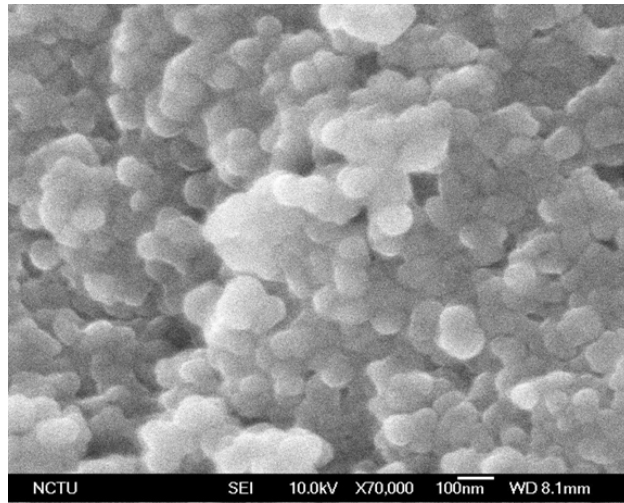
Tap water was used as the scrubbing liquid for the collection electrodes. Two peristaltic pumps (Model MP-1000, Eylea Co., Japan) were used to continuously pump water into and out of the overflow and collection reservoirs. The appropriate scrubbing water flow rate, important to water film thickness and uniformity (Tsai et al. 2008), was determined in this study. The goal was to minimize the flow rate in order to decrease the water waste and film thickness (which decreases the electric field due to water's resistivity), while also ensuring the film is uniform.

To determine the hydrophilicity of the coated surfaces, the morphology of the TiO_2 nanopowder coated on the frosted copper plate was first determined by SEM, and then the water contact angle was measured by using a Contact Angle System (FTA125, First Ten Angstroms, VA). As shown in Figure 3.2, there is a porous surface in our case which is not the same as the water-repellent leaves with epicuticular wax crystals in combination with papillose epidermal observed by Barthlott and Neinhuis (1997). When the water contact angle was measured, we found the frosted surface coated with TiO_2 nanopowder sucked in the water droplet forcing the droplet to spread out quickly. The contact angle was measured to be only $6.0\pm 4.2^\circ$, which is very small compared to $104.03\pm 1.73^\circ$ and $117.17\pm 2.83^\circ$ for the smooth copper plates and uncoated sand-blasted copper plates, respectively, as shown in Figure 3.3. It

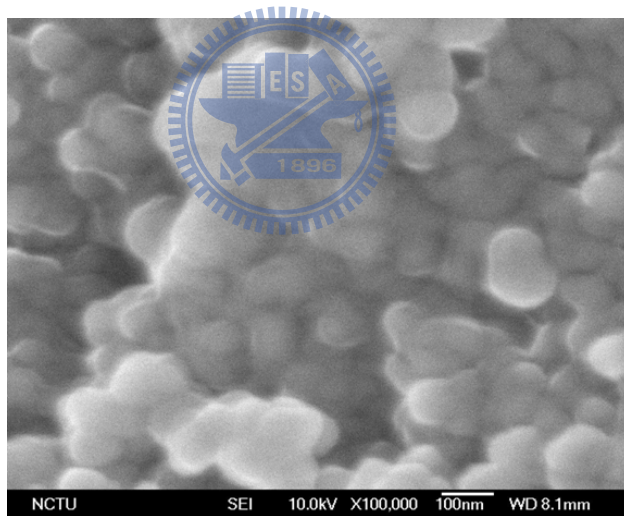
is certain that hydrophilicity can be achieved by this porous morphology to enhance the uniformity of the scrubbing water film.

Particle collection efficiency experiments were conducted at different aerosol flow rates and applied voltages under initially clean conditions to determine the optimum operation conditions. TiO_2 nanopowder was then used to create heavy loading conditions for comparing the collection efficiency of the dry and present wet ESP.



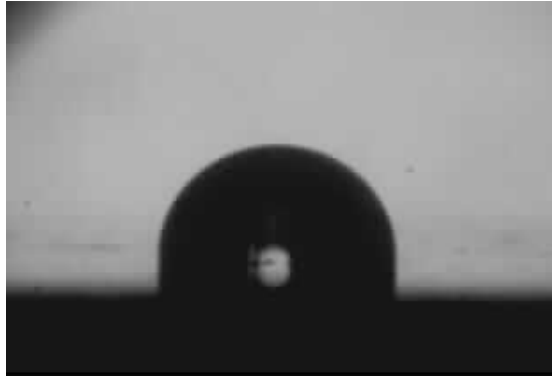


(a)

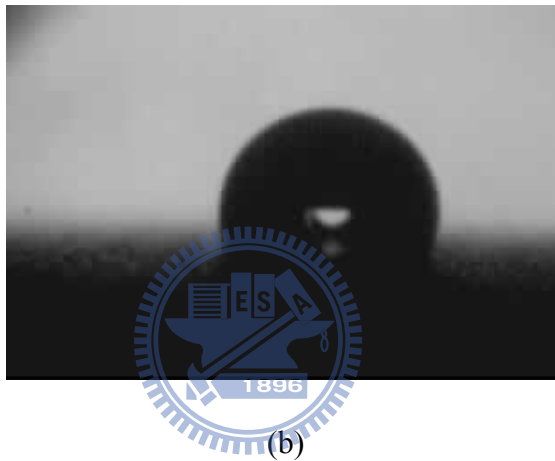


(b)

Figure 3.2 SEM image of micromorphological characteristic of the frosted copper plate coated with TiO_2 nanopowder. (a) X 70,000, (b) X 100,000.



(a)



(b)



(c)

Figure 3.3 Water contact angle on three copper plate surfaces. (a) smooth surface, (b) sand-blasted surface, and (c) sand-blasted surface coated with TiO_2 nanopowder.

3.1.2 Particle collection efficiency experiment and loading test

The particle collection efficiency experiments under initially clean conditions were conducted at aerosol flow rates of 5 and 10 L/min (corresponding to residence times of 0.39 and 0.19 seconds, respectively, over the total precipitation length of 48 mm, which is assumed to be three times the wire spacing) with applied voltages ranging from 3.8 to 4.3 kV. The experiment under each operation condition was tested for 6 to 8 hours. The experimental setup is shown in Figure 3.4. Polydisperse liquid corn oil particles (density of 0.9 g/cm³) and silver particles (density of 10.49 g/cm³) were generated by the evaporation-condensation technique (Scheibel et al. 1982) at an oven temperature of 260 and 1050 °C, respectively. Two rotameters were used to control carrier gas and cooling air flow rates to obtain the desired particle diameter and concentration. Before being introduced into the present wet ESP, all charged particles were removed using a wire-in-tube ESP allowing only zero-charged particles to enter the wet ESP. To generate an electric field and corona ions, high positive voltage was supplied to the corona wires using a high voltage D.C. power supplier (Model SL150, Spellman High Voltage Electronics Corporation, NY, USA). The voltage and corresponding corona current were read directly from the power supplier. A scanning mobility particle sizer (SMPS, model 3081, TSI Inc.) coupled with a condensation particle counter (CPC, model 3022, TSI Inc.) was used to measure the size distribution of the polydisperse particles. The characteristics and number size distribution of the test aerosols are shown in Table 3.1, respectively. The particle collection efficiency of the wet ESP, $\eta_{total}(d_p)$, was calculated by the following equation:

$$\eta_{total}(d_p)(\%) = \frac{C_{in}(d_p) - C_{out}(d_p)}{C_{in}(d_p)} \times 100\% \quad (3.1)$$

where $C_{in}(d_p)$ is the particle inlet concentration (cm⁻³) and $C_{out}(d_p)$ is the outlet concentration (cm⁻³) for particle of diameter d_p .

The particle collection efficiency experiment for monodisperse NaCl particle (particle density=2200 kg/m³) was also conducted in this study. The experimental setup is shown in Figure 3.5. Test particles were generated by the evaporation-condensation technique in an oven temperature at temperature of 650 to 700 °C. The generated particles were then passed through a nano-DMA (differential mobility analyzer, TSI Model 3085) to obtain monodisperse particles with d_p of 10 and 50 nm. The experiment was conducted at an aerosol flow rate of 5 L/min and at an applied voltage of +3.6~+4.3 kV. A condensation particle counter (CPC, model 3022, TSI Inc.) was used to measure particle number concentration. For 10 and 50 nm particles, the inlet concentration of the ESP was measured to be 1.2×10^9 (m⁻³) and 6.6×10^9 (m⁻³), respectively.

To study particle loading effect on the collection efficiency and possible particle reentrainment after particle loading, Degussa P25 TiO₂ nanopowder (resistivity of 0.75×10^6 Ω·cm) (Salah et al. 2004) was dispersed by a Jet-O-Mizer (Model 000, Fluid Energy Processing and Equipment Co., Hatfield, UK) at an aerosol flow rate of 5.67~56.62 L/min corresponding to a mass loading rate of 0.1-100 g/hr as shown in Figure 3.4. The particles that penetrated through the ESP (W_{out} , g) and the particles in the excess flow (W_{ex} , g) were measured by weighing the filters at the outlet of the wet ESP and the excess flow. After loading for two hours, the quantity of particles in the ESP per plate, W_{loaded} (g), was then calculated to be 1.2 ± 0.06 g/plate by the following equation:

$$W_{loaded} = \frac{W_{total} - W_{outlet} - W_{excess}}{2} \quad (3.2)$$

where W_{total} (g) is the total particle dispersed by the Jet-O-Mizer. In order to examine the collection efficiency of the present wet ESP for nanosized particles after 0.5~2 hr of heavy TiO₂ particle loading, corn oil particles were used instead of TiO₂ nanopowders (P25) because

very few particles below 100 nm were generated by standard dispersive technique as found in Tsai et al. (2009). A small-scale powder disperser (SSPD, model 3433, TSI Inc.) was also used to disperse the TiO₂ nanopowder for conducting the loading test (size distribution is shown in Table 3.1). However, the mass concentration was too low to generate the desired heavy loading condition. Therefore, corn oil particles generated from the evaporation-condensation technique were used to test the collection efficiency after heavy TiO₂ particle loading.

To examine possible redispersion of particles into gas stream after heavy TiO₂ nanoparticle loading in the dry ESP, a particle reentrainment test was conducted. After two hours of loading, clean air at a flow rate of 5 L/min was introduced into the dry ESP when the applied voltage was 4.3 kV. The scanning mobility particle sizer (SMPS, model 3081, TSI Inc.) was used to measure the reentrained particle size distributions at 135 second sampling interval.

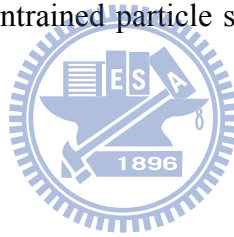


Table 3.1 Characteristics of the test particles

	Size range (nm)	CMD (nm)	GSD (nm)	Total number concentration (#/cm ³)
Corn oil, for efficiency test	16.8~615	103.18	1.64	2.38×10 ⁵
Silver, for efficiency test	5.23~107.5	12.9	1.53	7.51×10 ⁶
TiO ₂ *, for creating heavy particle condition	16.8~615	232.75	2.22	2.14×10 ⁴

* Generated by a small-scale powder disperser (SSPD, model 3433, TSI Inc.)

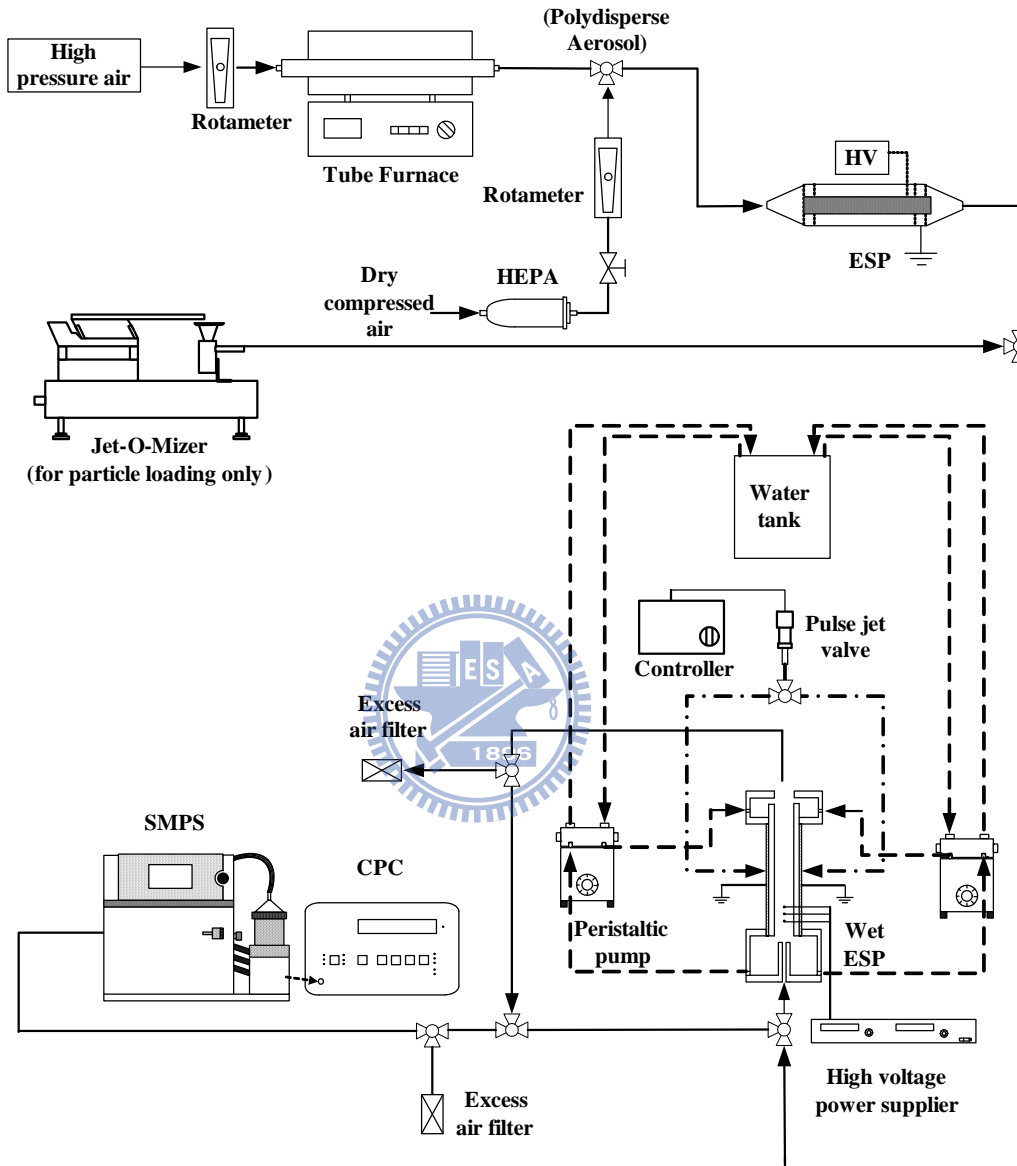


Figure 3.4 Experimental setup for particle collection efficiency and particle loading tests.

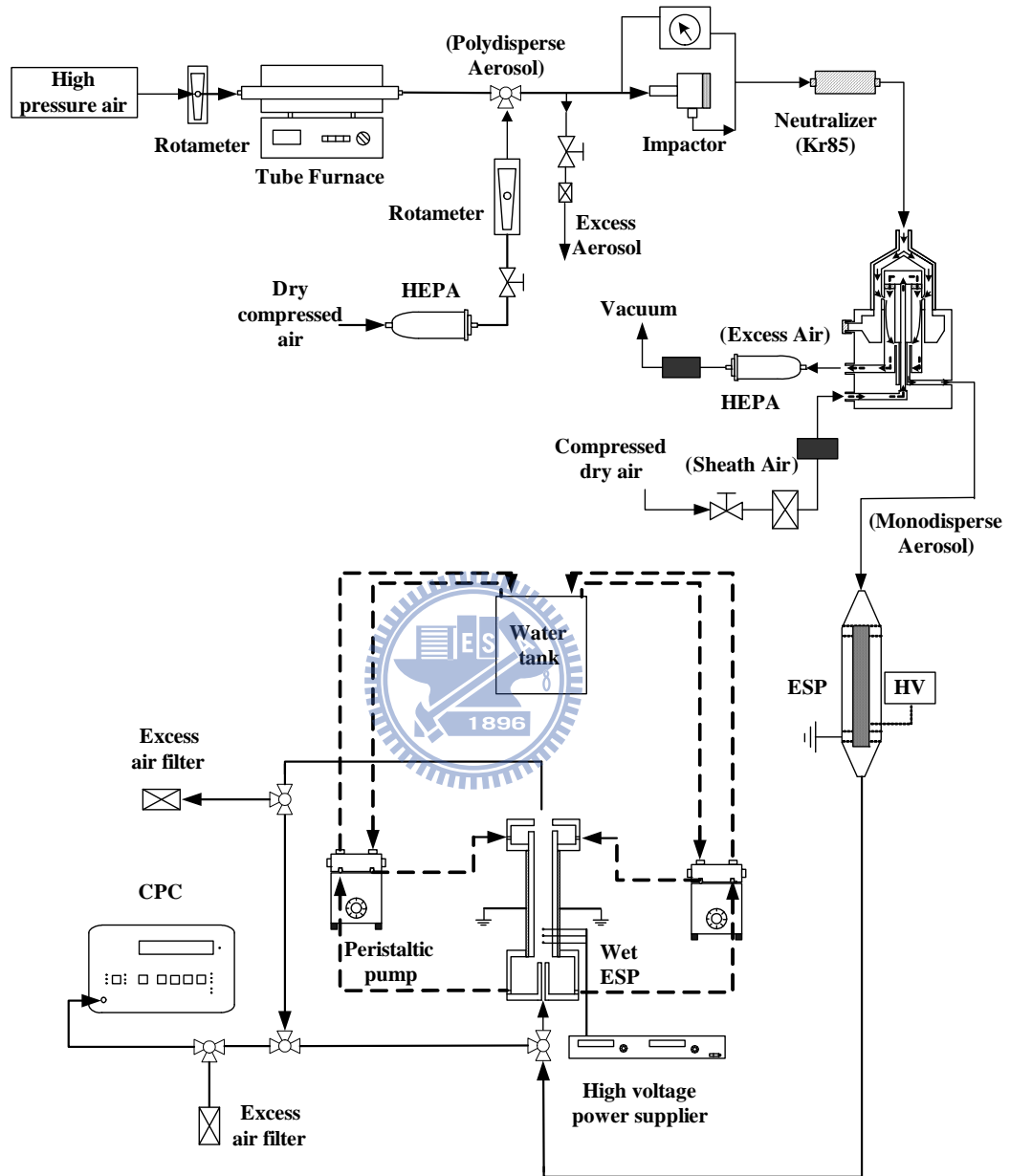


Figure 3.5 Experimental setup for monodisperse NaCl particle collection efficiency.

3.2 Numerical method

3.2.1 Flow field

The calculation domains for the dry ESP of Huang and Chen (2002) and the wet ESP (Lin et al. 2010) are shown as the hatched areas in Figures 3.6 (a) and (b), respectively. The dimensions of the present wet ESP were described in the previous experimental method section. The wire-in-plate dry ESP in Huang and Chen (2002) was 300 mm in length, 120 mm in width, and 76 mm in height. Three discharge wires had the diameter of 0.3 mm. The wire to wire spacing and wire to plate spacing was 42 and 60 mm, respectively.

A total of 19,368 (269 in x-direction, 72 in y-direction) non-uniform rectangular grids were used in each of the calculation domains. The average grid size was about 62.5 and 372 μm in x and y direction. The smallest size of 2.35 and 1.94 μm was assigned near the wall of the collection plate of the ESP in Huang and Chen (2002) and the present wet ESP, respectively. It was found that increasing the number of grids from 269 \times 72 to 269 \times 92 only resulted in a slight decreasing of particle diffusion loss from 38.5 to 37.6 % for 10 nm particles in the present wet ESP. Thus, a fixed number of grid of 269 \times 72 was used in the present simulation. The total number of iterations to reach convergence was about 10000 for solving the flow field.

The laminar flow field model was used in both cases because the flow Reynolds numbers based on the hydrodynamic diameter were 130.5 and 1124.4 in the wet ESP (Lin et al. 2010) and the dry ESP (Huang and Chen 2002), respectively, which were all smaller than 2000 (Hinds, 1999). The governing equations for the 2-D Navier-Stokes equations are

$$\rho_{air} \left(u \frac{\partial u}{\partial x} + v \frac{\partial u}{\partial y} \right) = - \frac{\partial P}{\partial x} + \mu_{air} \left(\frac{\partial^2 u}{\partial x^2} + \frac{\partial^2 u}{\partial y^2} \right) \quad (3.3)$$

$$\rho_{air} \left(u \frac{\partial v}{\partial x} + v \frac{\partial v}{\partial y} \right) = -\frac{\partial P}{\partial y} + \mu_{air} \left(\frac{\partial^2 v}{\partial x^2} + \frac{\partial^2 v}{\partial y^2} \right) \quad (3.4)$$

and the continuity equation is

$$\frac{\partial u}{\partial x} + \frac{\partial v}{\partial y} = 0 \quad (3.5)$$

where u and v (m/s) is the air velocity in x and y direction, respectively, and P is the pressure (Pa). The Navier-Stokes and continuity equations were discretized by means of the finite volume method and solved by the SIMPLER algorithm (Semi-Implicit Method for Pressure-Linked Equations) (Patankar, 1980).

3.2.2 Electric field and ion concentration distribution

The governing equation, Poisson's equation, for the electric potential distribution in the ESP was written as follows

$$\frac{\partial^2 V}{\partial x^2} + \frac{\partial^2 V}{\partial y^2} = -\frac{\rho_i}{\epsilon_0} \quad (3.6)$$

where V is the potential (Volt), ρ_i is the space charge density (C/m^3).

The space charge density ρ_i in equation (3.6) were calculated by convection-diffusion equation for ion concentration distribution as follows

$$\frac{\partial(u\rho_i + E_x Z_i \rho_i)}{\partial x} + \frac{\partial(v\rho_i + E_y Z_i \rho_i)}{\partial y} = D_i \left(\frac{\partial^2 \rho_i}{\partial x^2} + \frac{\partial^2 \rho_i}{\partial y^2} \right) \quad (3.7)$$

where D_i is the ion diffusion coefficient (m^2/s), Z_i is the ion mobility ($\text{m}^2/\text{s-V}$), E_x and E_y is the local electric field at x and y direction (Volt/m), respectively, which can be calculated as

$$-\frac{\partial V}{\partial x} = E_x \quad (3.8)$$

$$-\frac{\partial V}{\partial y} = E_y \quad (3.9)$$

Equations (3.6) and (3.7) were discretized by using the finite volume method and solved by the same computer code used in the flow field simulation. About 100000 iterations were needed to reach convergence. In equation (3.6), the sink term of the ion quenching of particles was neglected because the predicted ion concentration was much higher than the particle number concentration in this study. For example, when the applied voltage was +3.7 kV and -15.5, the average ion number concentration was calculated to be 2.26×10^{14} and 1.86×10^{14} (m^{-3}) in the dry and wet ESP, respectively, which was four orders of magnitude higher than the particle concentration. Similarly, in equation (3.7), the source term of the corona current generated by charged particles was neglected, either. To solve Equations (3.6) and (3.7), the ion density at the discharge wire surface must be calculated first as (McDonald et al. 1977)

$$\rho_{i,0} = \frac{2s_x J_p}{\pi Z_i r_c f \left[30\delta + 9\left(\frac{\delta}{r_c}\right)^{\frac{1}{2}} \right]} \times 10^{-3} \quad (3.10)$$

where s_x is the half wire to wire spacing (m), r_c is the wire radius (m), f is the wire roughness factor, δ is the relative density of air, and J_p is the average current density at the plate (A/m^2). J_p was calculated by an analytical equation (Cooperman 1981; Goo and Lee 1997) as follow

$$J_p = \frac{\varepsilon_0 Z_i}{16s_y^3} \left(\gamma + \sqrt{\gamma^2 + 192(V_0 - V_c)(s_y E_1)} \right) \quad (3.11)$$

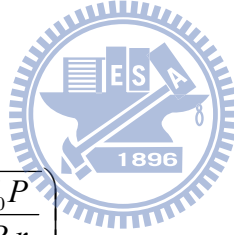
$$\gamma = 9(V_0 - V_c + s_y E_1)^2 - 12(s_y E_1)^2 \quad (3.12)$$

$$E_1 = \frac{\pi V_c}{2s_x \ln \frac{r_{eff}}{r_c}} \quad (3.13)$$

$$V_c = r_c E_c \ln \frac{r_{eff}}{r_c} \quad (3.14)$$

$$r_{eff} = \frac{4s_y}{\pi} \quad \text{for} \quad \frac{s_y}{s_x} \leq 2.0 \quad (3.15)$$

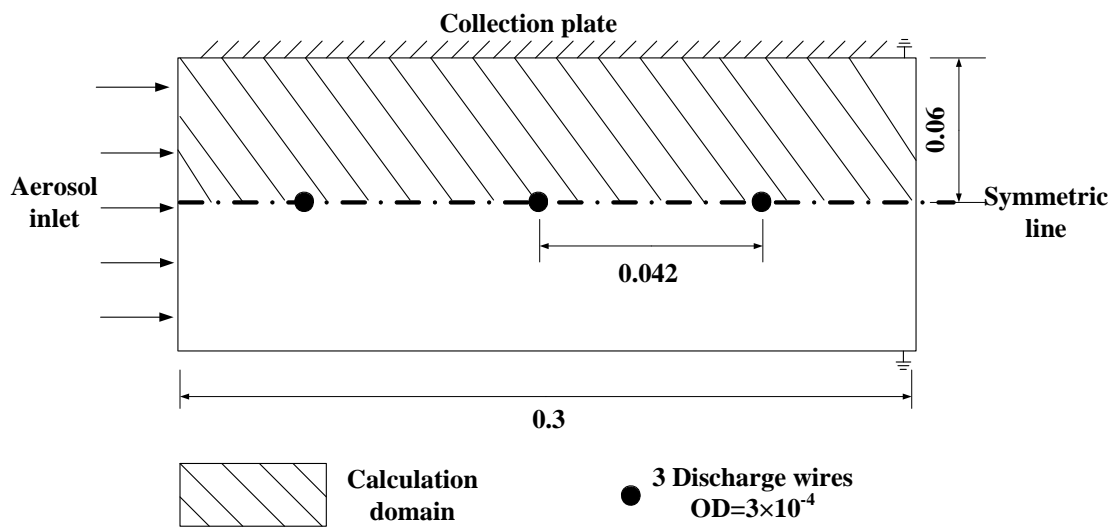
$$E_c = 3 \times 10^6 f \left(\frac{T_0 P}{T P_0} + 0.03 \sqrt{\frac{T_0 P}{T P_0 r_c}} \right) \quad (3.16)$$



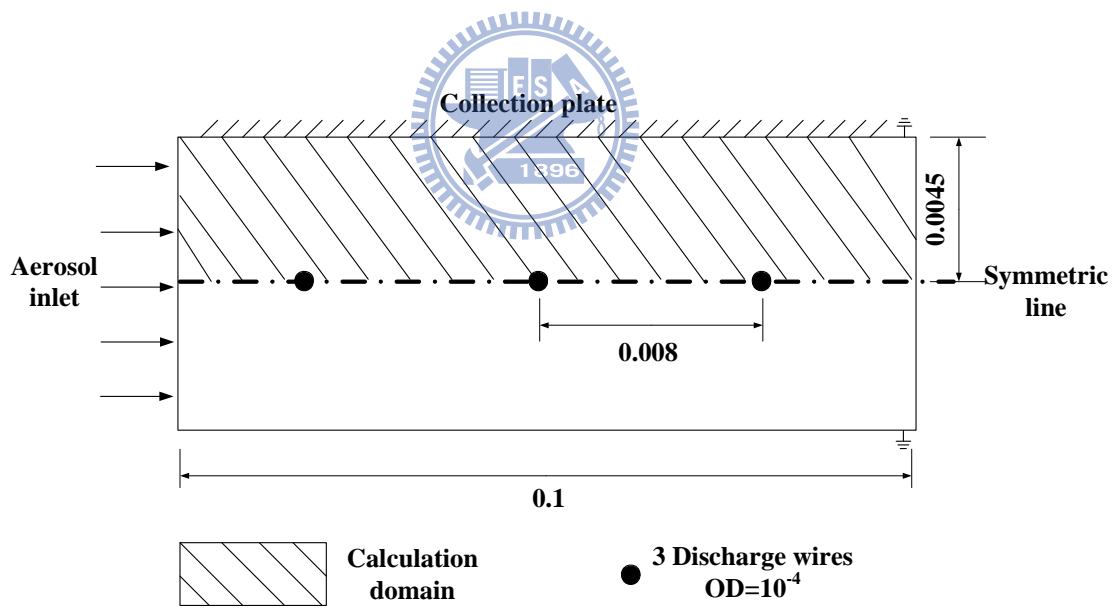
where V_0 is the applied voltage (V), V_c is the corona onset voltage (V), r_{eff} is the equivalent cylinder radius (m), E_c is the corona initiating electric field (V/m), $T_0=293$ (K), $P_0=1$ (atm). After obtaining J_p , the total current I (A) per discharge wire is calculated as (McDonald et al. 1977)

$$I = J_p 4s_x l \quad (3.17)$$

where l is the wire length (m).



(a)



(b)

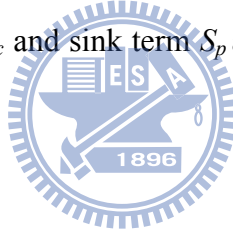
Figure 3.6 Calculation domain (a) the single-stage wire-in-plate dry ESP (Huang and Cheng 2002), (b) the single-stage wire-in-plate wet ESP (Lin et al. 2010). (unit: m)

3.2.3 Particle collection efficiency based on Eulerian method

The governing equation of the concentration of particles carrying q elementary charges, $N_{p,q}$, is

$$\frac{\partial(uN_{p,q} + E_x Z_p N_{p,q})}{\partial x} + \frac{\partial(vN_{p,q} + E_y Z_p N_{p,q})}{\partial y} = D_B \left(\frac{\partial^2 N_{p,q}}{\partial x^2} + \frac{\partial^2 N_{p,q}}{\partial y^2} \right) + S_c + S_p \quad (3.18)$$

where Z_p is the particle electrical mobility ($\text{m}^2/\text{s-V}$), which is defined by $Z_p = qeC_c / 3\pi\mu_{air}d_p$, D_B is the Brownian diffusion coefficient for particles (m^2/s), S_c is the source term, which represents the generation of particles with $q-1$ charges. In the turbulent flow case, D_B is replaced by D_{eddy} (m^2/s) calculated by equations (2.5)-(2.11) as described in section 2.2. In equation (3.18), the source term S_c and sink term S_p are given by (Adachi et al. 1985; Aliat et al. 2009)



$$S_c = \alpha_{q-1} N_{p,q-1} N_i \quad (3.19)$$

$$S_p = -\alpha_q N_{p,q} N_i \quad \text{for particles with } q \text{ elementary charges} \quad (3.20)$$

where α_q is the combination coefficient of ions for particles carrying q elementary charges (m^3/s), which is given by (Fuchs, 1963)

$$\alpha_q = \frac{\bar{c}_i^+ \xi \delta_r^2 \exp\left(\frac{-\phi(\delta_r)}{k_b T}\right)}{1 + \exp\left(\frac{-\phi(\delta_r)}{k_b T}\right) \frac{\bar{c}_i^+ \xi \delta_r^2}{4D_i a} \int_0^{a/\delta_r} \exp\left(\frac{\phi(a/x)}{k_b T}\right) dx} \quad (3.21)$$

where δ_r is the radius of the limiting sphere (m), ζ is the striking probability, which is assumed to be 1 for air ion by Fuchs (1963), and then recalculated by Hopple and Frick (1986), ϕ is the electrostatic potential between the particle and the ion (Adachi et al. 1985) (V), and a is the radius of particles (m). As will be discussed later, the recalculated ζ values by Hopple and Frick (1986) are adopted to investigate the aerosol penetration in the partial charging regime. All parameters used in equation (3.21) were calculated as follows:

$$x = a/r \quad (3.22)$$

$$\phi(r) = \int_r^\infty F(r)dr = \frac{e^2}{4\pi\epsilon_0} \left[\frac{q}{r} - \frac{\kappa_d - 1}{\kappa_d + 1} \frac{a^3}{r^2 - a^2} \right] \quad (3.23)$$

$$\delta_r = \frac{a^3}{\lambda_{ion}^2} \left[\frac{1}{5} \left(1 + \frac{\lambda_{ion}}{a} \right)^5 - \frac{1}{3} \left(1 + \frac{\lambda_{ion}^2}{a^2} \right) \left(1 + \frac{\lambda_{ion}}{a} \right)^3 + \frac{2}{15} \left(1 + \frac{\lambda_{ion}^2}{a^2} \right)^{5/2} \right] \quad (3.24)$$

$$\zeta = \left(\frac{r_a^2 \left(1 + \frac{2}{3k_b T} (\phi(\delta_r) - \phi(r_a)) \right)}{\delta_r} \right)^2 \quad (3.25)$$

$$D_i = \frac{k_b T Z_i}{e} \quad (3.26)$$

$$\bar{c}_i = \sqrt{\frac{8k_b T}{\pi(M_i/N_a)}} \quad (3.27)$$

$$\lambda_{ion} = 1.329 \frac{Z_i}{e} \sqrt{\frac{k_b T M_i M_{air}}{(M_i + M_{air}) N_a}} \quad (3.28)$$

where r is the distance between particles and ions center (m), r_a is the apsidal distance (m), M_i is the molecular weights of ions (kg/mol), M_{air} is the molecular weights of air (kg/mol), and N_a is the Avogadro number (6.023×10^{23} 1/mol). Equation (3.18) was also discretized by using the finite volume method and solved by the same computer code used in the flow field simulation. About 2000 iterations were needed to reach convergence.

For particles with $d_p \leq 20$ nm, the charging model of Marlow and Brock (1975) was also applied to examine the partial charging effect on the particle collection efficiency in the present simulation. The combination coefficient α_q was calculated as (Marlow and Brock, 1975)

$$\alpha_{q,MB} = \frac{\pi a^2 \bar{c}_i [1 + \sqrt{\pi h}]}{1 + \left[\lambda_d G_{IN} / 1 + \sqrt{\pi h} \right]} \quad (3.29)$$


where

$$h = \frac{\varepsilon_p - 1}{\varepsilon_p + 1} \frac{e^2}{2ak_b T} \quad (3.30)$$

$$\lambda_d = \sqrt{\pi} (a / \lambda_i) \left(\frac{M_i + M_{air}}{M_i} \right) \quad (3.31)$$

In Equation (3.29), G_{IN} is the first iterate correction to the flux, which was calculated to be

0.26.

After concentrations of particles with different charge levels ($q=0, 1, 2\dots$) were obtained, the particle collection efficiency of the ESP was calculated as

$$\eta = \left(1 - \frac{\sum_{q=0}^n \int_0^{s_y} N_{p,q,\text{outlet}}(y) u_{\text{outlet}}(y) dy}{\int_0^{s_y} N_{p,0,\text{inlet}}(y) u_{\text{inlet}}(y) dy} \right) \times 100\% \quad (3.32)$$

where $N_{p,0,\text{total}}(y)$ is the inlet uncharged particle number concentration, and $N_{p,q,\text{outlet}}(y)$ is the outlet number concentration of particles carrying q elementary charges.

3.2.4 Particle collection efficiency based on Lagrangian method

Based on Lagrangian method, the collection efficiency was determined by calculating particle trajectories in collaboration with particle charging equations in ESPs. The equation of particle motion and the charging rate along the trajectory were solved numerically by using the fourth order Runge-Kutta method. In the 2-D Cartesian coordinate, the particle equations of motion were given by

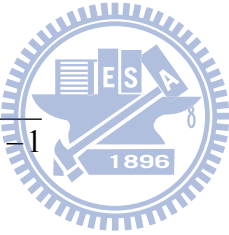
$$\frac{du_p}{dt} = C_D \text{Re}_p \frac{C_c}{24\tau} (u - u_p) + \frac{Z_p \bar{E}}{\tau} \quad (3.33)$$

$$\frac{dv_p}{dt} = C_D \text{Re}_p \frac{C_c}{24\tau} (v - v_p) + \frac{Z_p \bar{E}}{\tau} \quad (3.34)$$

where u_p and v_p are the particle velocity in x and y direction (m/s), respectively, C_D is the empirical drag coefficient, Re_p is the particle Reynolds number. C_D was expressed by Rader and Marple (1985) as

$$\begin{aligned}
C_d &= \frac{24}{\text{Re}_p} \quad \text{for } \text{Re}_p \leq 1 \\
&= \frac{24}{\text{Re}_p} (1 + 0.0916 \text{Re}_p) \quad \text{for } 1 < \text{Re}_p \leq 5 \\
&= \frac{24}{\text{Re}_p} (1 + 0.1586 \text{Re}_p^{2/3}) \quad \text{for } 5 < \text{Re}_p \leq 1000
\end{aligned} \tag{3.35}$$

Two charging models were adopted to predict particle charges in the continuum regime, and the predicted values were compared with each other in this study. The first model combined diffusion charging rate of Fuchs (1947) and field charging rate of Pauthenier and Moreau-Hanot (1932), which are shown in equation (3.36) and (3.37), respectively, as follows:

$$\frac{dq_{diffu}}{dt} = \frac{Z_i \rho_i q / \varepsilon_0}{\exp(qe^2 / 2\pi\varepsilon_0 d_p k_b T) - 1} \tag{3.36}$$


$$\frac{dq_{field}}{dt} = \frac{\rho_i}{e} Z_i \frac{q_{sat}}{4\varepsilon_0} \left(1 - \frac{qe}{q_{sat}}\right)^2 \tag{3.37}$$

$$q_{sat} = \frac{3\kappa_d}{\kappa_d + 2} \pi\varepsilon_0 d_p^2 E \tag{3.38}$$

where q_{sat} is the saturation charge (C), E is the electric field strength (V/m).

The second model developed by Lawless (1996) is shown as follows

$$\frac{dv}{d\tau} = \begin{cases} F(v, \omega) + f(\omega), & -3\omega \leq v \leq 3\omega \\ f(\omega)Be(v - 3\omega), & v > 3\omega \\ -v + f(\omega)Be(-v - 3\omega), & v < -3\omega \end{cases} \tag{3.39}$$

All parameters used in equation (3.39) are shown as follows

$$\omega = \frac{d_p e E}{2k_b T} \quad (3.40)$$

$$\nu = \frac{q \times e^2}{2\pi\epsilon_0 d_p k_b T} \quad (3.41)$$

$$f(\omega) = \begin{cases} \frac{1}{(\omega + 0.475)^{0.575}}, & \omega \geq 0.525 \\ 1, & \omega < 0.525 \end{cases} \quad (3.42)$$

3.2.4 Turbulent flow field in a pilot scale wet ESP

In order to examine the effect of variation of design parameters for ESPs on particle collection efficiency, a pilot scale wet ESP was simulated which had 750-1100 mm in length, 150-300 mm in width, and 6 m in height. There are 3-6 discharge wires each of which had the diameter of 1.3-2.5 mm. The wire to wire spacing and wire to plate spacing was 50-75 and 75-150 mm, respectively. A total of 21,744 (302 in x-direction, 72 in y-direction) non-uniform rectangular grids were used in this calculation domain.

The turbulent flow field model was used in this case. The time-averaged equations for mass, momentum, and energy are

$$\frac{\partial(\rho_{air} u)}{\partial x} + \frac{\partial(\rho_{air} v)}{\partial y} = 0 \quad (3.43)$$

$$\begin{aligned} & \frac{\partial}{\partial x} \left[\rho_{air} u^2 - (\mu_{air} + \mu_t) \frac{\partial u}{\partial x} \right] + \frac{\partial}{\partial y} \left[\rho_{air} uv - (\mu_{air} + \mu_t) \frac{\partial u}{\partial y} \right] \\ & = -\frac{\partial P}{\partial x} + \frac{\partial}{\partial x} \left(\mu_t \frac{\partial u}{\partial x} \right) + \frac{\partial}{\partial y} \left(\mu_t \frac{\partial v}{\partial x} \right) \end{aligned} \quad (3.44)$$

$$\begin{aligned} & \frac{\partial}{\partial x} \left[\rho_{air} uv - (\mu_{air} + \mu_t) \frac{\partial v}{\partial x} \right] + \frac{\partial}{\partial y} \left[\rho_{air} v^2 - (\mu_{air} + \mu_t) \frac{\partial v}{\partial y} \right] \\ &= -\frac{\partial P}{\partial x} + \frac{\partial}{\partial x} \left(\mu_t \frac{\partial u}{\partial y} \right) + \frac{\partial}{\partial y} \left(\mu_t \frac{\partial v}{\partial y} \right) \end{aligned} \quad (3.45)$$

$$\frac{\partial}{\partial x} (\rho_{air} uk) + \frac{\partial}{\partial y} (\rho_{air} vk) = \frac{\partial}{\partial x} \left(\frac{\mu_t}{\sigma_k} \frac{\partial k}{\partial x} \right) + \frac{\partial}{\partial y} \left(\frac{\mu_t}{\sigma_k} \frac{\partial k}{\partial y} \right) + \mu_t G - C_D \rho_{air} \varepsilon \quad (3.46)$$

$$\frac{\partial}{\partial x} (\rho_{air} u\varepsilon) + \frac{\partial}{\partial y} (\rho_{air} v\varepsilon) = \frac{\partial}{\partial x} \left(\frac{\mu_t}{\sigma_\varepsilon} \frac{\partial \varepsilon}{\partial x} \right) + \frac{\partial}{\partial y} \left(\frac{\mu_t}{\sigma_\varepsilon} \frac{\partial \varepsilon}{\partial y} \right) + \frac{\varepsilon}{k} (C_1 \mu_t G - C_2 \rho_{air} \varepsilon) \quad (3.47)$$

$$G = 2 \left(\frac{\partial u}{\partial x} \right)^2 + 2 \left(\frac{\partial v}{\partial y} \right)^2 + \left(\frac{\partial u}{\partial y} + \frac{\partial v}{\partial x} \right)^2 \quad (3.48)$$

$$\mu_t = C_\mu \frac{\rho_{air} k^2}{\varepsilon} \quad (3.49)$$

where μ_t is turbulent viscosity (kg/m-s), ε is turbulent dissipation rate (J/s-kg), and k is turbulent kinetic energy (J/s-kg). The parameters used in k - ε model are as follows:

σ_k	σ_ε	C_μ	C_D	C_1	C_2
1.0	1.3	0.09	1.0	1.44	1.92

CHAPTER 4

RESULTS AND DISCUSSION

4.1 Experimental results for the particle collection efficiency of the wet ESP

4.1.1 Flow rate, uniformity and thickness of the water film

Surface texture and liquid flow rate are two important factors that affect the uniformity of the water film (Tsai et al. 2008). As mentioned previously, the contact angle was greater than 100° for the smooth collection electrodes or uncoated sand-blasted electrodes. It was found that water film on these electrodes was not uniform. In comparison, for the TiO_2 coated, sand-blasted electrodes, scrubbing water was found to be uniform over the collection surfaces at the liquid flow rate per collection surface area ($0.075 \times 0.17 \text{ m}^2$) of 2.31 L/min/m^2 . Similar findings were reported by Tsai et al. (2008), Yu et al. (2001) and Liu et al. (2002). It was also found that channeling occurred when the liquid flow rate per collection surface area was lower than 2.31 L/min/m^2 . These findings demonstrate that both surface texture and liquid flow rate are important for creating a uniform water film. Comparing with the liquid flow rate of $4.44\text{-}6.22 \text{ L/min/m}^2$ used by Saiyasitpanich et al. (2006; 2007), the present design saved 48-63 % of the scrubbing water. The thickness (w) of the water film was calculated to be $0.1 \pm 0.18 \text{ mm}$ by the method presented in Tsai et al. (2008). With this small thickness, the water film was still found to decrease the corona current compared to a dry ESP with the same design except without scrubbing water or purge air flows. Figure 4.1 shows the comparison of the corona current between the dry and wet ESPs, at various supplied voltages. It is seen that at the same voltage, the corona current was decreased after supplying the scrubbing water on the collection plate surfaces, due to the resistivity of the water film. Hence, the wet ESP collection efficiency is expected to be lower than the dry ESP operating at the same voltage. Therefore, for the initially clean condition the operation voltage has to be increased for the

present wet ESP to have the same collection efficiency as the dry ESP. As will be shown later, the advantage of using scrubbing water flow and purge air flow becomes obvious when the collection surfaces are loaded heavily with TiO₂ nanopowder.

4.1.2 Particle collection efficiency of the wet ESP at different aerosol flow rates and applied voltages

Figure 4.2 shows the collection efficiency of the wet ESP as a function of corn oil diameter when the aerosol flow rate is 5 and 10 L/min and the applied voltage is 4.3 kV under the initially clean condition. The residence time of the aerosol in the present wet ESP was calculated to be 0.39 and 0.19 s for aerosol flow rates of 5 and 10 L/min, respectively. As seen in Figure 4.2, decreasing the flow rate from 10 to 5 L/min (or increasing the residence time from 0.19 to 0.39 sec) had a substantial effect on the collection efficiency as the Deutsch-Anderson equation dictates. At the flow rate of 5 L/min, the collection efficiency was 96.9-99.7 % for particles from 16.8 to 615 nm in electrical mobility diameter. The minimum collection of 96.9 % corresponds to the particle diameter of 126.3 nm. As the flow rate is increased to 10 L/min, the minimum collection efficiency is reduced to 84.1 % at the corresponding diameter of 70 nm.

According to particle charging theory, particle charge decreases with decreasing particle diameter, while the mechanical mobility increases rapidly with decreasing particle diameter (Hinds 1999). Therefore, the collection efficiency of ESPs for particles in the size range of 0.1 to 1 µm has a U-shape efficiency curve, as shown in Figure 4.2. Saiyasitpanich et al. (2006) also found a U-shaped collection efficiency curve for the wet ESP with a minimum of about 95 % for particles between 80 and 250 nm in diameter when the supplied voltage was 70 kV, gas residence time was 0.4 s, and the particle concentration was 15.9 mg/Nm³.

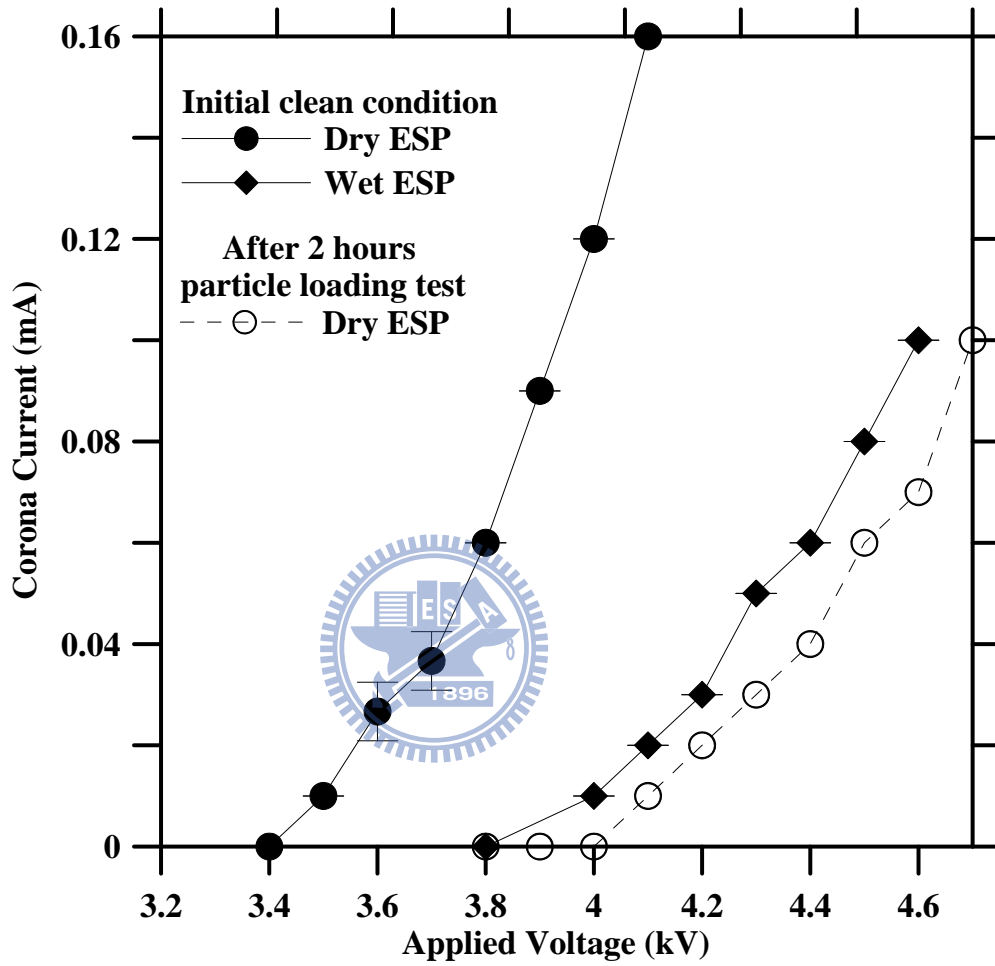


Figure 4.1 Corona current as a function of applied voltage in the dry and wet ESPs.

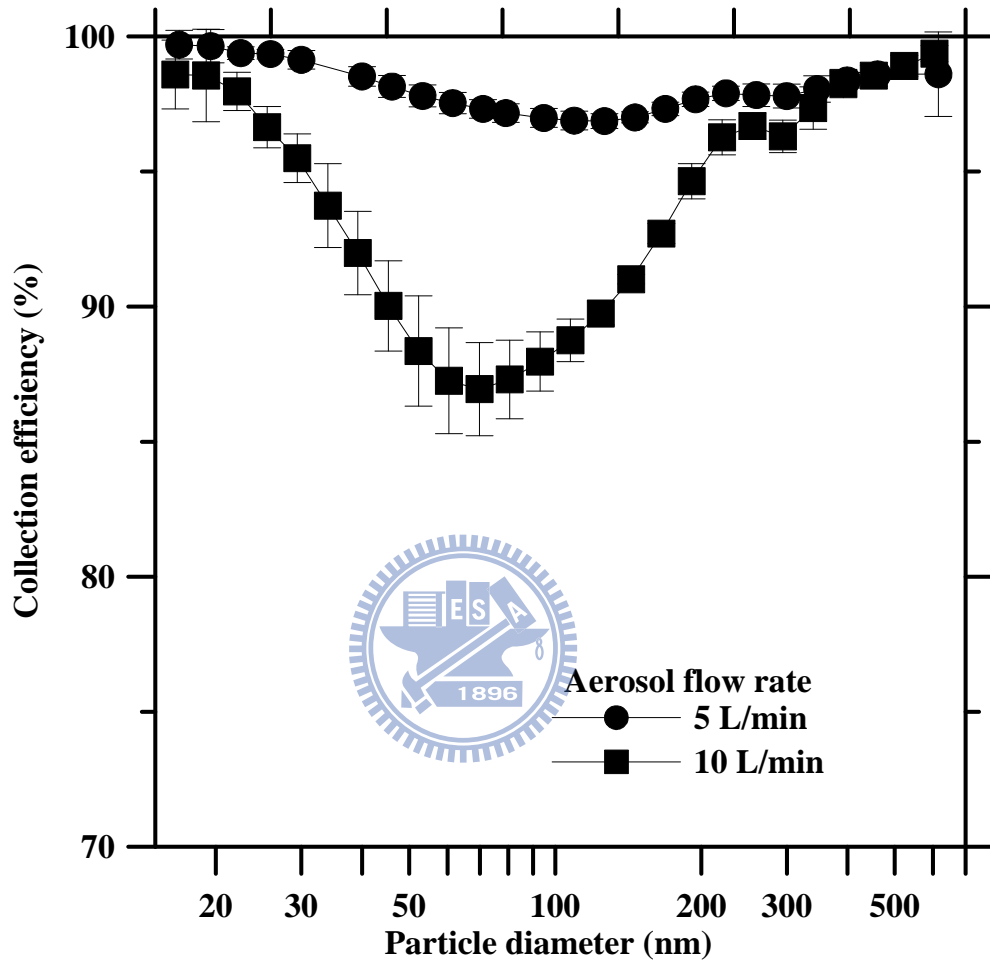


Figure 4.2 Collection efficiency of the present wet ESP for corn oil particles at the aerosol flow rate 5 and 10 L/min and the applied voltage of 4.3 kV. Each test was repeated 6 times.

Figure 4.3 shows the collection efficiency of the present wet ESP for corn oil particles in the size range of 16.8 to 615 nm under different applied voltages at the aerosol flow rate of 5 L/min. As shown in the figure, the corn oil particle collection efficiency also shows a U-shape efficiency curve for particles from 16.8 to 615 nm in electrical mobility diameter and the efficiency decreases with decreasing applied voltage because of the reduction of the electric field strength. When the applied voltage was decreased from 4.3 to 4.1 kV, the collection efficiency decreased slightly from 96.9-99.7 % to 93.9-99.4 %. The collection efficiency was further decreased to 74.2-82.4 % and 11.4-35.5 % for the same particle diameter range when the applied voltage was reduced to 3.9 and 3.8 kV, respectively. Based on these experimental results, it is certain that the present wet ESP can be operated to efficiently control fine and nanosized particles at an aerosol flow rate of 5 L/min, applied voltage of 4.3 kV, and scrubbing water flow rate per collection surface area of 2.31 L/min/m².

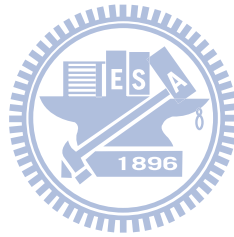
Figure 4.4 shows the collection efficiency of the present wet ESP for corn oil particles in the size range of 16.8 to 615 nm under different applied voltages at the aerosol flow rate of 10 L/min. The collection efficiency can be increased from 86.9-99.4 % to 98.2-100 % when the applied voltage was increased from 4.3 to 4.9 kV. This result suggested that the increase of aerosol penetration due to the decrease of residence time of particles in ESPs can be diminished by increasing the applied voltage. The spark over occurs when the applied voltage is increased to 5.5 kV, which is the operation limitation for the present wet ESP.

In the present wet ESP, high particle collection efficiency (99 %) was found for small nanoparticles (16.8 to 29.4 nm) with an applied voltage of 4.3 kV. This is attributed to the high electrostatic precipitation efficiency $\eta_{elec}(d_p)$ and diffusive deposition $\eta_{diff}(d_p)$ in this size range, which can be calculated by the following equations:

$$\eta_{elec}(d_p)(\%) = \frac{\eta_{total}(d_p)(\%) - \eta_{diff}(d_p)(\%)}{100\% - \eta_{diff}(d_p)(\%)} \times 100\% \quad (4.1)$$

$$\eta_{diff}(d_p)(\%) = \frac{C_{in} - C_{out,OFF}}{C_{in}} \times 100\% \quad (4.2)$$

where $C_{out,OFF}$ is the outlet particle number concentration of the wet ESP without supplying high voltages. As can be seen in Figure 4.5, the electrostatic precipitation efficiency decreased from 99.4 % to 97.2 % when the particle diameter increased from 16.8 to 615 nm. The diffusive deposition was found to be negligible for particles greater than 29.4 nm, and it increased from 4.0 to 17.4 % as particles decreased from 29.4 to 16.8 nm. These results demonstrate that diffusive deposition plays an important role for very small nanoparticles in the wet ESP.



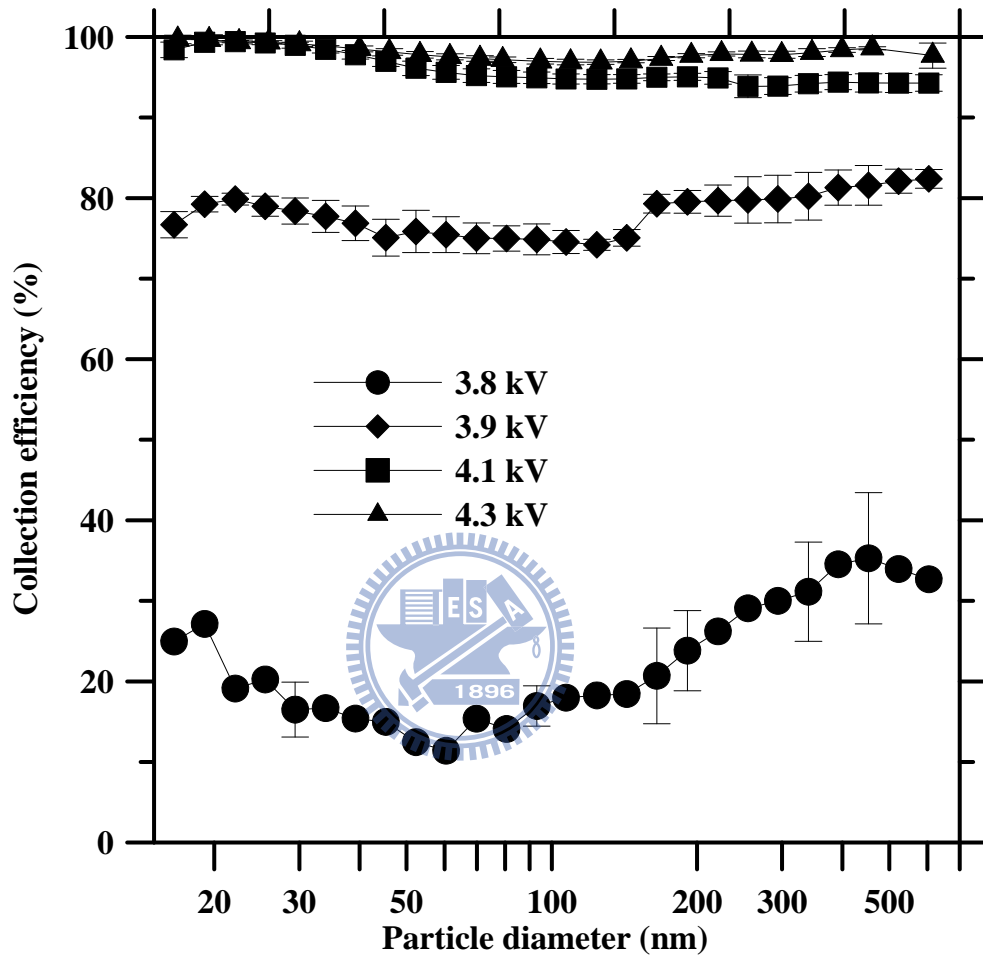


Figure 4.3 Collection efficiency of the present wet ESP for corn oil particles under different applied voltages. The aerosol flow rate is fixed at 5 L/min. Each test was repeated 6 times.

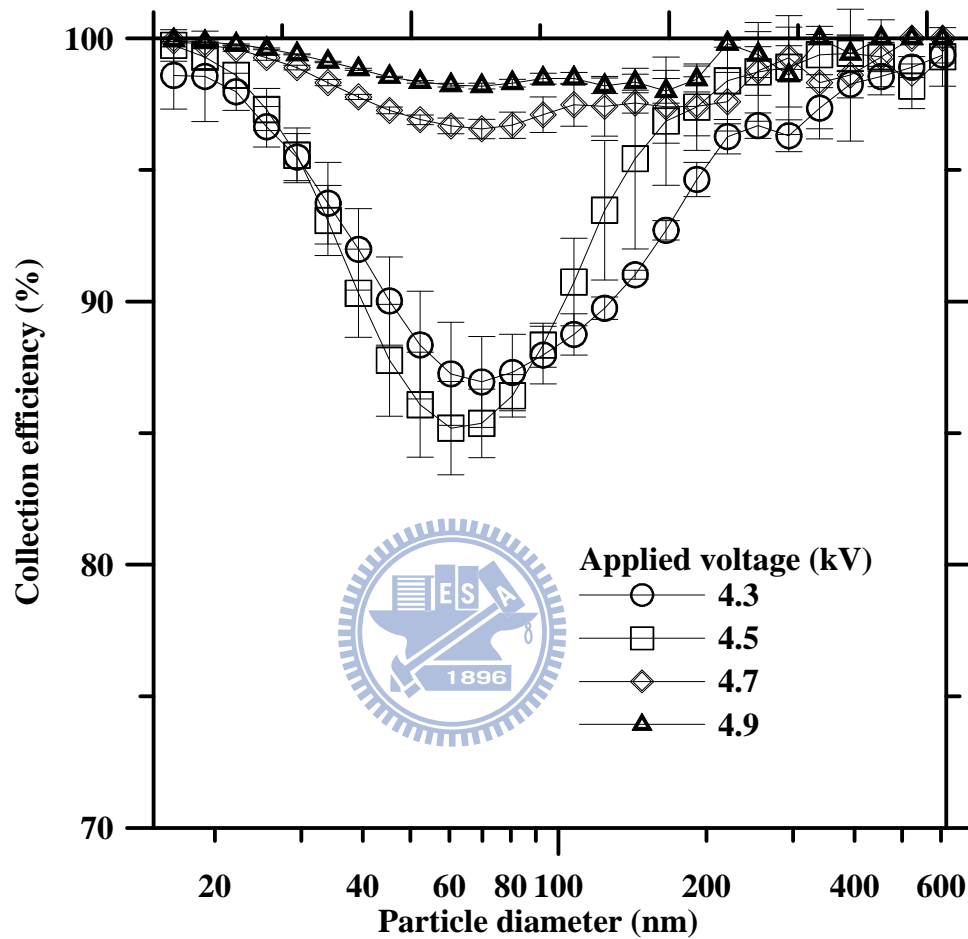


Figure 4.4 Collection efficiency of the present wet ESP for corn oil particles under different applied voltages. The aerosol flow rate is fixed at 10 L/min. Each test was repeated 6 times.

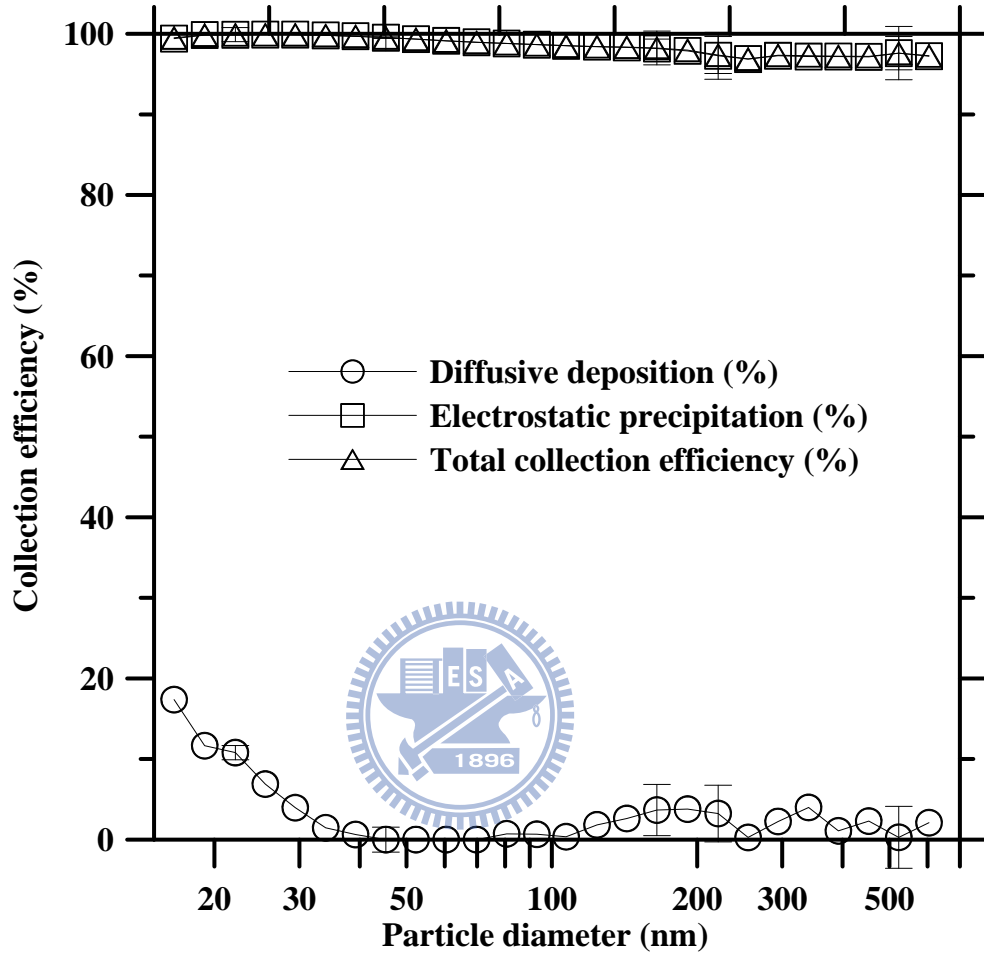


Figure 4.5 Electrostatic precipitation and diffusive deposition efficiencies of the polydisperse corn oil particles in the present wet ESP when the aerosol flow rate and the applied voltage are 5 L/min and 4.3 kV, respectively. Each test was repeated 6 times.

4.1.3 Particle loading test

The particle collection efficiency for corn oil particles was tested by the dry and wet ESP at an aerosol flow rate of 5 L/min and an applied voltage of 4.3 kV for a long operation time of 10 hours. The collection efficiency in the dry ESP was found to decrease only slightly from 99.2-100 % to 98.7-100 % for 10.4-149 nm particles after the 10-hour test (loaded corn oil: 5.04×10^{-5} mg/plate). Particle accumulation on the collected plates and wires was found to be negligible due to the small loaded particle mass. Similar tests for the wet ESP also showed that the collection efficiency was as high as the initial condition (99.1-98.4 % for 10.4-149 nm particles) after 10-hours of loading corn oil particles. Therefore, heavy loading conditions on the collection plates had to be generated by dispersing powders, such as TiO₂ nanopowder used in this study.

The collection efficiency was tested for the dry and wet ESP with an aerosol flow rate of 5 L/min, an applied voltage of 4.3 kV, and with a TiO₂ loading quantity of 0.6 ± 0.06 g/hr/plate (4 ± 0.06 g/m³). As shown in Figure 4.6, the collection efficiency decreased slightly from 96.9-99.7 % to 92.1-99.3 % for electrical mobility diameters of 16.8-615 nm in the dry ESP after 30 minutes of particle loading. However, after one hour of loading, the aerosol penetration increased sharply from 0.9-1.6 % to 12.4-55.4 % for the same range of electrical mobility diameters. The particle collection efficiency finally decreased below 35.0 % for all particles (Figure 4.6). This resulted from the reduction of the electric field strength due to the accumulation of TiO₂ particles on the collected plates and the discharge wires. As shown in Figure 4.1, it is evident that the corona current, and hence the electric field strength, decreases dramatically under the same applied voltage after two hours of heavy particle loading because of the additional resistivity of the dust layer.

Experimental results showed that after two hours of TiO₂ nanoparticle loading, the total number concentration of reentrained particles was 612.2 \#/cm^3 (16.8 to 615 nm) at the first

sampling interval of 135 seconds and then reduced to almost zero after that (Figure 4.7). Many particles were seen to be dislodged and redispersed back into the gas stream because the electrostatic voltage difference across the TiO₂ dust layer was very low. These reentrained particles were too small to settle by gravity and would leave dry ESPs (Richards, 1995).

Under the same loading conditions as the dry ESP, the collection efficiency of the present wet ESP for corn oil particles was measured to be as high as 97.6-99.5 % and 94.9-99.9 % for particles from 16.8 to 615 nm in electrical mobility diameter after 30 and 120 minutes particle loadings, respectively, as shown in Figure 4.8. The particle loaded mass used in this study, $4\pm 0.06 \text{ g/m}^3$, is much higher than 2.8-15.9 mg/Nm³ used in Saiyasitpanich et al. (2006; 2007). By direct observation, the continuous scrubbing water was seen to wash the collection plates clean and maintain a uniform water film. The pulse air jet was also capable of cleaning the discharge wires regularly. These were key factors in maintaining a high collection efficiency of the present wet ESP under heavy particle loading conditions.



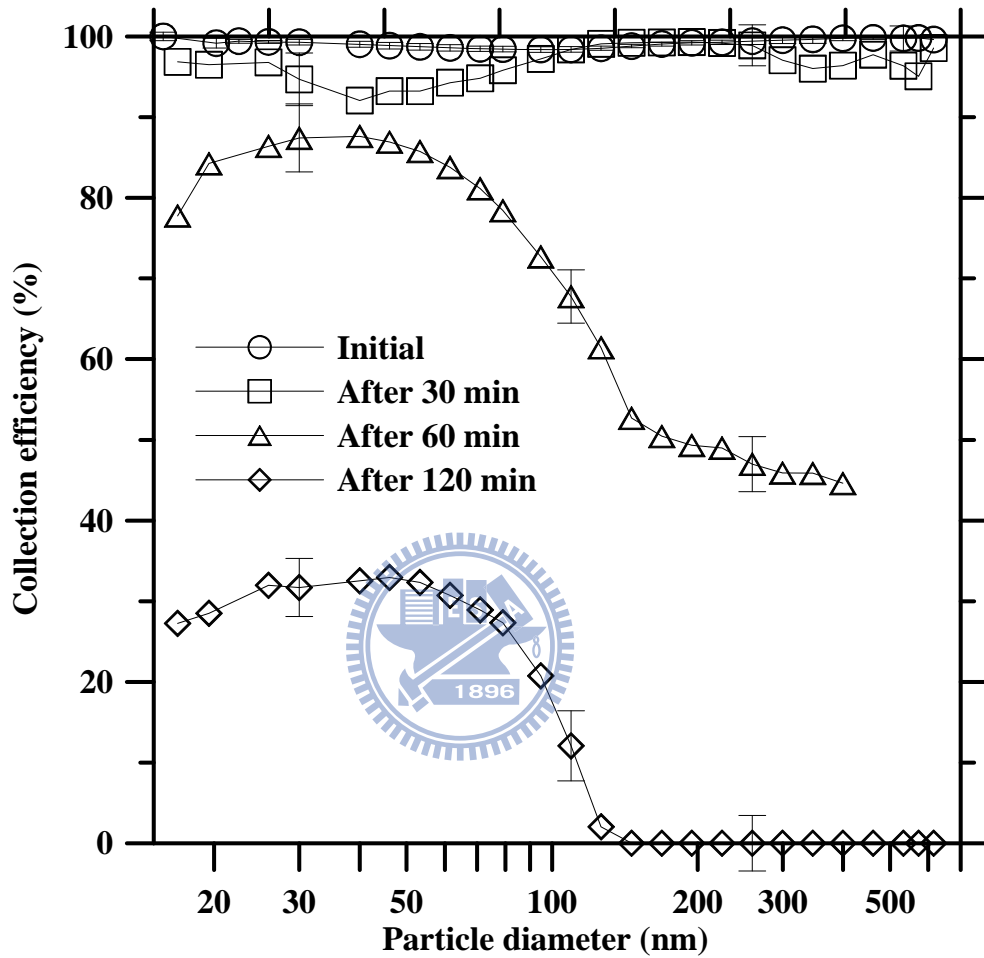


Figure 4.6 Collection efficiency for corn oil particles in the dry ESP at different TiO_2 nanopowder loadings. The applied voltage and aerosol flow rate are 4.3 kV and 5 L/min, respectively.

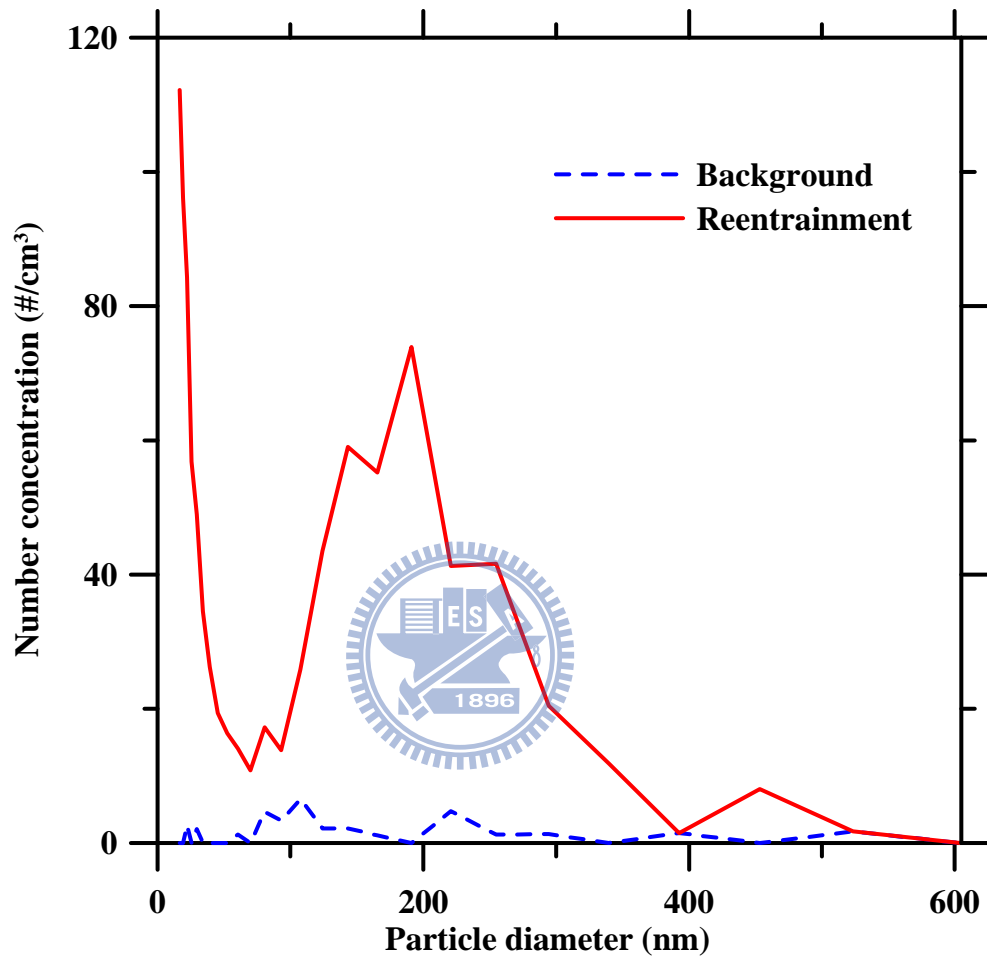


Figure 4.7 Particle reentrainment test in dry ESPs. The aerosol flow rate and applied voltage were 5 L/min and 4.3 kV.

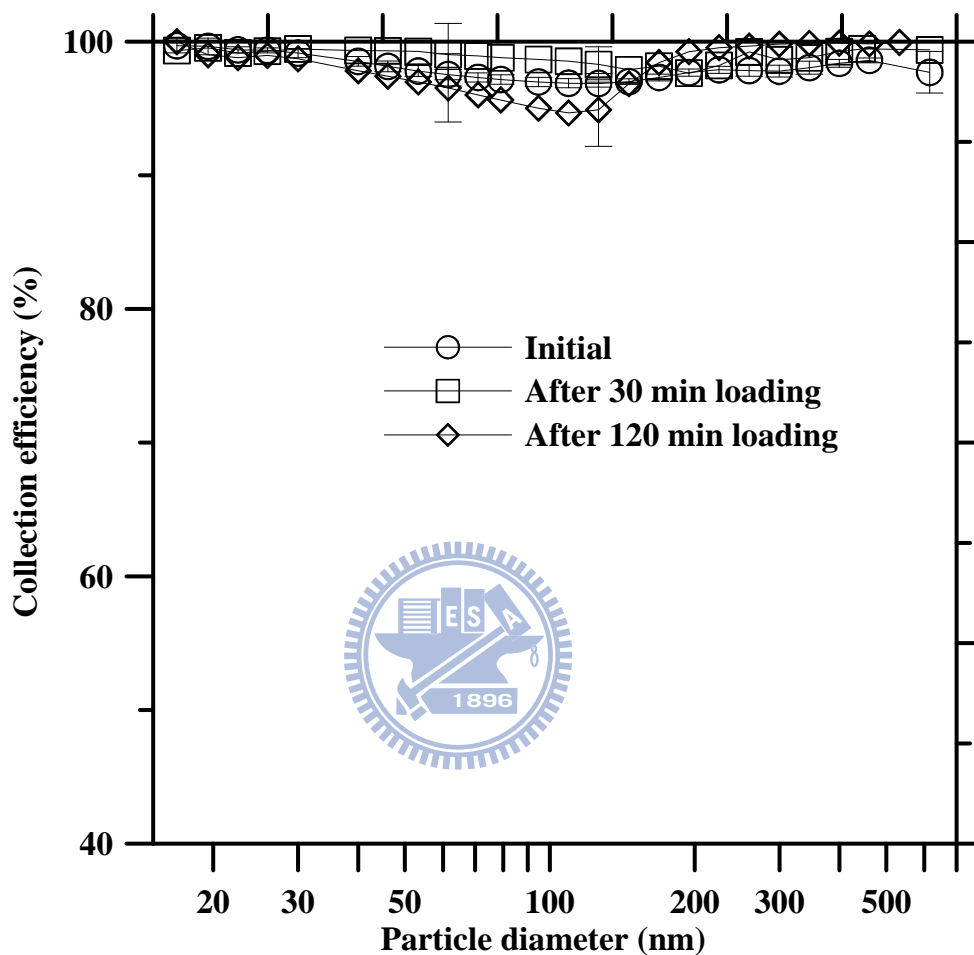


Figure 4.8 Collection efficiency for corn oil particles in the wet ESP at different TiO₂ nanopowder loadings. The applied voltage and aerosol flow rate are 4.3 kV and 5 L/min, respectively.

4.2 Numerical results based on Lagrangian method for the nanoparticle collection efficiency of ESPs

4.2.1 Particle charging and particle trajectory in the ESP

In order to examine the applicability of the present model based on the Lagrangian method for predicting particle charging and particle trajectory, the numerical results were compared with the values in two benchmark problems. In the first case, number of charges acquired by particles by the diffusion, field and combined charging mechanisms were calculated, and then compared with the analytical solutions and numerical solutions in Hinds (1999). When the electric field strength is 5×10^5 V/m, ion number concentration is 10^{13} (m^{-3}), and charging time is 1 s, the number of particle charges is calculated as shown in table 4.1. As shown in the table, the number of charges acquired by particles with various particle sizes by diffusion charging mechanism calculated by Lawless (1999) and Fuch's (1943) equations in the present model match with numerical solutions in Hinds (1999) very well. The combined charges calculated by Lawless equation (1999) and Pauthenier and Moreau-Hanot equation (1932) in the present model match with the numerical solutions in Hinds (1999) as well.

In the second benchmark problem, the particle charging and trajectory in an ESP were calculated and compared with the numerical results in Goo and Lee (1997). In this ESP, the wire to wire spacing was 5.08×10^{-2} m, the wire to plate spacing was 2.5×10^{-2} m, the radius of corona wire was 0.05×10^{-3} m, the air velocity was 2.0 m/s, and the applied voltage was 12.78 kV. Figure 4.9 shows the particle trajectory in the ESP in Goo and Lee (1997). As can be seen, the present numerical results match with the simulated results in Goo and Lee (1997). Figure 4.10 shows the number of charges acquired by particles along the particle trajectory as shown in Figure 4.9. As shown in figure 4.10, the present numerical results also match with the simulated results in Goo and Lee (1997).

Table 4.1 Comparison of different models for particle charging by field, diffusion, and combined charging.

Particle diameter r (μm)	Number of elementary units of charged acquired									
	Diffusion charging			Field charging				Combined charging		
	Eq. 15.24 (Hinds, 1999)	Numerical solution (Hinds, 1999)	Present model (Lawless, 1996)	Present model (Fuch's, 1943)	Eq. 15.25 (Hinds, 1999)	Present model (Lawless, 1996)	Present model (Pauthenier and Moreau-Hanot, 1932)	Numerical solution (Hinds, 1999)	Present model (Lawless, 1996)	Present model (Fuch's (1943) and P-M (1932))
0.1	2.7	4.1	4.0	4.0	1.6	1.63	1.62	5.6	5.6	5.7
0.4	15.7	16.3	16.2	16.2	25.9	26	26	40	40	42
1.0	47	41	41	41	162	163	162	162	193	204
4.0	237	163	163	163	2580	2604	2598	2680	2656	2761
10	673	407	407	407	16200	16277	16237	16540	16382	16723
40	3180	1630	1630	1630	259000	260439	259785	264000	261164	262674

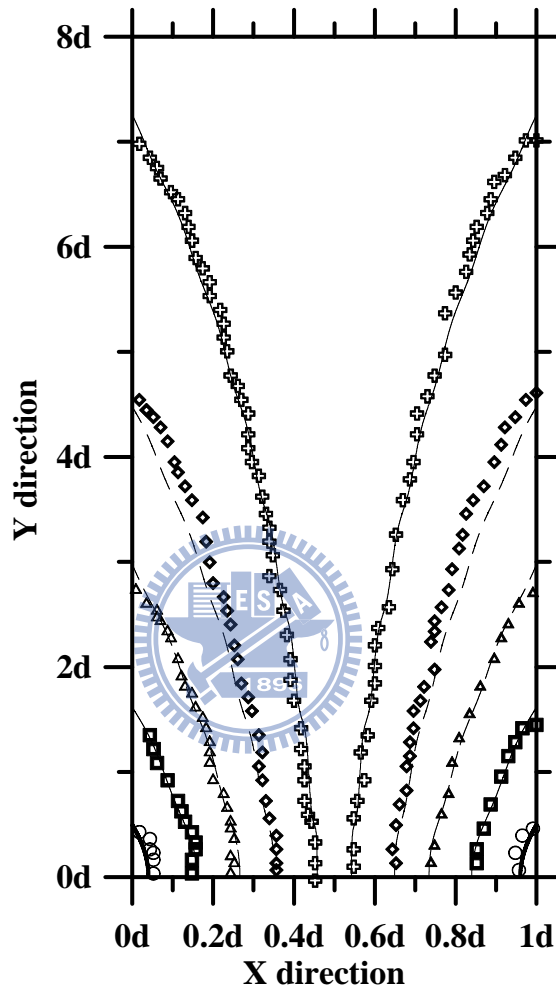


Figure 4.9 Comparison of the simulated particle trajectory between the present numerical results and those in Goo and Lee (1997) (Line: the present numerical results; open symbol: the numerical results in Goo and Lee (1997)).

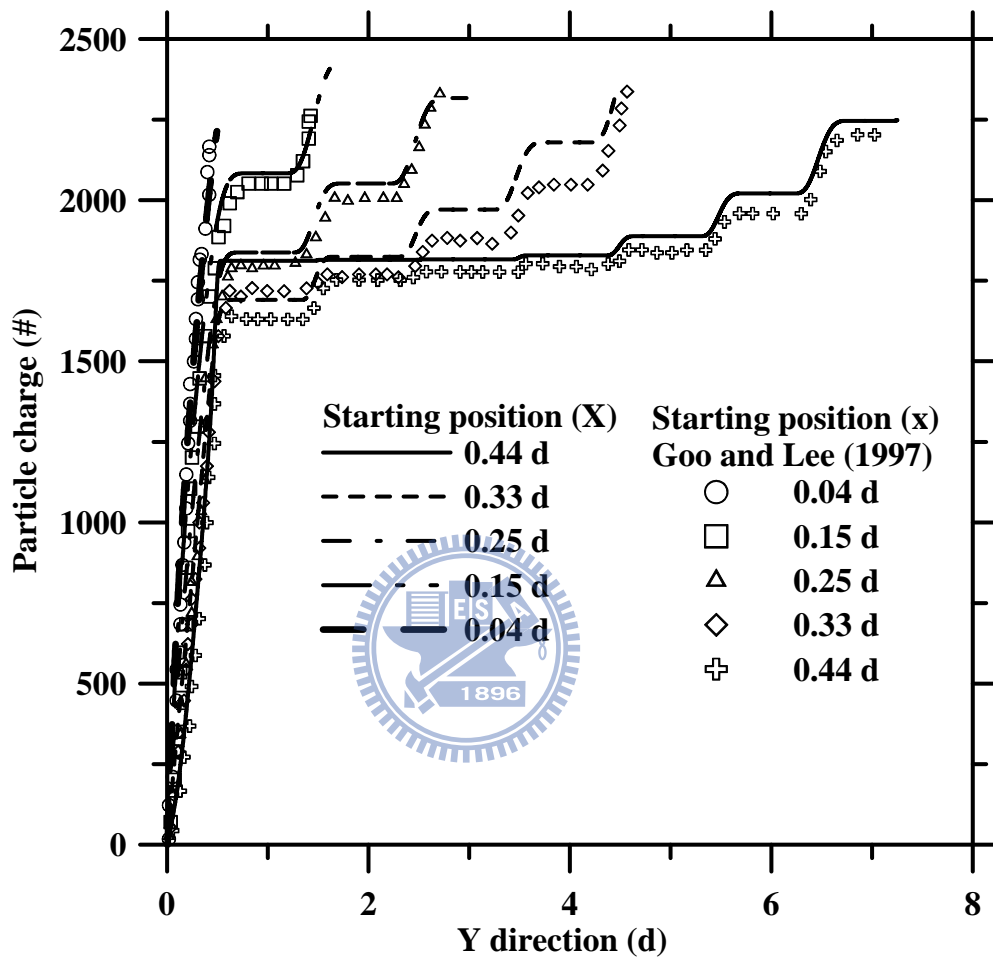


Figure 4.10 Comparison of the simulated particle charging between the present numerical results and those in Goo and Lee (1997) (Line: the present numerical results; open symbol: the numerical results in Goo and Lee (1997)).

4.2.2 Comparing the particle collection efficiency in the dry ESP of Huang and Chen (2002) and Chang and Bai (1999)

Figure 4.11 shows comparison of the aerosol penetration between the present numerical values and the experimental data of Huang and Chen (2002). The charging model of Lawless (1996) was used to predict particle charges for particles with $0.006 \leq d_p \leq 10 \mu\text{m}$. As shown in Figure 4.11, when the applied voltage is -15.5 kV, the simulated results are in reasonable agreement with the experimental data with deviation of 2.75-16.07 % for particles with diameter of 40-100 nm. However, for particles with diameter below 40 nm, the present model based on Lagrangian method using combined charging model to predict particle charges underestimates the aerosol penetration with deviation larger than 20 % as compared with the experimental data. When the applied voltage is -18.0 kV, the deviation between simulated results and the experimental data are also larger than 20 % for particles with diameter below 70 nm. Besides, the partial charging effect on the aerosol penetration for the particles with $d_p \leq 20 \text{ nm}$ at both applied voltages can't be predicted correctly. These results coincide with the theoretical results in Lawless (1996), who concluded that the limit of applicability of the combined charging model is 100 nm (Lawless 1996). Thus, the appropriate charging model, Fuchs model (1963) and the model of Marlow and Brock (1975), should be adopted to calculate charges of particles with $d_p \leq 100 \text{ nm}$. The simulated results based on these two models are shown in section 4.3.

When the applied voltage is -26.4 kV, the simulated aerosol penetration increases from 0.0 to 26.3 % with increasing particle diameter from 100 to 400 nm, and then decreases from 26.3 % to 0.0 % particle diameter from 400 to 1500 nm. The numerical results agreed reasonably with the experimental data with deviation of 0.54-14.57 % for particles with $100 \leq d_p \leq 1000 \text{ nm}$.

Figure 4.12 shows comparison of the particle collection efficiency between the present

numerical values and the experimental data of Chang and Bai (1999). In the ESP of Chang and Bai (1999), the wire to wire spacing was 300 mm, wire to plate spacing was 60 mm, and wire diameter was 0.5 mm. The aerosol flow rate and the applied voltage were 109 L/min and 27.0 kV, respectively. The numerical results are also in reasonable agreement with the experimental data in Chang and Bai (1999) with deviation of 1.49-12.46 %. These results could be attributed to the fact that Lawless' model predicts particle charges accurately for particles in the continuum charging regime ($Kn \ll 1$) (Lawless 1997). Lawless concluded that when the electric field strength is very strong, diffusion charging can be neglected for particles with $d_p > 1 \mu\text{m}$; whereas diffusion charging should never be neglected for submicron particles (Marquard 2007). This is a very important conclusion for predicting particle charges using combined charging model in the continuum regime.



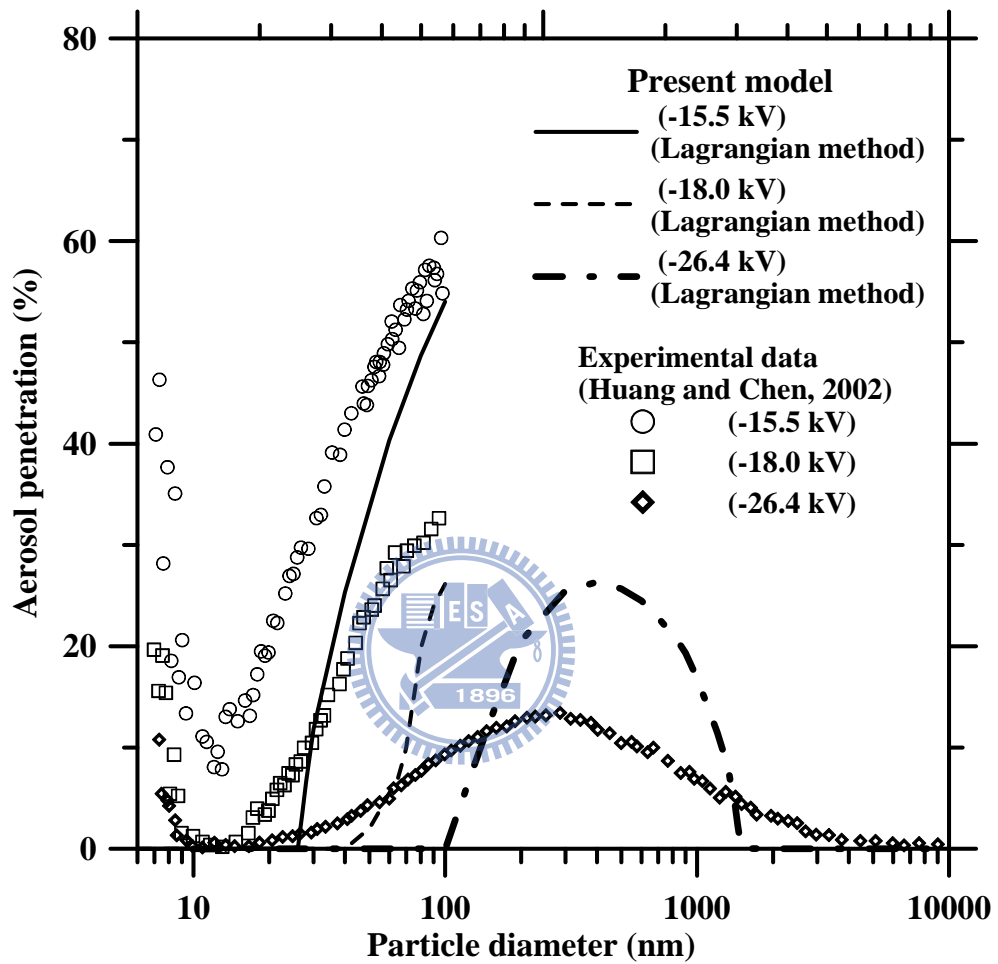


Figure 4.11 Comparison of particle collection efficiency in the single-stage wire-in-plate dry ESP between numerical results and experimental data in Huang and Chen (2002) at the aerosol flow rate of 100 L/min.

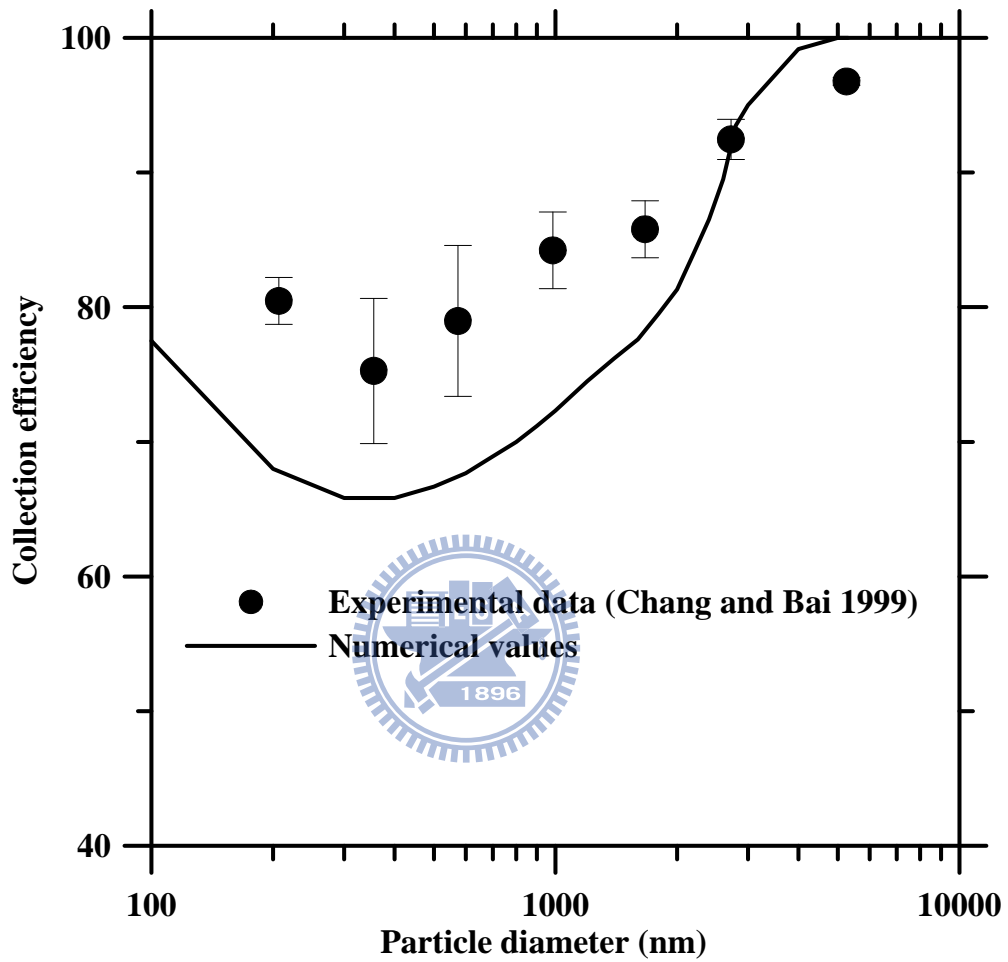


Figure 4.12 Comparison of particle collection efficiency in the single-stage wire-in-plate dry ESP between numerical results and experimental data in Chang and Bai (1999) at an aerosol flow rate of 109 L/min and an applied voltage of 27.0 kV.

4.3 Numerical results based on Eulerian method for the nanoparticle collection efficiency of ESPs

4.3.1 Characteristics of the V-I curve, electric field and ion concentration distribution

Figure 4.13 shows the comparison of V-I curve between the theoretical values and the experimental data in the dry ESP of Huang and Chen (2002) and the wet ESP. Applying the ion mobility in the range of $1.35 \times 10^{-4} \sim 1.90 \times 10^{-4} \text{ m}^2/\text{V/s}$ for negative ions and $1.15 \times 10^{-4} \sim 1.40 \times 10^{-4} \text{ m}^2/\text{V/s}$ for positive ions, good agreement was obtained. The range of ion mobility was taken from previous researches and shown in Table 4.2 (Adachi et al. 1985; Hoppel and Frick 1986; Hussin et al. 1983; Mohnen 1977; Wiedensohler et al. 1986; Wen et al. 1984; Wiedensohler and Fissan 1991). In the mobility range, the variation of the collection efficiency for particles with $2 \leq d_p \leq 100 \text{ nm}$ was found to be insignificant, which was calculated to decrease from 3.44~0.5 % to 5.70~0.0 % when the applied voltage was increased from -15.5 to -21.5 kV in the dry ESP of Huang and Chen (2002), and decreased from 3.7 to 0.0 % when the applied voltage was increased from +3.6 to +4.3 kV for 10 nm particles in the wet ESP. Thus, a fixed value of $1.35 \times 10^{-4} \text{ m}^2/\text{V/s}$ for negative ions and $1.15 \times 10^{-4} \text{ m}^2/\text{V/s}$ for positive ions was used to calculate the particle collection efficiency.

The present simulated electric potential and ion concentration distribution were also compared to the analytical solutions in a wire-in-tube ESP case (Marquard et al. 2005), and numerical results were found to match with analytical solutions as shown in Figure 4.14. Therefore, the present model is able to predict electric field strength and ion concentration distribution in ESPs. Figures 4.15 and 4.16 show the electric potential and the ion density distribution in the wire-in-plate wet ESP at an applied voltage of +3.7 kV and an air flow rate was of 5 L/min, respectively. The electric potential is shown to be symmetric with respect to the y-axis around the discharge wire. The ion density distribution also tends to be symmetric with respect to the y-axis around the discharge wire. The average ion density at the outlet of

the wet ESP, $7.38 \times 10^{-6} \text{ C/m}^3$, was calculated to be slightly higher than $4.69 \times 10^{-7} \text{ C/m}^3$ at the inlet of the wet ESP due to the influence of air flow convection. The profiles of the electric potential and the ion concentration distribution in the dry ESP of Huang and Chen (2002) were found to be similar to those in the wet ESP, and are not shown here.

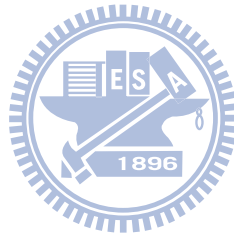


Table 4.2 Ion molecular weight, ion mobility, and the corresponding ion diffusion coefficient used in previous researches.

Z_i (m ² /V/s)		M_i (kg/mol)		D_i (m ² /s)		Reference
Positive ion	Negative ion	Positive ion	Negative ion	Positive ion	Negative ion	
1.40×10^{-4}	1.90×10^{-4}	0.109	0.050	3.6×10^{-6}	4.9×10^{-6}	Adachi et al. (1985)
1.40×10^{-4}	1.90×10^{-4}	0.130	0.100	3.6×10^{-6}	4.9×10^{-6}	Mohnen (1977)
1.40×10^{-4}	1.90×10^{-4}	0.130	0.130	3.6×10^{-6}	4.9×10^{-6}	Wen et al. (1984)
1.40×10^{-4}	1.60×10^{-4}	0.140	0.101	3.6×10^{-6}	4.1×10^{-6}	Wiedensohler and Fissan (1991)
1.35×10^{-4}	1.60×10^{-4}	0.148	0.130	3.5×10^{-6}	4.1×10^{-6}	Wiedensohler et al. (1986)
1.33×10^{-4}	1.84×10^{-4}	0.200	0.100	3.4×10^{-6}	4.7×10^{-6}	Hoppel and Frick (1990)
1.20×10^{-4}	1.35×10^{-4}	0.150	0.090	3.1×10^{-6}	3.5×10^{-6}	Hoppel and Frick (1986)
1.15×10^{-4}	1.39×10^{-4}	0.140	0.101	3.0×10^{-6}	3.6×10^{-6}	Hussin et al. (1983)
1.15×10^{-4}	1.425×10^{-4}	0.290	0.140	3.0×10^{-6}	3.7×10^{-6}	Reischl et al. (1996)
1.15×10^{-4}	1.65×10^{-4}	N.D.	N.D.	3.0×10^{-6}	4.2×10^{-6}	Alonso et al. (2009)

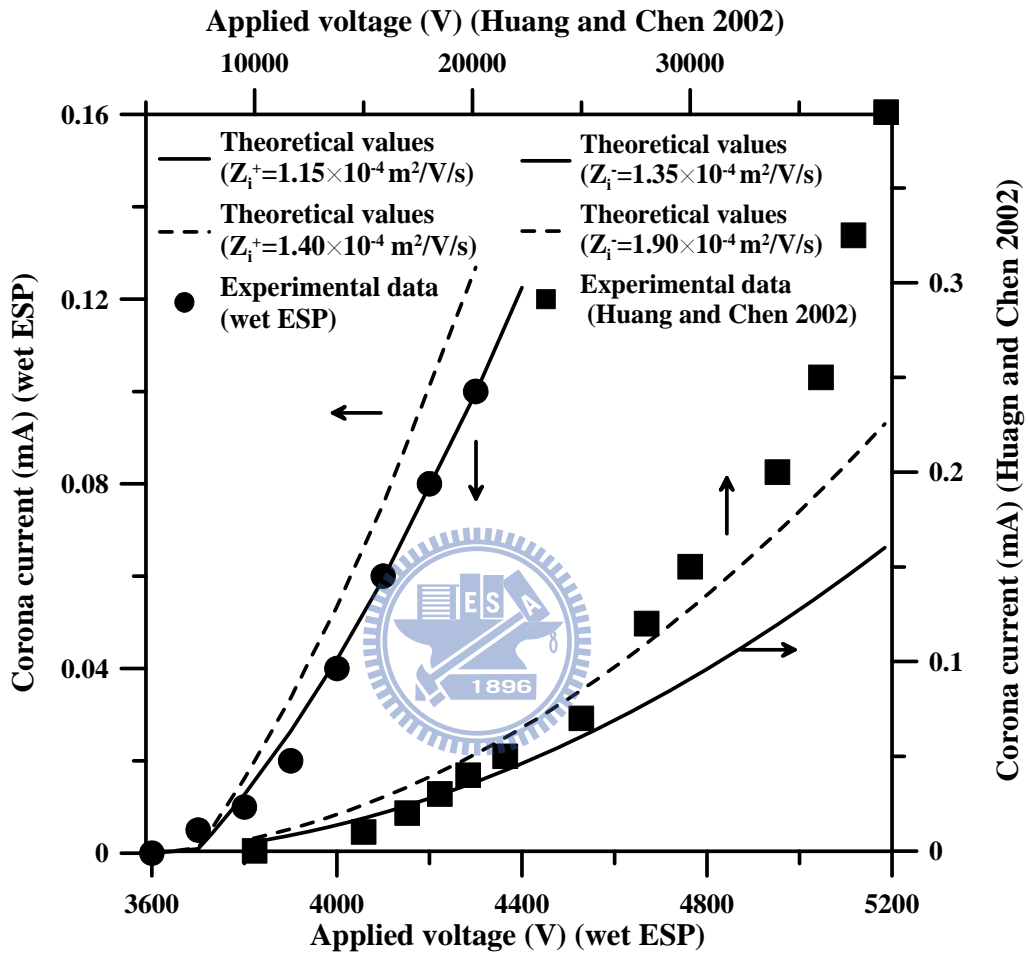
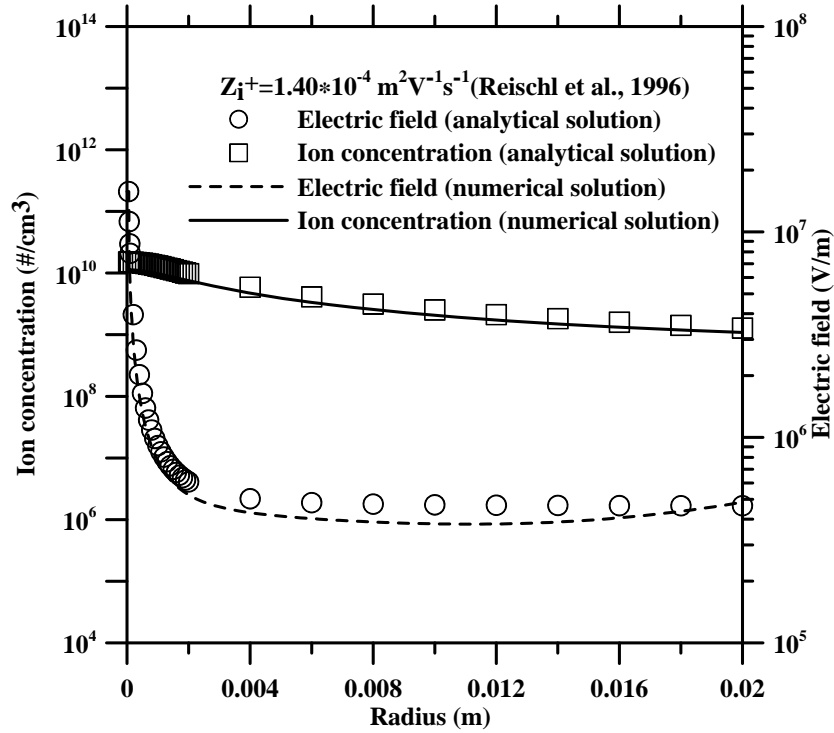
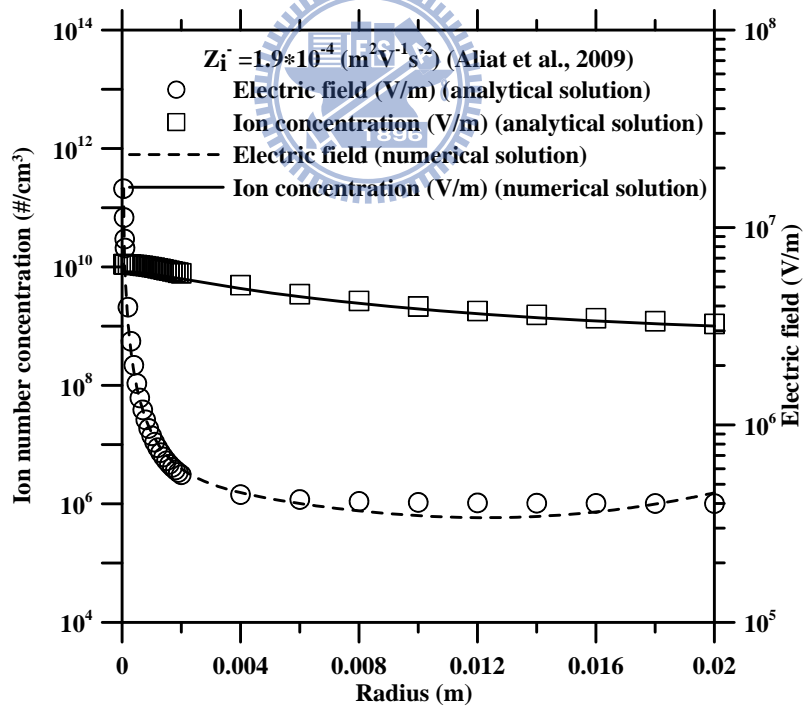


Figure 4.13 Comparison of Corona current as a function of applied voltage between theoretical results and experimental data in the ESP.



(a)



(b)

Figure 4.14 Comparison of electric field strength and ion concentration distribution between numerical results and analytical solutions in a wire-in-tube ESP for (a) positive ions, and (b) negative ions.

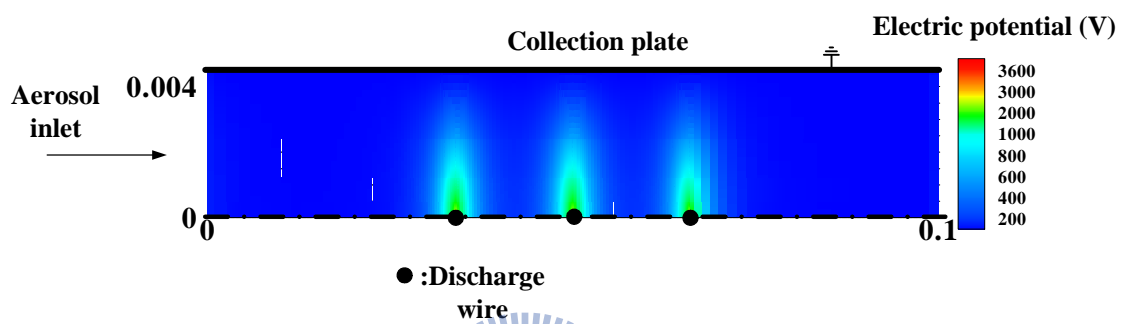


Figure 4.15 Electric potential distribution at the applied voltage of +3.7 kV in the wet ESP.

(Note: The scale in y direction is magnified 4.5 times relative to that in x direction.)

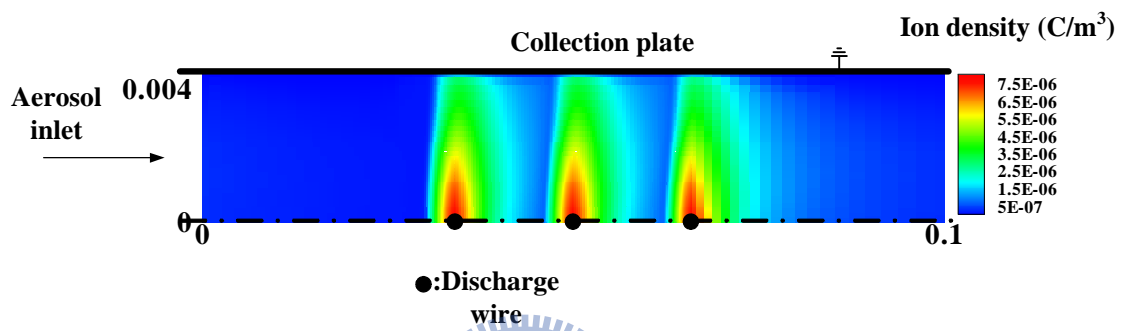


Figure 4.16 Ion concentration distribution at the applied voltage of +3.7 kV in the wet ESP.

(Note: The scale in y direction is magnified 4.5 times relative to that in x direction.)

4.3.2 Comparing the particle collection efficiency in the dry ESP of Huang and Chen (2002)

Figure 4.17 shows comparison of the particle collection efficiency between the present numerical values and the experimental data of Huang and Chen (2002). When the aerosol flow rate and the applied voltage was 100 L/min and -15.5~-21.5 kV, respectively, the numerical results based on Fuchs model (1963) agreed reasonably with experimental data with a deviation of 0.4-11.3 % for particles with $40 \leq d_p \leq 100$ nm. The calculated penetration efficiencies were 11.3-22.7 % lower than the experimental data for particles with $20 \leq d_p \leq 40$ nm.

For particles with $d_p \leq 20$ nm, the present model with particle charge calculated by using Fuchs model (1963) was shown to over-predict the particle collection efficiency with a large deviation of over 20 % as compared to the experimental data, as shown in Figure 4.17. In order to predict the collection efficiency for particles below 20 nm accurately, the charging model of Marlow and Brock (1975) was used in the present simulations. The aerosol penetration was calculated to increase from 0.0 to 38.4 % for an applied voltage of -18.0 kV, 0.1 to 51.9 % for an applied voltage of -16.0 kV, and 8.52 to 54.4 % for an applied voltage of -15.5 kV with decreasing particle diameter from 20 to 2 nm. As shown in Figure 4.17, better agreement between the simulated values and the experimental data was obtained with deviation of 0.8-13.1 % at the applied voltage of -15.5~-21.5 kV. This result could be attributed to the fact that the model of Marlow and Brock (1975) predicts better combination coefficient than Fuchs model (1963) for particles with $d_p < 20$ nm (Pui et al. 1988; Romay and Pui 1992). The model of Marlow and Brock (1975) considers the velocity distribution of the ions in the vicinity of the particle, which is an important factor for predicting particle charging in the transition and free molecule regimes (Pui et al. 1988). Therefore, it can be concluded that the model of Marlow and Brock (1975) is more appropriate than Fuchs model for predicting particle charging and the collection efficiency in the partial charging regime ($d_p < 20$ nm) in the ESP.

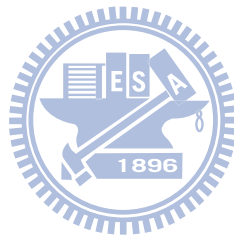
In Figure 4.17, the ion molecular weight is assumed to be 0.140 kg/mol. The effect of the ion molecular weight on the particle collection efficiency was also examined in the present simulation. Table 4.2 shows molecular weights of positive and negative ions measured by previous researchers. According to Fuchs theory (1963), the combination coefficient is related to ion molecular weight (Equation (3.21)). For negative ions, when the ion molecular weight increases from the minimum of 0.05 kg/mol to the maximum of 0.140 kg/mol shown in Table 4.2, the particle collection efficiency was found to decrease (data not shown) with decreasing α_0 from $3.69 \times 10^{-15} \sim 2.13 \times 10^{-12}$ to $2.85 \times 10^{-15} \sim 1.77 \times 10^{-12}$ for particles with $2 \leq d_p \leq 100$ nm. Good agreement between the calculated particle collection efficiency and the experimental data was found to correspond to the ion molecular weight of 0.140 kg/mol. Choosing the minimum ion molecular weight of 0.05 kg/mol leads to a less than 10 % deviation between the calculated particle collection efficiencies. For example, when the applied voltage is -15.5 kV, the calculated particle penetration ranges from 12.4~17.7 % for 10 nm particles, and 40.8~43.2 % for 50 nm particles, corresponding to the molecular weight range of 0.05 to 0.14 kg/mol.

To elucidate the aerosol penetration due to the partial charging effect, the concentration distribution of 6 nm particles carrying 0 and 1 charge was calculated at an applied voltage of -15.5 kV and an aerosol flow rate of 100 L/min, as shown in Figure 4.18. In Figure 4.18 (a), high concentration of particles carrying zero charge appears at the outlet of the dry ESP. These uncharged particles can't be collected by electrostatic forces on the collection electrodes, and thus penetrate through the ESP. The average outlet concentration was calculated to be 8.40×10^7 for uncharged particles and $3.54 \times 10^6 \text{ m}^{-3}$ for singly charged particle, leading to an average particle charge of 0.04 and an aerosol penetration of 33.0 % when the inlet particle concentration was $1.67 \times 10^8 \text{ m}^{-3}$.

When the applied voltage was increased to -21.5 kV, the partial charging effect was less severe than that at the applied voltage of -15.5 kV. It is because the electric field strength and

the ion concentration become higher and the particle collection efficiency is enhanced.

For particles with $d_p \geq 20$ nm at the applied voltage of -15.5 kV, the average particle charge was found to increase from 0.99 to 6.64 with increasing particle diameter from 20 to 100 nm. The partial charging effect on the collection efficiency became insignificant. In this size range, high aerosol penetration was due to weak electric field strength, which can be reduced by applying higher electric field strength in the ESP.



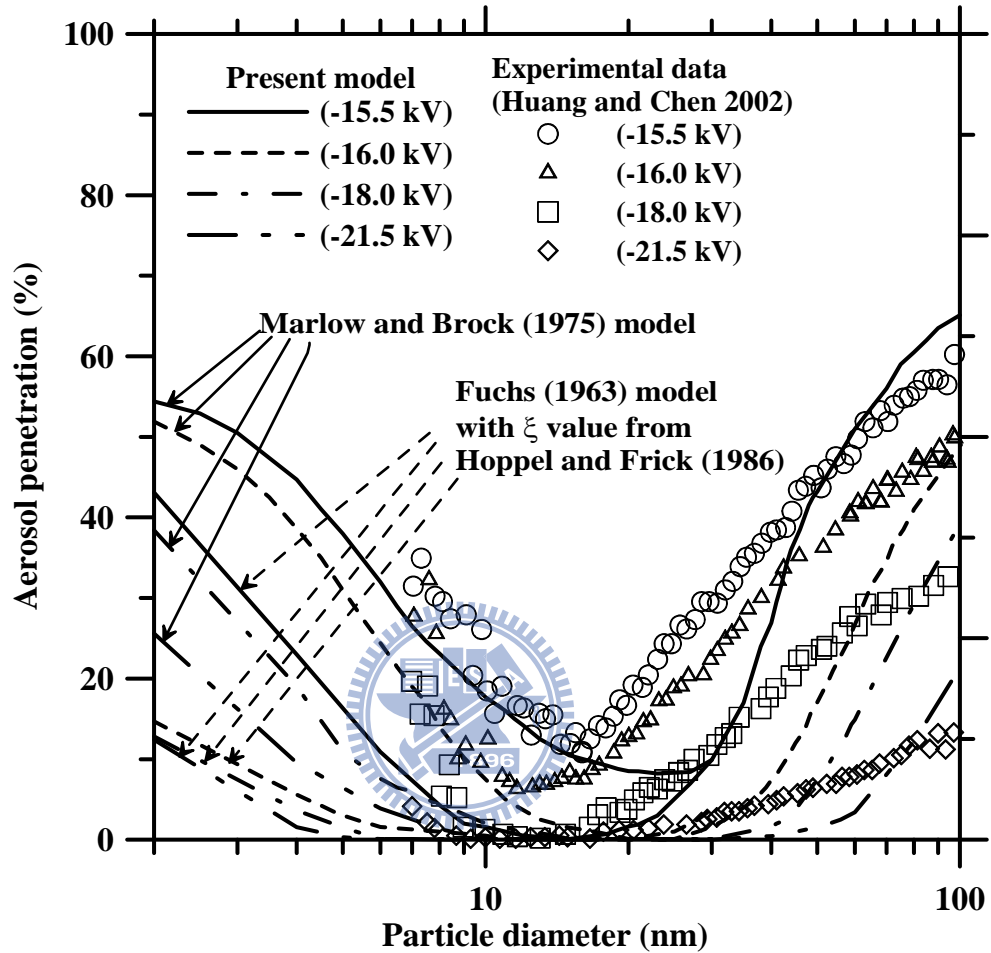


Figure 4.17 Comparison of particle collection efficiency in the single-stage wire-in-plate dry ESP between numerical results and experimental data in Huang and Chen (2002) at the aerosol flow rate of 100 L/min.

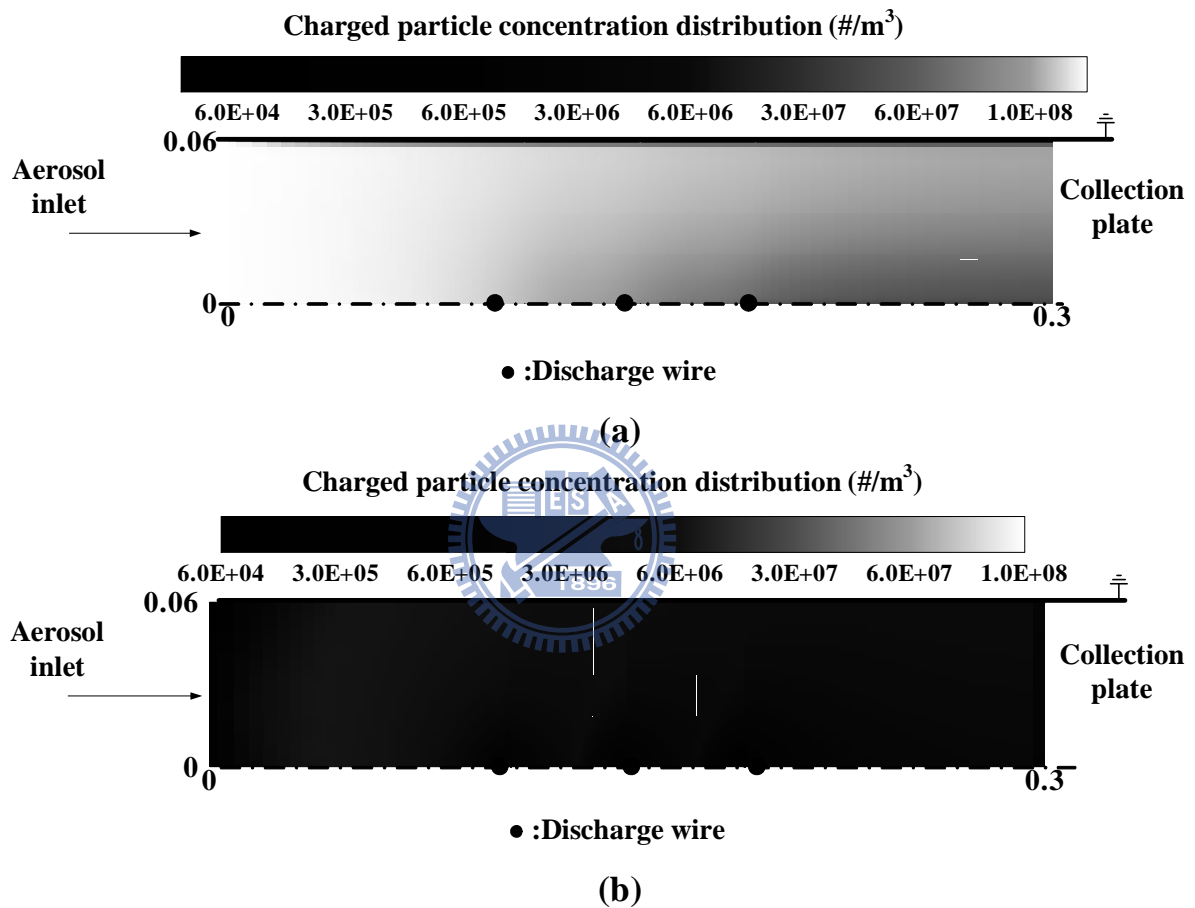


Figure 4.18 Number concentration distribution of 6 nm particles carrying 0 and 1 charges in the single-stage wire-in-plate dry ESP (Huang and Chen 2002) when the applied voltage and air flow rate was -15.5 kV and 100 L/min, respectively. (a) 0 charge, (b) 1 charge.

4.3.3 Comparing the particle collection efficiency in the present wet ESP

Figure 4.19 shows comparison of the particle collection efficiency between numerical values and experimental data for 10 and 50 nm NaCl particles in the present single-stage wire-in-plate wet ESP. As the figure shows, when Fuchs model is adopted to calculate the particle charge, the simulated collection efficiencies at the applied voltage of +3.6~+4.3 kV agree with the experimental data with deviation of 0.10-10.8 % and 4.50-14.1 % for 10 and 50 nm particles, respectively. For 10 nm particles, when the model of Marlow and Brock (1975) is used to calculate the particle charge, reasonable agreement between the predicted and the experimental collection efficiency is also obtained with a deviation of 0.10-8.71 %.

In Figure 4.19, the effect of the ion molecular weight on the particle collection efficiency is also shown. Within the range of positive ion molecular weight from 0.109 to 0.290 kg/mol, the corresponding α_0 and α_1 can be calculated based on Fuchs theory as shown in Table 4.3. The calculated collection efficiency ranges from 74.2~79.4 % to 100 % for 10 nm particles, and from 40.9~44.9 % to 100 % for 50 nm particles, respectively, at the applied voltage of +3.7~4.3 kV. For comparison, the particle collection efficiency ranges from 60.0~64.4 % to 100 % for 10 nm particles at the applied voltage of +3.7~4.3 kV, based on Marlow and Brock's charging model. Again, it shows that there are no significant differences in the particle collection efficiency when different ion molecular weights are used.

Figures 4.20 (a)-(c) show the number concentration distribution of 50 nm particles carrying 0, 1 and 4 charges in the wet ESP at an applied voltage of +3.7 kV, an air flow rate of 5 L/min, and an ion molecular weight of 0.290 kg/mol. As shown in the figure, the concentration of particles with 0 charge decreases with increasing x distance from the entrance of the wet ESP, where some particles are charged by positive ions to acquire 1-4 charges and some of which are collected by the collection electrodes due to electrical force. This can be observed from the location of the highest charged particle concentration near the

collection electrode surface as shown in Figures 4.20 (b) and (c). Besides, large amount of particles carrying 1~4 charges penetrate through the present wet ESP because the electrostatic force is not high enough for collecting the charged particles. The average concentration of particles at the exit of the wet ESP was calculated to be 8.66×10^4 , 1.27×10^7 , 4.48×10^7 , 1.03×10^7 , and $2.60 \times 10^5 \text{ m}^{-3}$ for particles carrying 0-4 charges, respectively, leading to an average outlet particle charge of 1.97 when the inlet particle concentration was $8.70 \times 10^7 \text{ m}^{-3}$. When the applied voltage was increased to +4.3 kV, the collection efficiency reached up to 99 % and the particles carried an average charge of 3.19.

For 10 nm particles, particles with an average outlet concentration of 4.62×10^7 and $2.79 \times 10^6 \text{ m}^{-3}$ carrying with 0 and 1 charge, respectively, were found to penetrate through the wet ESP operating at + 3.7 kV. The average outlet particle charge was 0.06, or partial charging occurred which led to a decrease of particle collection efficiency (Figure 4.19). When the applied voltage was increased to +4.3 kV, the partial charging effect became insignificant, and the collection efficiency of particles with an average charge of 2.00 reached up to 99 %.

Table 4.3. Combination coefficient of positive ion with 50 and 10 nm NaCl particles calculated by using different ion molecular weights shown in Table 1 based on Fuchs theory.

$d_p=50$ nm			$d_p=10$ nm		
M_{ion} (kg/mol) positive ion	α_0 (m ³ /s)	α_1 (m ³ /s)	M_{ion} (kg/mol) positive ion	α_0 (m ³ /s)	α_1 (m ³ /s)
0.109	7.36E-13	1.97E-13	0.109	3.42E-14	1.00E-15
0.130	7.03E-13	1.86E-13	0.130	3.21E-14	9.81E-16
0.140	6.88E-13	1.81E-13	0.140	3.13E-14	9.71E-16
0.148	6.78E-13	1.78E-13	0.148	3.07E-14	9.62E-16
0.150	6.75E-13	1.77E-13	0.150	3.05E-14	9.60E-16
0.200	6.22E-13	1.60E-13	0.200	2.73E-14	9.03E-16
0.290	5.55E-13	1.39E-13	0.290	2.35E-14	8.13E-16

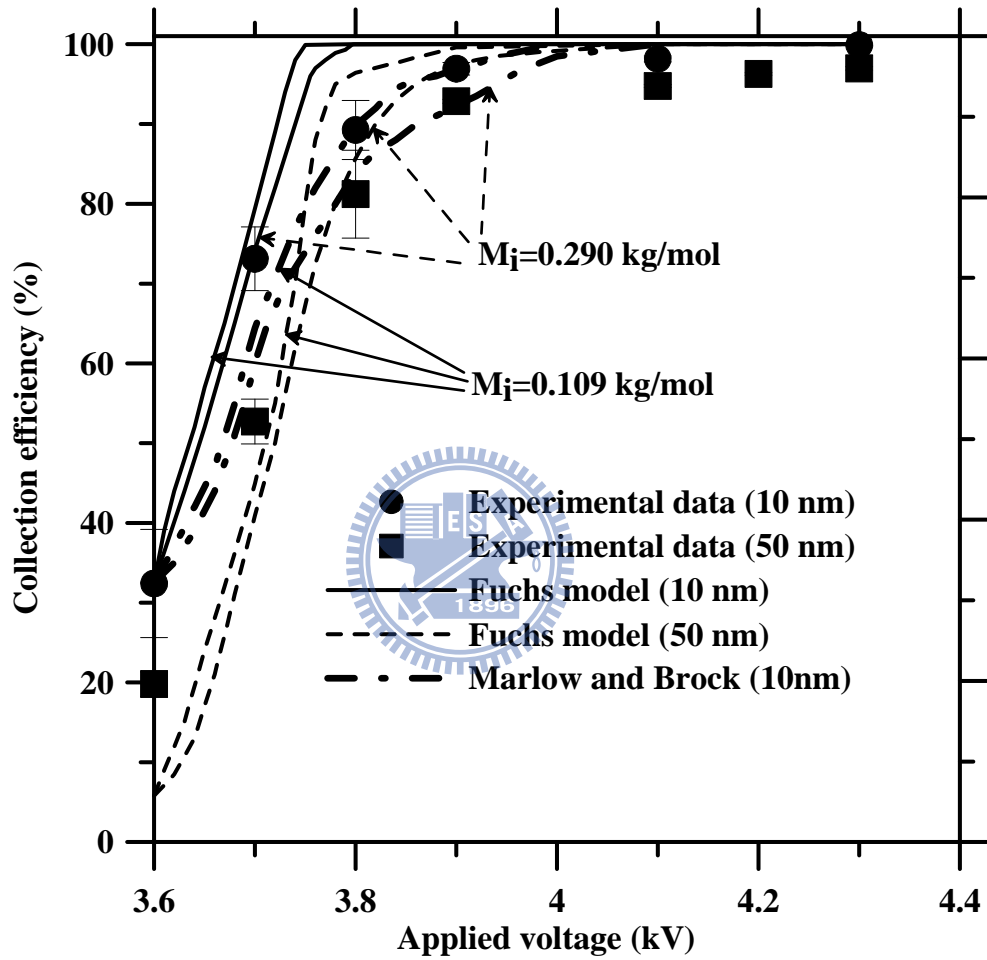


Figure 4.19 Comparison of particle collection efficiency in the single-stage wire-in-plate wet ESP between numerical results and experimental data at the air flow rate of 5 L/min.

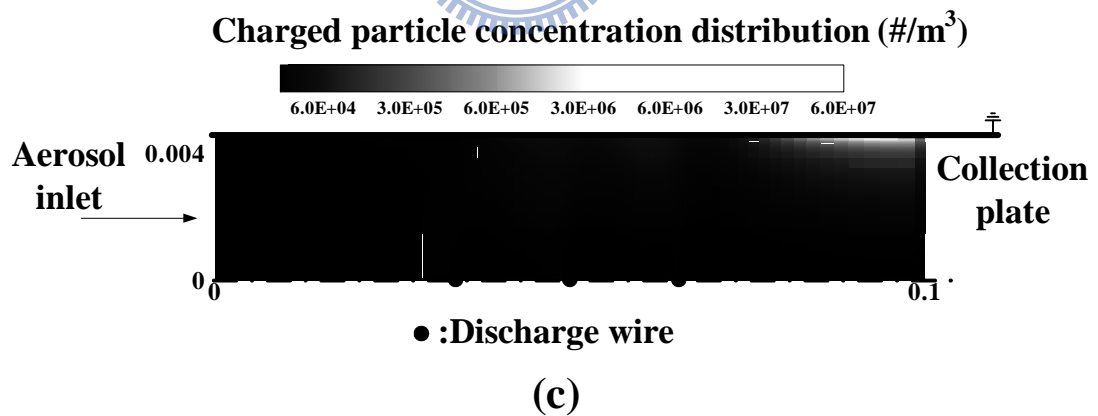
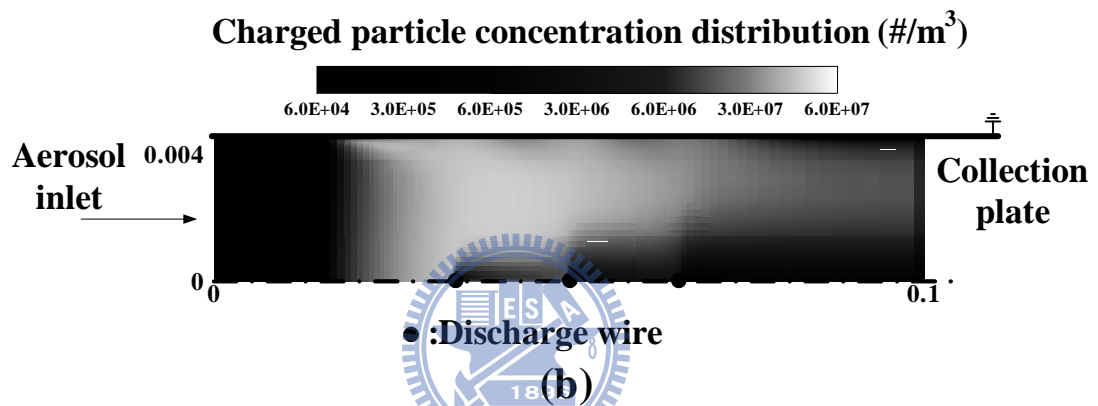
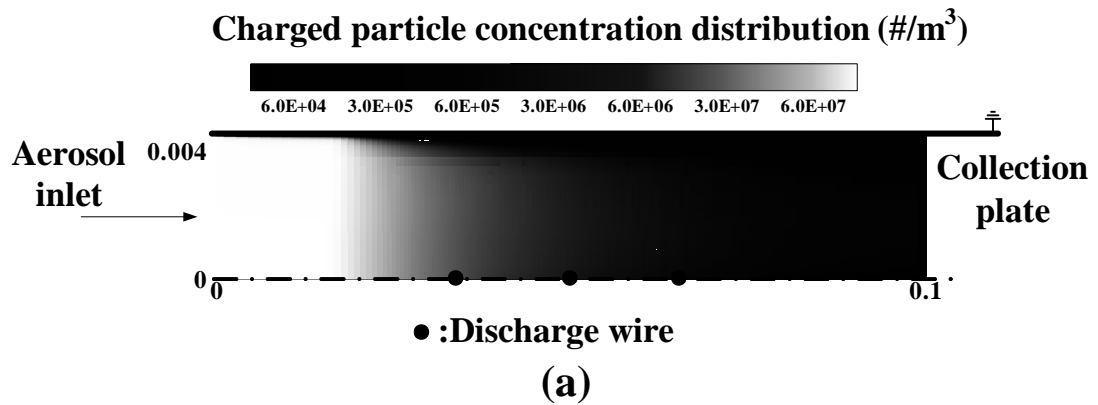


Figure 4.20 Number concentration distribution of 50 nm particles carrying 0-4 charges in the single-stage wire-in-plate wet ESP when the applied voltage and air flow rate was +3.7 kV and 5 L/min, respectively. (a) 0 charge, (b) 1charge, (c) 4 charges. (Note: The scale in y direction is magnified 4.5 times relative to that in x direction.

Figure 4.21 shows comparison of the particle collection efficiency between numerical values and experimental data for silver particles in the size range of 5.23~107.5 nm. As the figure shows, the particle collection efficiency decreased from 64.2 to 36.9 % and 86.9 to 63.7 % with decreasing particle diameter from 45.3 to 8.06 nm when the applied voltage were +3.7 and +3.8 kV, respectively. The collection efficiency increased from 38.2 to 54.7 % and 63.7 to 68.8 % for particles with diameter of 5 nm when the applied voltages were +3.7 and +3.8 kV, respectively. It is because the higher diffusion deposition of 5 nm particles than the particles with $d_p \geq 8.06$ nm. When Fuchs model is adopted to calculate the particle charge, the simulated collection efficiencies at the applied voltage from +3.7 to +3.9 kV agree with the experimental data with deviation of 0.70-18.9 %, 0.10-19.8 %, and 0.10-4.80 %, respectively. At the applied voltage of +3.7-+3.9 kV, the partial charging effect on the collection efficiency for particles with $d_p \leq 20$ nm was found. When the applied voltage was increased to +4.3 kV, the partial charging effect on the collection efficiency was diminished due to high electric field strength and ion concentration, and the particle collection efficiency reached up to 97.7-99.8 %.

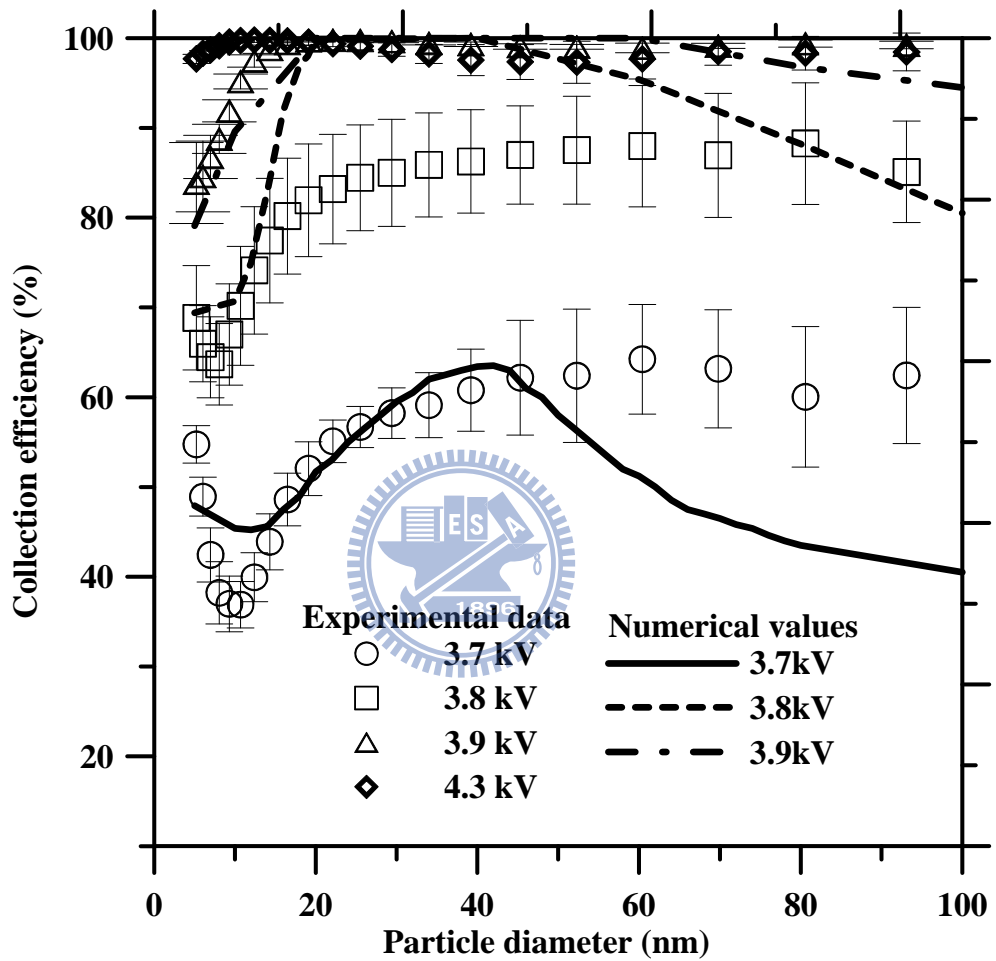


Figure 4.21 Collection efficiencies of the polydisperse silver particles in the present wet ESP when the aerosol flow rate and the applied voltage are 5 L/min and +3.7-+3.9kV, respectively. Each test was repeated 6 times.

4.4 Numerical modeling of a pilot scale wet ESP

Typical design parameters for ESPs are shown in Table 4.4. Based on the range of parameters as shown in this table, the effect of different parameters on particle collection efficiency for ESPs was investigated. Figure 4.22 shows turbulent flow field in the simulated pilot scale wet ESP, which is 750 mm in length, 300 mm in width, and 6 m in height.

Figure 4.23 shows collection efficiencies of particles in the pilot scale wet ESP under different design parameters. When the applied voltage was 70 kV, the air velocity was 1 m/s, the wire to wire spacing was 75 mm, the wire to plated spacing was 150 mm ($s_y/s_x=2.0$), and the diameter of 3 discharge wires was 2.5 mm, the collection efficiency for particles with $5 \leq d_p \leq 100$ nm was calculated to be 14.5-29.3 %. When the ratio of s_y/s_x was changed from 2.0 to 1.0 by shortening the wire to plate spacing from 150 to 75 mm, the collection efficiency for particles of the same size range was increased to 22.5-58.4 %. It is obvious that a decrease of the wire to plate spacing results in an increase in particle collection efficiency.

When the wire to wire spacing was 75 mm, wire to plate spacing was 75 mm, and the air velocity was 0.6 m/s, the particle collection efficiency was increased to 62.3-94.8 % by adding three additional discharge wires with the diameter of 2.5 mm, as shown in Figure 4.22. Under these conditions, the collection efficiency was calculated to slightly decrease to 56.6-92.5 % when the ratio of s_y/s_x was 1.5 by shortening the wire to wire spacing from 75 to 50 mm. This is because the average current density at collection plates decreases with decreasing wire to wire spacing at a fixed applied voltage as shown in MacDonald et al. (1977).

The particle collection efficiency of the pilot scale ESP with s_y/s_x of 1.0 can be further increased to 64-96.2 % by reducing the wire diameter to 1.3 mm at the air velocity of 0.6 m/s. This result can be attributed to the fact that a decrease in the wire diameter leads to a lower starting voltage and higher average current density at collection plates for the same applied voltages (MacDonald et al. 1977).

In summary, at a fixed applied voltage and aerosol velocity, the collection efficiency of ESPs can be increased by reducing the wire diameter, increasing the number of discharge wires, and decreasing the wire to plate spacing.

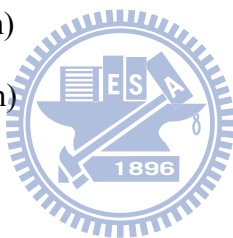
Figure 4.24 shows the comparison of the collection efficiency for particles with $5 \leq d_p \leq 100$ nm in the ESP which have 3-12 discharge wires (diameter=2.5 mm). When the collection efficiencies in the ESP which has n discharge wires, η_n , were calculated by using the present numerical model, the collection efficiency in the ESP which has m discharge wires, η_m , can be predicted by

$$\eta_m (\%) = [1 - (1 - \eta_n)^{m/n}] \times 100\% \quad (4.3)$$

where m is a multiple of n. As shown in Figure 4.24 (a), the simulated collection efficiencies in the ESP with 6 discharge wires are in good agreement with those calculated by using Equation (4.3). Thus, Equations (4.3) can be used to predict particle collection efficiency in the ESP with multiple discharge wires. Figure 4.24 (b) shows simulated particle collection efficiency obtain by using the present model in the ESP with 6 discharge wires, and the collection efficiency calculated by using Equation (4.3) in the ESP with 12 discharge wires. As shown in this Figure, the nanoparticle collection efficiency can be increased to 87.84-99.9% by adding additional 6 discharge wires without changing other parameters.

Table 4.4 Typical design parameter for ESPs (http://yosemite.epa.gov/oaqps/EOGtrain.nsf/DisplayView/SI_412A_0-5?OpenDocument).

Parameter	Range
Wire to wire spacing (m)	0.15-0.3
Wire to plate spacing (m)	0.075-0.15
Wire diameter (mm)	1.3-3.8
Aerosol velocity (m/s)	0.6-2



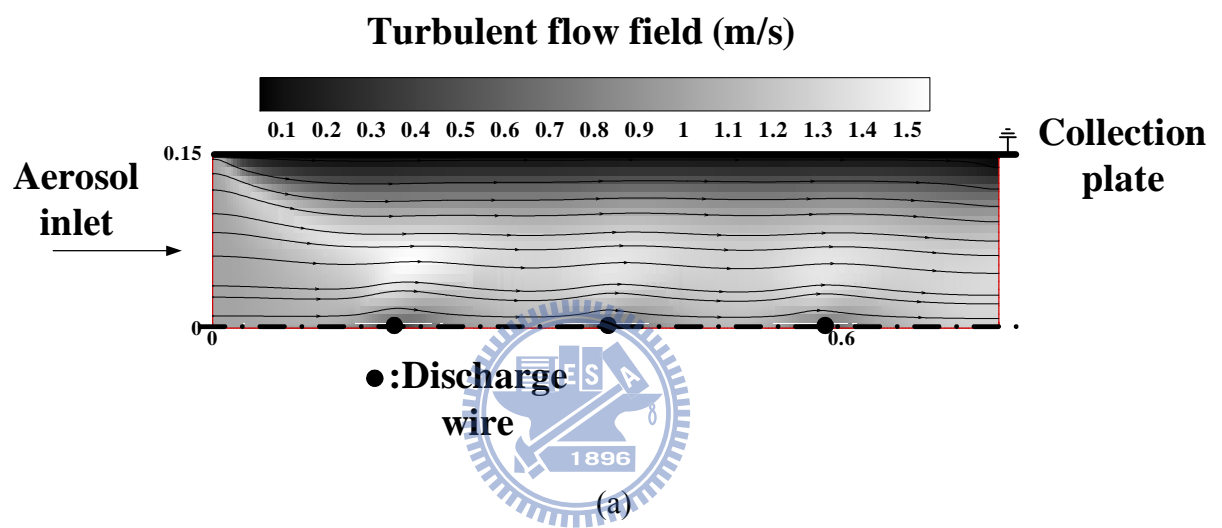


Figure 4.22 Turbulent flow field in the simulated pilot scale wet ESP, (a) simulated result calculated by using SIMPLER algorithm (Patankar 1980).

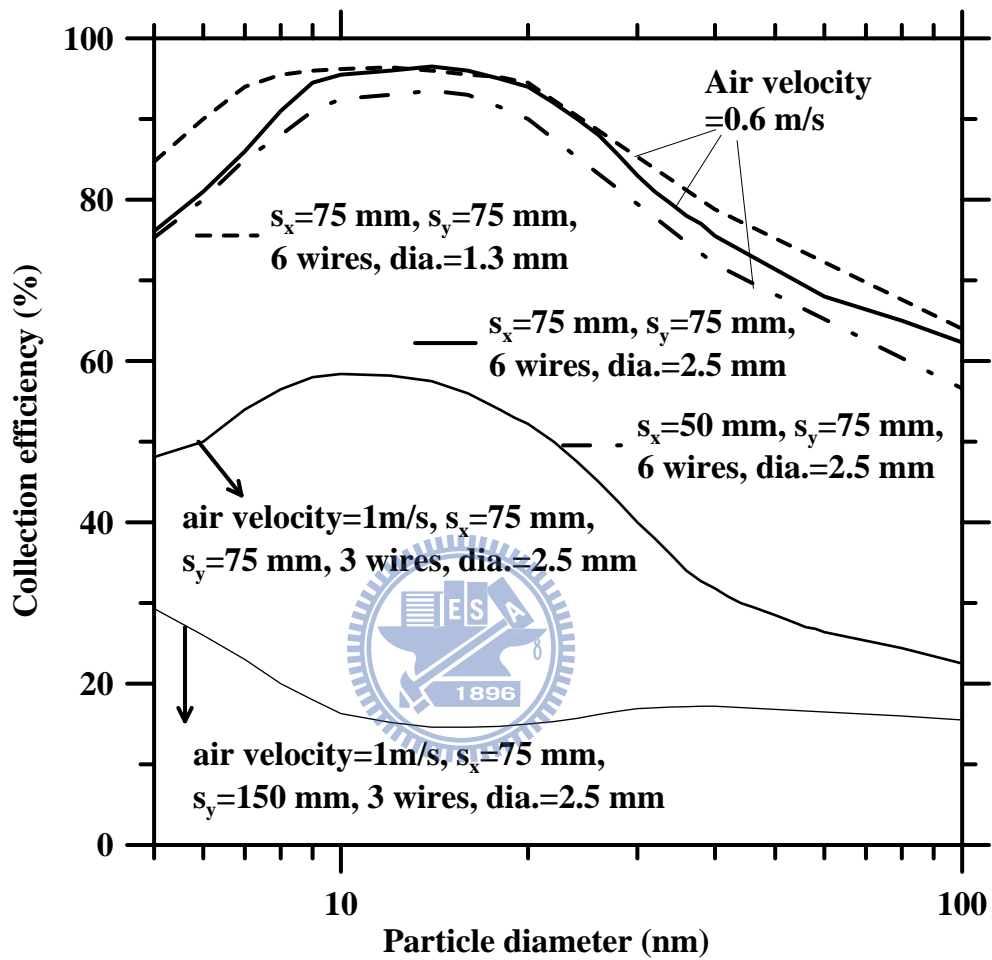
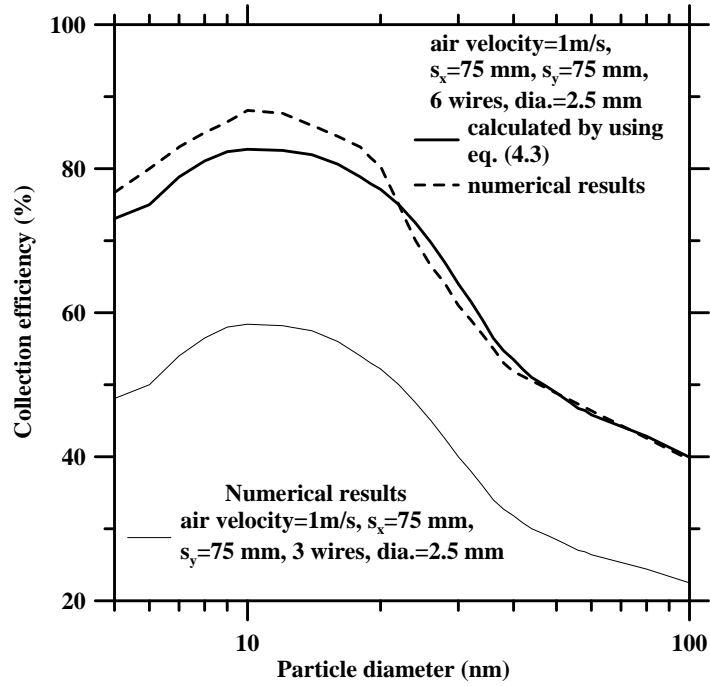
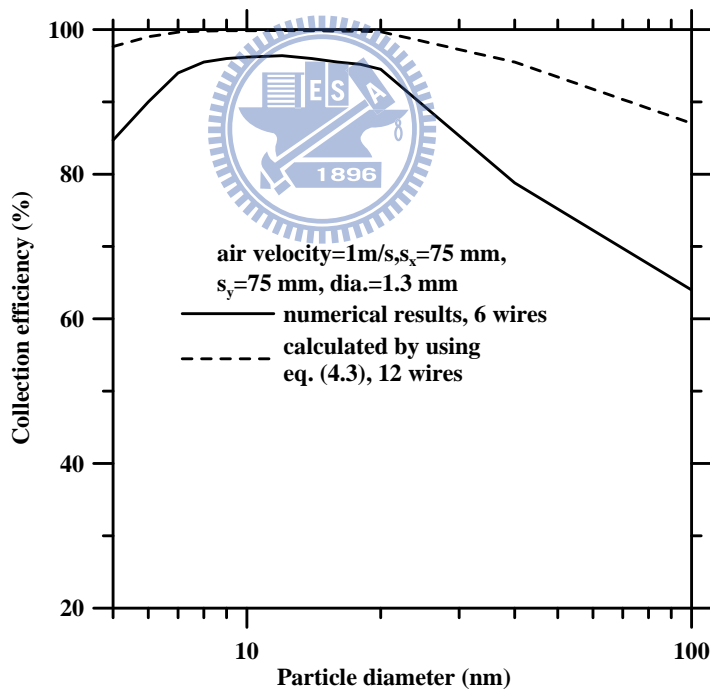


Figure 4.23 Collection efficiencies of particles in the pilot scale wet ESP under different design parameters. The applied voltage was 70 kV.



(a)



(b)

Figure 4.24 Comparison of the collection efficiency for particles with $5 \leq d_p \leq 100$ nm in ESPs which have 3, 6, or 9 discharge wires (diameter=2.5 mm). (a) The ESPs have 3 and 6 wires, (b) The ESP have 6 and 9 wires.

CHAPTER 5

CONCLUSIONS AND RECOMMENDATIONS

5.1 Conclusions

This study designed and developed a parallel-plate single-stage wet ESP to control fine and nanosized particles without the need of rapping. Sand-blasted copper plates coated with TiO₂ nanopowders were used as collection plates to enhance hydrophilicity for the scrubbing water film. A pulse jet valve was used to clean the corona wires regularly. Corn oil particles were used to conduct particle collection efficiency experiments with different applied voltages and aerosol flow rates under an initially clean condition. TiO₂ nanopowder was used to create heavy loading conditions to compare the particle collection efficiency of the dry and present wet ESP.

The experimental results showed that the present wet ESP can be operated to efficiently control fine and nanosized particles at an aerosol flow rate of 5 L/min, applied voltage of 4.3 kV and scrubbing water flow rate per collection surface area of 2.31 L/min/m² under the initially clean condition.

Under heavy loading conditions with a TiO₂ loading quantity of 0.6±0.06 g/hr/plate, the dry ESP particle collection efficiency decreased below 35 % for corn oil particles in the electrical mobility diameter range of 16.8-615 nm after two hours of loading. Under the same loading conditions, the collection efficiency for corn oil particles in the same size range was measured to be as high as 94.9-99.9 % for the wet ESP. This is because the uniform scrubbing water film and the pulse jet can effectively clean the collection plates and the corona wires, respectively, to keep the collection efficiency high.

For practical applications, the present lab-scale wet ESP could be scaled up to a size that allows treatment at high aerosol flow rates. When particles deposit on the collection electrode in the wet ESP, they will be removed by scrubbing water and will not accumulate on the

collection electrode. Therefore, it is expected that the present wet ESP can be used to control fine and nanosized particulates emitted from nanomaterial manufacturing processes without the typical problems associated with dry ESPs, such as particle reentrainment due to rapping and back corona due to the formation of the dust cake with high specific resistivity. In addition, since the particle collection efficiency of the present wet ESP is very high, it can be used as airborne particle samplers. The collected liquid samples can be analyzed further for chemical compositions.

In order to predict the particle collection efficiency in ESPs, a detailed 2-D mathematical model was developed to predict the flow field, the electric field strength, the ion concentration, the charged particle concentration distribution in the single-stage wire-in-plate ESPs. The predicted electric field strength and ion concentration distribution was calculated to match with analytical solutions in a benchmark problem of the wire-in-tube ESP. The comparison of the numerical collection efficiencies based on Fuchs charging model (1963) and the experimental data of the dry ESP in Huang and Chen (2002) shows reasonable agreement with a deviation smaller than 20 % for particles with $30 \leq d_p \leq 100$ nm. For $d_p < 20$ nm, the predicted aerosol penetration based on the charging model of Marlow and Brock (1975) were found to match better with the experimental data than that based on Fuchs charging model. Aerosol penetration was found to increase with decreasing particle diameter from 20 to 2 nm due to the partial charging effect. In the wet ESP of Lin et al. (2010), the predicted collection efficiencies are also shown to be in good agreement with the experimental data for 50 and 10 nm particles, respectively.

The numerical results show that partial charging can occur which reduces collection efficiency for particles smaller than 20 nm when the applied voltage is not high enough. Increasing the applied voltage of the ESPs can minimize the partial charging effect and increases the nanoparticle collection efficiency to nearly 100 %.

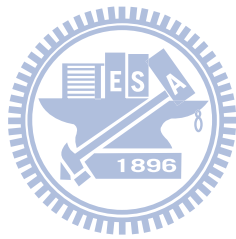
For particles with $0.1 \leq d_p \leq 10$ μm , the numerical model based on Lagrangian method

was found to predict particle collection efficiency accurately comparing with the experimental data in Huang and Chen (2002) and Chang and Bai (1999). This is because the combined charging model can be used to predict particle charges accurately in the continuum charging regime ($Kn \ll 1$).

The present numerical model has been validated carefully and can be used to facilitate the design and scale-up of the single-stage wire-in-plate wet ESPs to control the emission of fine and nanosized particles. Furthermore, the present model provides detailed spatial distribution of charged nanoparticles with the consideration of nonuniform distribution of flow field, electric field strength and ion concentration, which enables the design of efficient electrostatic nanoparticle samplers for sampling and characterization of nanoparticles.

5.2 Recommendations

1. In the present numerical model, the effect of the particle reentrainment, particle loading, EHD flow and the particle shape on the collection efficiency in ESPs was not taken into consideration. To investigate the effect of the above physical properties on the particle collection efficiencies in ESPs, more improvements in the present numerical model are need.
2. Different shapes of wires such as spiked band, pipe and double-spike, and pipe and double-spike were used to decrease the corona onset voltage and increase the ion concentration due to those high roughness factors (Jedrusik and Swierczok 2006). The effect of the discharge wires' shapes on the particle collection efficiency in ESPs should be further studied.
3. The numerical model for predicting particle collection efficiency in ESPs which have discharge wires with irregular shape is still in need. A 3-D numerical model needs to be developed to simulate the electric field and ion concentration distribution generated by



REFERENCES

- Adachi, M., Kousaka, Y., and Okuyama, K. (1985). Unipolar and Bipolar Diffusion Charging of Ultrafine Aerosol Particles, *J. Aerosol. Sci.* 16:109-123.
- Aliat, A., Hung, C. T., Tsai, C. J., and Wu, J. S. (2009). Implementation of Fuchs Model of Ion Diffusion Charging of Nanoparticles Considering the Electron Contribution in DC-Corona Chargers in High Charge Densities, *J. Phys. D: Appl. Phys.* 42:1-10.
- Alonso, M., Santos J. P., Hontañón E., and Ramiro E. (2009). First Differential Mobility Analysis (DMA) Measurements of Air Ions Produced by Radioactive Source and Corona, *Aerosol Air Qual. Res.* 9:453-457.
- Altman, R., Offen, G., Buckley, W., and Ray, I. (2001a). Wet Electrostatic Precipitation: Demonstrating Promise for Fine Particulate Control-Part I. *Power Eng.* 105:37-39.
- Altman, R., Buckley, W., and Ray, I. (2001b). Wet Electrostatic Precipitation: Demonstrating Promise for Fine Particulate Control-Part II. *Power Eng.* 105: 42-44.
- Asbach, C. (2004). Development and evaluation of a highly efficient gas particle partitioner with minimal effect on the gas composition. Ph. D. thesis, University Duisburg-Essen.
- Bayless, D. J., Alam, M. K., Radcliff, R., and Caine, J. (2004). Membrane-based Wet Electrostatic Precipitation. *Fuel Process. Technol.* 85:781-798.
- Chang, C. L., and Bai, H. (1999). An Experimental Study on the Performance of a Single Discharge Wire-Plate Electrostatic Precipitator with Back Corona. *J. Aerosol Sci.* 30:325-340.
- Cooperman, G. (1981). A New Current-Voltage Relation for Duct Precipitators Valid for Low and High Current Densities, *IEEE Trans. Ind. Appl.* IA-17:236-239.
- Fjeld, R. A., and McFarland, A. R. (1986). Continuum Field-Diffusion Theory for Bipolar

- Charging of Aerosols, *J. Aerosol Sci.* 14:541-556.
- Fuchs, N. A. (1947). The Charges on the Particles of Aerocolloids, *Izv. Akad. Nauk. SSSR, Ser. Geogr. Geofiz.* 11:341-348.
- Fuchs, N. A., (1963). On the Stationary Charge Distribution on Aerosol Particles in a Bipolar Ionic Atmosphere, *Geophys. Pura. Appl.* 56:185-193.
- Goo, J. G., and Lee, J. W. (1997). Stochastic Simulation of Particle Charging and Collection Characteristics for a Wire-Plate Electrostatic Precipitator of Short Length. *J. Aerosol Sci.* 28:875-893.
- Griffitt, R. J., Weil, R., Hyndman, K. A., Denslow, N. D., Powers, K., Taylor, D., and Barber, D. S. (2007). Exposure to Copper Nanoparticles Causes Gill Injury and Acute Lethality in Zebrafish (*Danio rerio*), *Environ. Sci. Technol.* 41:8178-8186.
- Hoppel, W. A., and Frick, G. M. (1986). Ion-Aerosol Attachment Coefficients and the Steady-State Charge-Distribution on Aerosols in A bipolar Ion Environment, *Aerosol Sci. Technol.* 5:1-21.
- Hoppel, W. A., and Frick, G. M. (1990). The Nonequilibrium Character of the Aerosol Charge-Distributions Produced by Neutralizers, *Aerosol Sci. Technol.* 12:471-496.
- Hinds, W. C. (1999). *Aerosol Technology*. John Wiley & Sons, New York, p. 30.
- Hinds, W. C. (1999). *Aerosol Technology*. John Wiley & Sons, New York, p. 245-257.
- Huang, S. H., and Chen, C. C. (2002). Ultrafine Aerosol Penetration through Electrostatic Precipitators. *Environ. Sci. Technol.* 36:4625-4632.
- Huang, S. H., and Chen, C. C. (2003). Loading Characteristics of a Miniature Wire-Plate Electrostatic Precipitator. *Aerosol Sci. Technol.* 37:109-121.
- Hussin, A., Scheibel, H. G., Becker, K. H., and Porstendoerfer, J. (1983). Bipolar Diffusion

- Charging of Aerosol-Particles .1. Experimental Results within the Diameter Range 4-30-nm, *J. Aerosol Sci.* 14:671-677.
- Kim, H. H., Yamamoto, I., Takashima, K., Katsura, S., and Mizuno, A. (2000). Incinerator Flue Gas Cleaning Using Wet-Type Electrostatic Precipitator. *J. Chem. Eng. JPN.* 33:669-674.
- Jedrusik, M., Swierczok, A. (2006). Experimental Test of Discharge Electrode for Collecting of Fly Ash of Different Pysico-Chemical Properties. (<http://www.isesp.org/ICESP%20X%20PAPERS/PDFS/Paper%202B1Jedrusik.pdf>)
- Lawless, P. A., (1996). Particle Charging Bounds, Symmetry Relations, and an Analytic Charging Rate Model for the Continuum Regime, *J. Aerosol. Sci.* 27:191-215.
- Li, M., and Christofides, P. D. (2006). Collection Efficiency of Nnanosize Particles in a Two-Stage Electrostatic Precipitator, *Ind. Eng. Chem. Res.* 45:8484-8491.
- Lin, G. Y., Tsai, C. J., Chen, S. C., Tzu, M. C., and Li, S. N. (2010). An Efficient Single-Stage Wet Electrostatic Precipitator for Fine and Nanosized Particle Control, *Aerosol Sci. Technol.* 44:38-45.
- Liu, Q., Wu, X., Wang, B., and Liu, Q. (2002). Preparation and Super-Hydrophilic Properties of TiO₂/SnO₂ Composite Thin Films. *Mater. Res. Bull.* 37:2255-2262.
- Lundgren, D. A., Marple, V. A., and Herrick, R. A. (1995). Electrostatic Precipitator Assembly. U.S. Patent 5 395 430.
- Marek, K., Jaroslaw, D., and Jerzy, M. (2005). Particle Precipitation Efficiency in an Electrostatic Precipitator. *J. Electrostat.* 63:761-766.
- Marlow, W. H. and Brock, J. R. (1975). Unipolar Charging of Small Aerosol Particles, *J. Coll. Interface Sci.* 50:32-38.

- Marquard, A., Kasper, M., Meyer, J., and Kasper, G. (2005). Nanoparticle Charging Efficiencies and Related Charging Conditions in a Wire-Tube ESP at DC Energization, *J. Electrostat.* 63:693-698.
- McDonald, J. R., Smith, W. B., and Spencer, H. W. III (1977). A mathematical model for calculating electrical conditions in wire-duct electrostatic precipitation devices, *J. Appl. Phys.* 48:2231-2243.
- Mohnen, V. A. (1977). Electrical Processes in Atmospheres. D. Steinkopff, Darmstadt. P.1-17.
- Oglesby, S. J., and Nichols, G. B. (1978). *Electrostatic Precipitation: Computer model*, Marcel Dekker, Inc., New York, p. 157-210.
- Oberdörster, G., Oberdörster, E., and Oberdörster, J. (2005). Nanotoxicology: An Emerging Discipline Evolving from Studies of Ultrafine Particles, *J. Environ. Health Perspect.* 113:823-839.
- Pasic, H., Alam, M. K., and Bayless, D. J. (2001). Membrane Electrostatic Precipitator, U.S. Patent, 6 231 643 B1.
- Park, J. H. and Chun, C. H. (2002). An Improved Modelling for Prediction of Grade Efficiency of Electrostatic Precipitators with Negative Corona, *J. Aerosol. Sci.* 33:673-694.
- Park, S. J., Kim, S. S. (2000) Electrohydrodynamic Flow and Particle Transport Mechanism in Electrostatic Precipitators with Cavity Walls, *Aerosol. Sci. Technol.* 33:205-221.
- Park, S. J., Kim, S. S. (2003). Effects of Electrohydrodynamic Flow and Turbulent Diffusion on Collection Efficiency of an Electrostatic Precipitator with Cavity Walls, *Aerosol. Sci. Technol.* 37:574-586.

- Patankar, S. V. (1980). *Numerical Heat Transfer and Fluid Flow*, Washington: Hemisphere Publishing Co.
- Pauthenier, M., and Moreau-Hanot, M. (1932). Charging of Spherical Particles in an Ionizing Field. *J. Phys. Radium* 3:590-613.
- Pui D., Y. H., Fruin, S., and McMurry, P. H. (1988). Unipolar Diffusion Charging of Ultrafine Aerosols, *Aerosol Sci. Technol.* 8:173-187.
- Reischl, G. P., Mäkelä, J. M., Karch, R., and Nucid, J. (1996). Bipolar Charging of Ultrafine Particles in the Size Range Below 10 nm, *J. Aerosol. Sci.* 27:931-949.
- Richards, J. (1995). *Control of Particulate Emissions*. APTI Course 413; EPA: Washington, DC, p. 6-20-6-23.
- Saiyasitpanich, P., Keener, T. C., Lu, M., Khang, S. J., and Evans, D. E. (2006). Collection of Ultrafine Diesel Particulate Matter (DPM) in Cylindrical Single-Stage Wet Electrostatic Precipitators. *Environ. Sci. Technol.* 40:7890-7895.
- Saiyasitpanich, P., Keener, T. C., Khang, S. J., and Lu, M. (2007). Removal of Diesel Particulate Matter (DPM) in a Tubular Wet Electrostatic Precipitator. *J. Electrostat.* 65:618-624.
- Salah, N. H., Bouhelassa, M., Bekkoushe, S., and Boultif, A. (2004). Study of Photocatalytic Degradation of Phenol. *Desalination.* 166:347-354.
- Scheibel, H. G., and Porstendörfer, J. (1982). Generation of Monodisperse Ag- and NaCl Aerosols With Particle Diameters between 2 and 300 nm. *J. Aerosol Sci.* 14:113-126.
- Talaie, M. R., Fathikaljahi, J., Taheri, M., and Bahri, P. (2001). Mathematical Modeling of Double-Stage Electrostatic Precipitators Based on a Modified Eulerian Approach, *Aerosol Sci. Technol.* 34:512-519.

- Talaie, M. R. (2005). Mathematical Modeling of Wire-Duct Single-Stage Electrostatic Precipitators, *J. Hazard. Mater.* B124:44-582.
- Tsai, C. J., Lin, G. Y., and Chen, S. C. (2008). A parallel Plate Wet Denuder for Acidic Gas Measurement. *AIChE J.* 54:2198-2205.
- Tsai, C. J., Wu, C. H., Leu, M. L., Chen, S. C., Huang, C. Y., Tsai, P. J., and Ko, F. H. (2009). Dustiness test of nanopowders using a standard rotating drum with a modified sampling train. *J. Nanopart. Res.* 11:121-131.
- U.S. Environmental Protection Agency. (2003). Air Pollution Control Technology Fact Sheet; EPA-452/F-03-030, EPA: Washington, DC.
- Wen, H. Y., Reischl, G. P., and Kasper, G. (1984). Bipolar Diffusion Charging of Fibrous Aerosol-Particles .1. Charging Theory, *J. Aerosol. Sci.* 15:89-101.
- Wiedensohler, A., and Fissan, H. J. (1991). Bipolar Charging-Distributions of Aerosol-Particles in High-Purity Argon and Nitrogen, *Aerosol Sci. Technol.* 14:358-364.
- Wiedensohler, A., Lütkenmeier, E., Feldpausch, M., and Helsper, C. (1986). Investigation of the Bipolar Charge-Distribution at Various Gas Conditions, *J. Aerosol. Sci.* 17:413-416.
- Yoo, K. H., Lee, J. S., and Oh, M. D. (1997). Charging and Collection of Submicron Particles in Two-Stage Parallel-Plate Electrostatic Precipitators. *Aerosol. Sci. Technol.* 27:308-323.
- Yu, J., Zhao, X., Zhao, Q., and Wang, G. (2001). Preparation and Characterization of Super-Hydrophilic Porous TiO₂ Coating Films. *Mater. Chem. Phys.* 68:253-259.
- Zhuang, Y., Kim, Y. J., Lee, T. G., and Biswas, P. (2000). Experimental and Theoretical Studies of Ultra-Fine Particle Behavior in Electrostatic Precipitators, *J. Electrostat.* 48:245-260.

VITA

Name: Guan-Yu Lin

Date of Birth: Apr. 5, 1982

Place of Birth: Taichung, Republic of China

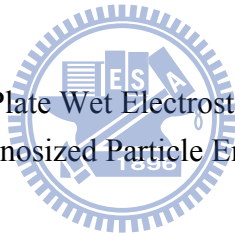
Education:

2006.8-2010.10 National Chiao Tung University, Hsin-Chu, Taiwan, Rpublic of China, Ph. D. program in Environmental Engineering

2004.6-2006.8 National Chiao Tung University, Hsin-Chu, Taiwan, Republic of China, M. S. program in Environmental Engineering

2000.6-2004.6 Tunghai University, Taichung, Taiwan, Rpublic of China, B. S. program in Environmental Science and Engineering

Title of Dissertation: A Wire-in-Plate Wet Electrostatic Precipitator for Controlling Fine and Nanosized Particle Emission



簡 歷

作者：林冠宇

出生日期：民國 71 年 4 月 5 日

出生地：台灣，台中

學歷：國立交通大學環境工程研究所博士班，95 年 8 月-99 年 10 月

國立交通大學環境工程研究所碩士班，93 年 6 月-95 年 8 月

私立東海大學環境科學與工程系，89 年 6 月 93 年 6 月

論文題目：一個控制細微粒及奈米微粒排放的電極線-平板型濕式靜電集塵器

PUBLICATION LIST

Journal papers

1. Chuen-Jinn Tsai, Hsi-Chen Lin, **Kuan-Yu Lin**, Tung-Sheng Shih, Kai-Chung Chang, I-Fu Hung, C.G. Deshpande (2006). Sampling Time Effect on 2,4-Toluene Diisocyanate Concentrations by Different Samplers, *Separation Science and Technology*, 41: 1799-1812.
2. Chuen-Jinn Tsai, **Guan-Yu Lin**, Sheng-Chieh Chen (2008). A Parallel-Plate Wet Denuder for Acidic Gas Measurement, *AIChE J.* 54:2198-2205.
3. **Lin, G. Y.**, Tsai, C. J., Chen, S. C., Tzu, M. C., and Li, S. N. (2010). An Efficient Single-Stage Wet Electrostatic Precipitator for Fine and Nanosized Particle Control, *Aerosol Sci. Technol.* 44:38-45.
4. **Lin, G. Y.**, Tsai, C. J. (2010). Numerical Modeling of Nanoparticle Collection Efficiency of Single-Stage Wire-in-Plate Electrostatic Precipitator, *Aerosol Sci. Technol.* (accepted).
5. Tsai, C. J. **Lin, G. Y.**, Chen, H. L., Huang, C. H., and Alonso, M. (2010). Enhancement of Extrinsic Charging Efficiency of a Nanoparticle Charger with Multiple Discharging Wires, *Aerosol Sci. Technol.* 44:807-816.
6. Ku, Y. P., Yang, C., Tsai, C. J., and **Lin, G. Y.** (2010). An Online Parallel-Plate Wet Denuder Technique for Monitoring Acetic Acid Gas, *AAQR*, Oct. (in press).

Conference papers

1. Tsai, C. J., **Lin, G. Y.**, Chen, H. L., and Chen, S. C. (2008). "Development of a Nanoparticle Charger", Abstract, EAC 2008, Thessaloniki, Greece, Aug. 24-29.
2. Chen, S. C., Tsai, C. J., Wu, C. H., Chang, C. S., **Lin, G. Y.**, Chen, S. J., Tsai, J. H., Lin, C. C., Chou, C. C. K., Huang, W. R., Roam, G. D., Wu, W. Y., Smolik, J., and Pui, D. Y.

3. **Lin, G. Y.**, Tsai, C. J., Chen, T. M., Lee, S. N. (2009). “A Parallel-Plate Wet Electrostatic Precipitator for Nanoparticle Control”, Abstract, NanOEH 2009, Helsinki, Finland, Aug. 26-29.
4. Tsai, C. J., Chien, C. L., Chen, H. L., **Lin, G. Y.** (2010). “Experimental and Numerical Study of a Nanoparticle Charger by using Sheath Air Flow”, Abstract, IAC 2010, Helsinki, Finland, Aug. 29-Sep. 3.
5. **Lin, G. Y.**, Chien, C. L., Tsai, C. J. (2010), “A mathematical model for predicting the nanosized particle collection efficiency in a single-stage wire-in-plate wet electrostatic precipitator”, Abstract, IAC 2010, Helsinki, Finland, Aug. 29-Sep. 3.

Patents

1. 蔡春進、林冠宇 (2010), “平板式濕式分離器、包含此平板式濕式分離器之用於連續式採樣及分析之系統及用於將氣體吸收及氧化之設備”, 中華民國專利, 證書號數: I327641。
2. 具有脈衝噴氣清洗放電電極線的濕式靜電集塵器(patent pending)。
3. 利用包覆空氣提升奈米微粒充電效率的方法及裝置(patent pending)。